Titre: Title:	Organic Ion-Gated Transistors
Auteur: Author:	Tian Lan
Date:	2020
Type:	Mémoire ou thèse / Dissertation or Thesis
Référence: Citation:	Lan, T. (2020). Organic Ion-Gated Transistors [Thèse de doctorat, Polytechnique Montréal]. PolyPublie. https://publications.polymtl.ca/5499/

POLYTECHNIQUE MONTRÉAL

affiliée à l'Université de Montréal

Organic Ion-Gated Transistors

TIAN LAN

Département de génie physique

Thèse présentée en vue de l'obtention du diplôme de *Philosophiæ Doctor*

Génie des matériaux

Octobre 2020

POLYTECHNIQUE MONTRÉAL

affiliée à l'Université de Montréal

Cette thèse intitulée :

Organic Ion-Gated Transistors

présentée par **Tian LAN**

en vue de l'obtention du diplôme de *Philosophiæ Doctor*

a été dûment acceptée par le jury d'examen constitué de :

Yves-Alain PETER, président

Clara SANTATO, membre et directrice de recherche

Denis SELETSKIY, membre

Dongling MA, membre externe

ACKNOWLEDGMENTS

First, I would like to express my thanks to Professor Clara Santato, my research supervisor, for her scientific guidance and help during the last five years. My grateful thanks are also extended to Professor Francesca Soavi (Università di Bologna) and Massimo Marcaccio (Università di Bologna) for their valuable advice and discussions. I would like to thank Professor Fabio Cicoira for access to his lab.

I acknowledge my profound gratitude to the China Scholarship Council for financial support. I am also grateful to CMC Microsystems for microfabrication grants through their programs MNT Financial Assistance and Solutions.

I would like to thank Christophe Clément, Patricia Moraille, Yves Drolet, Marie-Hélène Bernier and Francis Boutet for technical assistance during these years.

In addition, my special thanks go to the people I worked with, my colleagues: Jonathan, Xiang, Irina, Arun, Shiming, Martin, Zhaojing, Xu, Eduardo, Manuel, Yang, Jian, Orlando, Dominic, Julian, Gabriel, Xin, for their support and help in my research work. Meanwhile, I would like to give thanks to my friends: Wayne, Charles, Patrick, Ying, Nan, Yufei, Zunming, Jeff, Richard, Gilbert, Frank, Joseph, Baiyu, Chunyan, Jinyan, Haoyang, Chao, Yanyu, Yujiao, Ting, Xingjia, Zhihui, Steve, Roger as well. Thank you all very much.

Furthermore, I would like to thank my committee members: Professor Yves-Alain Peter, Professor Denis V. Seletskiy and Professor Dongling Ma for volunteering their time to read this thesis, hear my defense, and make valuable comments.

Finally, I would like to express my gratitude and thanks to my beloved parents for their unconditional love and support.

RÉSUMÉ

Les transistors jouent un rôle essentiel dans le développement de l'électronique, qui à son tour affecte notre société, en particulier dans le progrès scientifique, technologique, de l'information et de l'éducation.

Ces dernières années, les transistors à grille ionique (IGTs) utilisant des liquides ioniques comme milieu de déclenchement ont attiré beaucoup d'attention. Les IGTs remplacent les diélectriques conventionnels couramment utilisés, tels que SiO_2, afin d'obtenir une densité de porteurs de charge élevée (environ 10^{15} cm^{-2}) à basse tension (<2 V). Cela est dû à la capacité élevée (environ 1-10 $\mu F/cm^2$) des doubles couches électriques (épaisseur typique de 2-4 nm) formées à l'interface entre le milieu de déclenchement ionique/canal de transistor.

Les IGTs sont un exemple de la technologie iontronique, un domaine interdisciplinaire émergent qui réunit l'électronique et l'ionique. L'iontronique couvre différents aspects fondamentaux, y compris l'électrochimie, le génie électrique, la science des matériaux, etc. Dans cette thèse, l'accent des transistors à grille ionique est mis sur les propriétés électroniques des materiaux constituant le canal du transistor car celles-ci sont controlées par le mouvement ionique. On parle, en effet, de déclenchement ionique.

Les liquides ioniques sont un type d'électrolytes liquides «sans solvant». Ils possèdent des propriétés physicochimiques uniques. En effet, ils ont une pression de vapeur négligeable. De plus, ils ont une conductivité ionique relativement élevée (0.1-20 mS cm^{-1}) et une large gamme de viscosité (10-1000 mPa·s). De plus, les liquides ioniques présentent de larges fenêtres électrochimiques (jusqu'à 5 V) et une stabilité thermique élevée (jusqu'à 300 ^oC).

Les matériaux semi-conducteurs organiques ont été étudiés et appliqués en électronique organique au cours des quatre à cinq dernières décennies, par exemple dans les cellules solaires organiques, les diodes électroluminescentes organiques, les transistors organiques, etc. Dans cette

thèse de doctorat, nous nous concentrons sur de matériaux organiques constitutés de petites molécules et polymers: le phenyl−C_{61}−butyric acid methyl ester (PCBM), le poly[N-9'-heptadecanyl-2,7 -carbazole-alt-5,5-(4',7'-di-2-thienyl-2',1',3'-benzothiadiazole)] (PCDTBT) et le poly (3-hexylthiophene) (P3HT). Ces matériaux peuvent être traités en solution et présentent une absorption optique et une flexibilité mécanique au profit du développement de l'électronique de prochaine generation. Ceux-ci inclut une peau électronique artificielle, des systèmes intégrés portables et des écrans flexibles.

Le cœur de cette thèse est de faire progresser les connaissances sur le mécanisme et le potentiel technologique du déclenchement ionique. Cela vise à mieux comprendre l'intégration des liquides ioniques avec des matériaux organiques dans la configuration du transistor. Il comprend des propriétés électrochimiques, électriques et mécaniques.

Les mécanismes de dopage des transistors à grille ionique utilisant le sémiconducteur de type n PCBM interfacés avec deux liquides ioniques différents: [EMIM][TFSI] et [PYR_{14}][TFSI], ont été étudiés. Des mesures de voltamétrie cyclique (CV) ont été effectuées en configuration transistor dans l'interval de potentiel électrochimique compris entre 0.5 V et -1.9 V par rapport à une électrode de référence carbone: trois séries de pics de réduction et d'oxidation correspondants ont été observés. Une corrélation entre les propriétés redox et de transport de porteurs de charge a été proposée.

En suite, de transistors à grille ionique utilisant les semi-conducteurs de type p [N-9'-heptadecanyl-2,7-carbazole-alt-5,5-(4',7'-di-2-thienyl-2',1',3'-benzothiadiazole)] (PCDTBT, connu pour sa remarquable stabilité en conditions ambiantes) et poly (3-hexylthiophene) (P3HT) comme matériaux de canal ont été fabriqués.

L'étude sur la façon dont le photo-gating module le courant des transistors a été réalisée dans des conditions de lumière solaire simulée sur des transistors PCDTBT à déclenchement ionique. En outre, la stabilité à l'air et la flexibilité du dispositive ont également été explorées en configuration IGT. Ces deux caractéristiques ouvrent un large éventail de possibilités

d'applications en électronique organique. La stabilité opérationnelle à l'air dans les transistors PCDTBT à déclenchement ionique a été atteinte: la durée de conservation de dispositifs était d'environ 150 heures. La stabilité opérationnelle en conditions ambiantes a également été étudiée.

Une contribution clé de cette thèse est le développement de transistors P3HT avec différents poids moléculaires à déclenchement ionique sur des substrats flexibles en polyimide. Le poids moléculaire du P3HT est connu pour affecter les propriétés fonctionnelles des couches minces correspondantes et, finalement, les performances des dispositifs basés sur ceux-ci. Ici, les caractérisations électriques ont été effectuées à deux rayons de courbure différents (R = 10 mm et R = 5 mm). De plus, des mesures de cycle de flexion à R = 5 mm jusqu'à 1500 cycles ont été menées avec succès.

ABSTRACT

Transistors play a key role in the development of electronics, which in turn affects our society, particularly in the scientific, technological, information and education domains.

In recent years, ion-gated transistors (IGTs) making use of ionic liquids as gating media have gained a lot of attention. They replace the commonly used conventional dielectrics, such as SiO_2, to achieve low-operating voltages (< 2 V) and high charge carrier density (ca. ~10^{15} cm^{-2}). This is due to the high capacitance (ca 1-10 μF/cm^2) of the electrical double layer formed at the ion gating medium-transistor channel interface.

IGTs are an example of iontronic technology, an emerging interdisciplinary field that brings electronics and ionics together. Iontronics covers various fundamental aspects of electrochemistry, electrical engineering, materials science. The emphasis of ion-gated transistors is on the electronic properties of transistor channel materials as controlled by ionic motion, namely ion-gating.

Ionic liquids are a type of "solvent-free" liquid electrolyte. They possess unique physicochemical properties. In particular, they have negligible vapor pressure, relatively high ionic conductivity (0.1-20 mS cm^{-1}) and a wide range of viscosity (10-1000 mPa·s). They also exhibit wide electrochemical windows (up to 5 V) and high thermal stability (up to 300 ºC).

Organic semiconducting materials have been studied and applied in organic electronics for the past four or five decades, in organic solar cells, organic light-emitting diodes, organic transistors and so on. In this PhD thesis, we focus on the organic small molecule material phenyl−C_{61}−butyric acid methyl ester (PCBM) and polymer materials poly[N-9'-heptadecanyl-2,7 -carbazole-alt-5,5-(4',7'-di-2-thienyl-2',1',3'-benzothiadiazole)] (PCDTBT) and poly (3-hexylthiophene) (P3HT). These materials feature solution processability, optical absorption and mechanical flexibility benefiting the development of next generation

electronics, specifically, artificial electronic skin, wearable integrated systems and flexible displays.

The purpose of this PhD thesis is to better understand the mechanism and technological potential of ion-gating. We aim to gain insight into the integration of ionic liquids with organic materials in transistor configuration. This includes electrochemical, electrical and mechanical properties.

To investigate the doping mechanism, ion-gated transistors making use of *n*-type semiconductor PCBM interfaced with two different ionic liquids, [EMIM][TFSI] and [PYR_{14}][TFSI], were fabricated. Cyclic voltammetry (CV) measurements were carried out in transistor configuration within the electrochemical potential between 0.5 V and -1.9 V with a carbon reference: three sets of reduction peaks and corresponding anodic peaks were observed. A correlation between redox and charge carrier transport properties was attempted.

Ion-gated transistors making use of the *p*-type semiconductors poly [N-9'-heptadecanyl-2,7 -carbazole-alt-5,5-(4',7'-di-2-thienyl-2',1',3'-benzothiadiazole)] (PCDTBT, known for its remarkable stability in ambient conditions) and poly (3-hexylthiophene) (P3HT) as channel materials were fabricated.

The study on how photo-gating modulates transistor current was carried out under simulated solar light conditions on ion-gated PCDTBT transistors.

Air-stability and flexibility were explored in IGT configuration as well. These two characteristics open a wide range of possibilities for applications in organic electronics. The air-operational stability in ion-gated PCDTBT transistors was achieved: the shelf time of the devices was about 150 hours. The operational stability in ambient conditions was also investigated. One key contribution of this thesis is the development of ion-gated P3HT transistors with different molecular weights on flexible polyimide substrates. The molecular weight of P3HT is known to affect the functional properties of corresponding thin films, and ultimately, the performance of devices based thereon. Here the electrical characterizations were carried out at two different

bending radii (R= 10 mm and R= 5 mm). Additionally, bending cycle measurements at R=5 mm up to 1500 cycles were successfully conducted.

TABLE OF CONTENTS

LIST OF TABLES

LIST OF FIGURES

LIST OF SYMBOLS AND ABBREVIATIONS

A	The active region area under illumination
AFM	Atomic force microscopy
Au	Gold
BC-BG	Bottom contacts - bottom gate
BC-TG	Bottom contacts - top gate
BF_4^-	Tetrafluoroborate
BHJ	Bulk heterojunction
BODIPY-BF2	4,4-difluoro-4-bora-3a, 4a-diaza-s-indacene
C	Specific capacitance
C_i	Capacitance per unit area of gate dielectric layer
CMOSFET	Complementary metal oxide semiconductor field-effect transistor
C_{60}	Buckminsterfullerene
$(C_4H_9)_4NPF_6$	Tetrabutylammonium hexafluorophosphate
CV	Cyclic voltammetry
D	Drain electrode
d	Thickness of the dielectric
EMIM	1-ethyl-3-methylimidazolium
ECT	Electrochemical transistor
EDLs	Electric double layers

EGT	Electrolyte gated transistors
FET	Field effect transistor
G	Gate electrode
g_m	Transconductance
HOMO	highest occupied molecular orbital
I_D	Drain-source current
I_{DS}	Drain-source current
I_{ds}	Drain-source current
$I_{ds,lin}$	Drain-source current in the linear regime
$I_{ds,saturation}$	Drain-source current in the saturation regime
I_{dsat}	Saturation drain current
I_{dark}	I_{ds} under dark conditions
I_G	Gate-source current
I_{gs}	Gate-source current
I_{light}	I_{ds} under light conditions
I_{off}	Current in off state of transistor
I_{on}	Current in on state of transistor
ILs	Ionic liquids
IGTs	Ion-gated transistors
IPA	Isopropyl alcohol
k	Boltzmann constant
k	Relative permittivity

kDa	Kilodalton
L	Channel length
LUMO	Lowest unoccupied molecular orbital
Li	Lithium
MEH-PPV	Poly[2-methoxy-5-(2-ethylhexyloxy)-1,4-phenylenevinylene]
MHz	Mega Hertz
MOSFET	Metal-oxide-semiconductor field-effect
MW	Molecular weight
MPa	Mega pascal
mS	Millisiemens
NIR	Near infrared
NTFT	n-type thin film transistor
OFET	Organic field-effect transistors
OLEDs	Organic light-emitting diodes
OPTs	Organic phototransistors
OPVs	Organic photovoltaic cells
p	Two-dimensional charge carrier density
P	Photosensitivity
PCBM	Phenyl-C_{61}-butyric acid methyl ester
PCDTBT	Poly[N-9’-heptadecanyl-2,7-carbazole-alt-5,5-(4’,7’-di-2-thienyl-2’,1’,3’-benzothiadiazole)]
PDA	Polydopamine

PDMS	Polydimethylsiloxane
P3HT	Poly (3-hexylthiophene)
PET	Polyethylene terephthalate
PF_6^-	Hexafluorophosphate
PI	Polyimide
P_{light}	The illumination power intensity
PMMA	Poly(methyl methacrylate)
PR-TRMC	Pulse radiolysis time-resolved microwave conductivity
Pt	Platinum
PTFT	p-type thin film transistor
PVA	Poly(vinyl alcohol)
PYR_{14}	1-butyl-1-methylpyrrolidinium
q	Elementary charge
Q'	Mobile charges
Q	Charge density
R	Curvature radii
R	Photoresponsivity
rms	Root mean square roughness
RTILs	Room temperature ionic liquids
r_v	The sweeping rate
S	Source electrode
S	Subthreshold voltage

SECM	Scanning Electrochemical Microscopy
t	Time
TBA^+	Tetrabutylammonium
$(TBA)BF_4$	Tetrabutylammonium tetrafluoroborate
TCNQ	7,7,8,8-tetracyanoquinodimethane
TEA^+	Tetraethylammonium
TEGDME	Tetraethylene glycol dimethyl-ether
TFT	Thin film transistor
TFSI	bis(trifluoromethylsulfonyl)imide
THA^+	Tetrahexylammonium
THF	Tetrahydrofurane
Ti	Titanium
TOA^+	Tetraoctylammonium
UV	Ultraviolet
V_D	Drain-source voltage
V_{DS}	Drain-source voltage
V_{ds}	Drain-source voltage
V_G	Gate-source voltage
V_{GS}	Gate-source voltage
V_{gs}	Gate-source voltage
V_{sat}	Voltage at pinch-off point
V_{so}	Switch-on voltage

V_{th}	Threshold voltage
W	Channel width
$W_{overlap}$	Length of overlapping electrodes
XRD	X-ray Diffraction
ε_0	Vacuum permittivity
μ	Charge carrier mobility
σ	Single bond
π	Double bonds
2D	Two-dimensional
3D	Three-dimensional

LIST OF APPENDICES

CHAPTER 1 INTRODUCTION

In this chapter, we briefly introduce transistors, including history, technology, structure and working mechanisms along with working principles of ion-gated transistors. In addition, we discuss thin films of small organic electronic molecules and polymers used in this work as channel materials. A discussion of the research issues and motivations involved will further clarify the relevance and impact of the scientific and technological findings of this PhD thesis.

1.1 History of transistors

In 1907, the transistor precursor, a thermionic valve, was invented.[1] In 1925, the working principle of a field-effect transistor was proposed and filed as a patent by Julius Edgar Lilienfeld, an Austro-Hungarian physicist.[2] In 1947, a real working transistor, i.e. a point-contact transistor, was invented at Bell Labs, by scientists John Bardeen, William Shockley and Walter Brattain.[3-4] In 1956, the Nobel Prize in Physics was awarded to these three scientists for their "researches on semiconductors and their discovery of the transistor effect".[5] In 1948, William Shockley from Bell Labs invented the first bipolar junction transistor.[6] In 1953, the company Philco developed a surface-barrier germanium transistor, which is the first high-frequency (up to 60 MHz) transistor.[7] Intensive research on transistors was carried out in academia and industry at that time. In 1954, Morris Tanenbaum developed the first working silicon transistor at Bell Labs.[8] In the same year, Texas Instruments produced the first commercial silicon transistor, which is a benchmark in transistor history.[9] Initially, in the semiconductor industry, a lot of attention was focused on junction transistors, bulky devices that are difficult to manufacture. In 1959, Mohamed Atalla and Dawon Kahng co-invented metal oxide semiconductor field-effect transistors (MOSFETs).[10] MOSFETs have a wide range of uses because they are capable of being mass-produced and miniaturized. In 1963, Chih-Tang Sah and Frank Wanlass at Fairchild

Semiconductor invented the complementary metal oxide semiconductor field-effect transistor (CMOSFET). [11]

In 1962, based on the work on MOSFETs, thin film FETs were developed by Paul K. Weimer at RCA.[12] The architecture of thin film transistors consists of the source and drain electrodes on a thin layer of semiconductor (conducting channel) along with a thin layer of insulator in between the metal gate contact and the conducting channel.

Semiconducting materials are key to the development of thin film transistors. Due to their low cost, solution processability and mechanical flexibility, organic semiconducting materials gained a lot of attention (see below).

Organic field-effect transistors (OFETs) adopt the architecture of thin film FETs and attract enormous interest from academia and industry, due to their competitive performance with that of amorphous silicon TFTs in terms of field-effect mobility and ON/OFF ratio (see below).

The invention of transistors is a huge step forward in the development of techno-science. Due to the existence of transistors, more and more electronic devices have been invented: the transistor radio in the 1950s, transistorized portable television in 1960 and the pocket calculator in 1971. Nowadays, transistors are embracing new opportunities presented by flexible, stretchable, biocompatible electronics, such as wearable systems, flexible displays and artificial skin.

1.2 Thin film transistors

Very simply stated, a transistor is a device consisting of three terminals, called source (S), drain (D) and gate (G). The source and drain electrodes are in direct contact with the semiconductor. The region that lies between the two individual electrodes forms the transistor channel. S and D are associated with the injection and extraction of the charge carriers. In between the gate electrode and the semiconductor channel, there exists a dielectric layer. Normally, S is grounded (common ground of the device) and the potential applied between D and S induces the

drain-source current. The gate is used to modulate the channel conductivity (degree of doping in the channel).[7, 47]

Thin film transistors (TFTs) consist of thin films of an active semiconductor layer, a dielectric layer and three electrodes, namely gate (G), source (S) and drain (D). The channel is defined by the source and drain geometry in terms of width (W) and length (L), as shown in Figure 1-1. In TFTs, a variety of semiconductor materials can be used as channel material e.g., silicon, metal oxides or organic semiconductors.

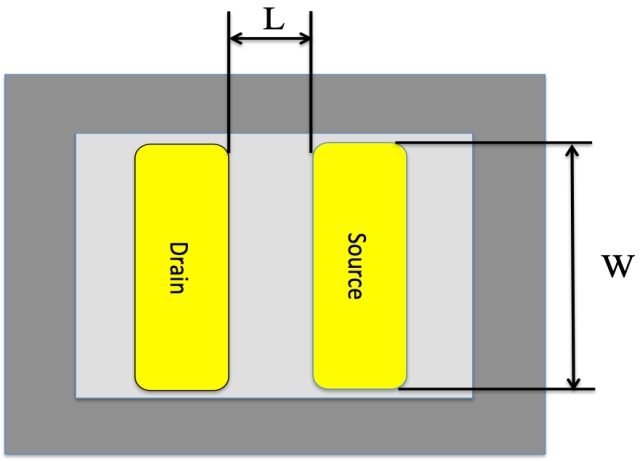

Figure 1-1 Geometry of drain and source electrodes in a thin film transistor (top view).

Thin film transistor configurations, along with transistor working principles and characteristics will be introduced in the following sub-chapters. Each parameter and component of a TFT has an impact on the transistor performance and could be adjusted and optimized for various applications.

1.2.1 Thin film transistor configuration

With different sequences of deposition of the materials in TFTs, there are four main distinguishable TFT architectures, as shown in Figure 1-2.

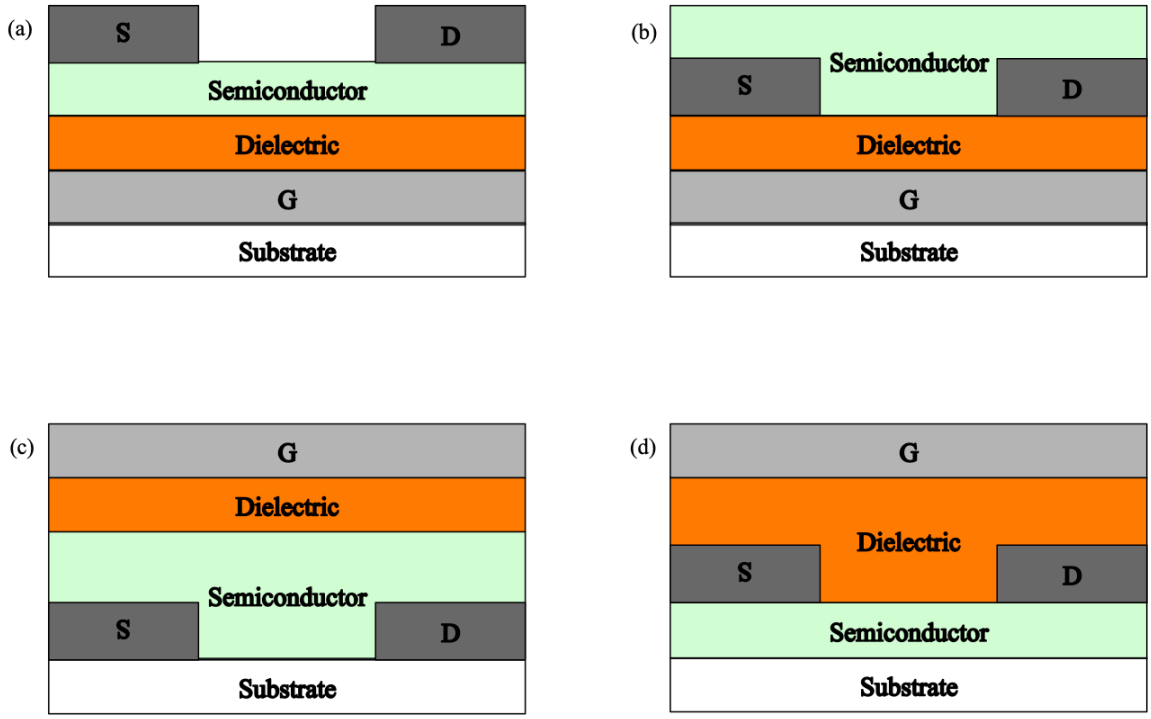

Figure 1-2 Schematic cross-sections of TFT structures. (a) Bottom gate staggered TFT, (b) Bottom gate coplanar TFT, (c) Top gate staggered TFT, (d) Top gate coplanar TFT.

Transistor configuration has an influence on the performance of the devices. Each TFT structure presented in Figure 1-2 has its advantages and disadvantages. There is an energy barrier at the interfaces between the organic semiconductor and the source or drain metal contacts limiting the charge carrier injection between semiconductor and contacts. Previous studies have shown that bottom gate and top gate staggered TFTs exhibit less influence from the energy barrier compared to bottom gate and top gate coplanar TFTs.[13-18] The impact on charge carrier injection efficiency can be reduced through the surface modification of the source and drain contacts in bottom-gate coplanar TFTs.[19-20]

In the four main device configurations, charge carrier transport takes place mainly at the interface between semiconductor and dielectric.[21] Charge carriers are injected close to the semiconductor-dielectric interface in bottom gate and top gate coplanar TFTs, whereas the

injected charges need to travel through the semiconductor to reach the channel for bottom gate and top gate staggered TFTs.

1.2.2 Operation principles

Since TFTs are a special type of MOSFETs, their working principles are similar to a conventional MOSFET. Based on different types of semiconductors working as the channel materials, charge carriers with different polarity are induced in the semiconductor: for p-type semiconductors, negative gate bias is applied, holes are induced; for n-type semiconductors, positive gate bias is applied, electrons are induced.

Output and transfer curves are two main characteristics to extract the most important figures of merit of the transistors as shown in Figure 1-3. The output curves present the drain-source current (I_{ds}) as a function of the drain-source voltage (V_{ds}) at various gate-source voltages (V_{gs}). On the other hand, transfer curves show the correlation between I_{ds} and V_{gs} at different V_{ds}. The voltage applied on the gate electrode is used to control the channel conductance, which is dependent on the number of mobile charge carriers in the transistor channel. For example, with n-type semiconductors as the channel material, with positive V_{gs}, mobile electrons will be induced next to the semiconductor-dielectric interface, leading to an increase in channel conductance. Higher conductivity could be achieved by increasing at higher positive V_{gs}. Conversely, when a negative bias is applied to the gate electrode, the channel conductance is reduced, due to the repulsion of the electrons from the semiconductor-dielectric interface with consequent decrease in the density of charge carriers (electrons) in the transistor channel. For p-type semiconductors (majority of mobile charge carriers are holes), the transistor channel would be more conductive with a negative bias applied to the gate electrode.

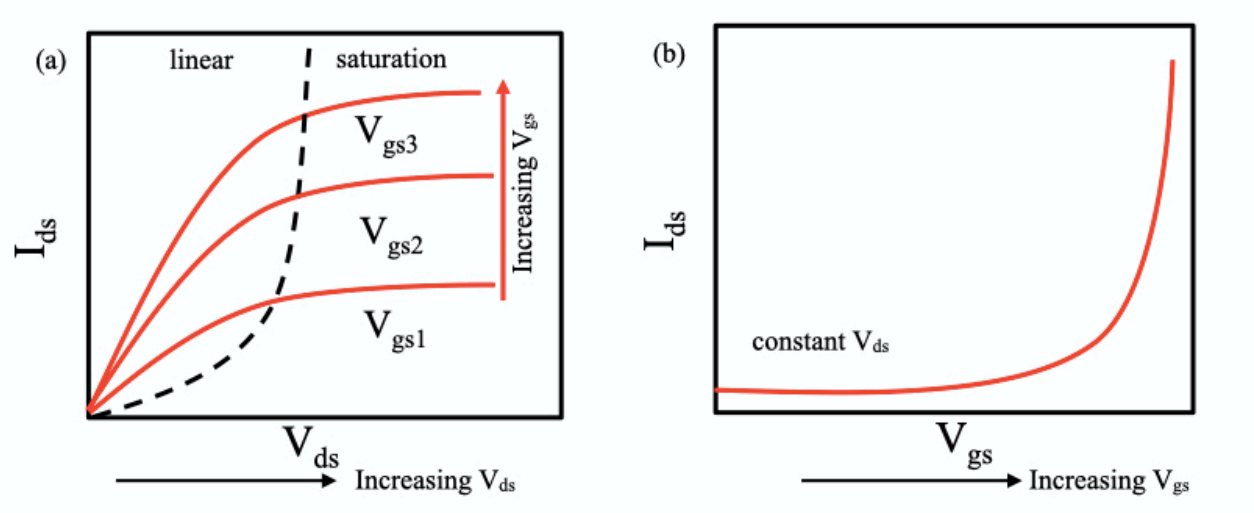

Figure 1-3 Output (I_{ds}-V_{ds}) (a) and transfer (I_{ds}-V_{gs}) (b) characteristics of thin film transistors. Dash line (cutoff line) separating the linear and saturation operation regimes is indicated in (a).

For n-type TFTs (NTFTs), the relationship of I_{ds} and V_{ds} is approximately linear at low V_{ds} values, in the output characteristics. When V_{gs} is much higher than V_{ds} and there are no defects at the semiconductor-dielectric interface, the distribution of the majority charge carriers in the channel is nearly uniform. With the increase of V_{ds}, a decrease in charge carriers near the drain electrode is observed under the influence of the semiconductor potential, leading to a deviation of I_{ds} from linear behavior. When V_{ds} reaches a certain value, the *pinch-off* point is built, the number of charge carriers near the drain electrode is nearly zero and moving to source electrode with further increase of V_{ds}. As the applied V_{ds} continues to increase and goes beyond the voltage needed to form the *pinch-off* point (V_{sat}), the number of charges arriving at the *pinch-off* point does not change, reaching a saturation regime instead under the condition of $V_{ds} > V_{sat}$. At the same time, the *pinch-off* point moves closer to the source. This indicates that further increase in V_{ds} does not affect I_{sat}, despite the reduction in effective channel length. For p-type TFTs (PTFTs) an analogous situation is observed.

In the linear regime, I_{ds} it can be approximated through equation (1):

$$I_{ds,\ lin} = \frac{W\mu C_i}{L}\left((V_{gs} - V_{th})V_{ds} - \frac{V_{ds}^2}{2}\right), \quad V_{ds} < (V_{gs} - V_{th}) \quad (1)$$

Where C_i is the capacitance per unit area of gate dielectric layer, μ is the charge carrier mobility and V_{th} is the threshold voltage (see below).

For I_{ds} in saturation regime, equation (1) can be approximated through equation (2)

$$I_{ds,\ sat} = \frac{W\mu C_i}{2L}\left(V_{gs} - V_{th}\right)^2, \quad V_{ds} > (V_{gs} - V_{th}) \quad (2)$$

which presents a linear relationship between the square root of the channel current and gate voltage.

1.2.3 Main characteristics of thin film transistors

The charge carrier mobility (a charge carrier's magnitude of drift velocity per unit electric field, which is used to describe the charge carrier transport efficiency) can be derived from I_{ds} in the linear and saturation regimes from the equation (1) and (2) shown above:

Linear: $\mu_{lin} = \frac{L}{WC_iV_{ds}}\frac{dI_{ds}}{dV_{gs}}$ (3)

Saturation: $\mu_{sat} = \frac{2L}{WC_i}\left(\frac{d\sqrt{I_{ds,sat}}}{dV_{gs}}\right)^2$ (4)

The detailed derivation steps of mobility in the linear region are shown as follows:

The capacitance per unit area of a dielectric (specific capacitance) (F m^{-2}) can be written as:

$$C = \kappa\frac{\varepsilon_0}{d} \quad (5)$$

Where k is the relative permittivity (dielectric constant), ε_0 is the vacuum permittivity and d is the thickness of the dielectric.[18]

The charge density (Q) could be expressed in C cm^{-2} at condition of V_{ds}=0 by

$$Q = C(V_{gs} - V_{th}) \quad (6)$$

When V_{ds} increases, the charge density could be written as:

$$Q = C(V_{gs} - V_{th} - V_{ds}) \quad (7).$$

In the linear region as shown in Figure 1-3, at the condition of V_{gs}-V_{th}>$V_{ds,}$ the transistor current I_{ds} could be yielded by the charge density across the channel width W, with bias applied between drain and source electrodes,

$I_{ds} = QWv = QW\mu E$ (8),

Where Q is the charge density, v is the velocity of the charge carrier, E is the electric field in the channel i.e., V_{ds}/L, L is the channel length and μ is the charge carrier mobility.

Equation (6) could be rewritten as:

$I_{ds} = QW\mu\frac{V_{ds}}{L}$ (9)

From (9), the charge carrier mobility could be given by:

$\mu = \frac{L}{W}\frac{I_{ds}}{V_{ds}Q}$ (10)

Introducing (6) into (10) would achieve the equation (3).

The charge carrier mobility is a very important parameter to evaluate the performance of semiconductors, as fast device operation needs high mobility values.

The ON/OFF ratio is typically extracted from the transfer curve, representing the ratio between the channel current when the transistor is in the on-state mode and when the transistor is switched off. When the transistor is not operating, it is better to avoid power consumption by minimizing the off current. Thus the on/off ratio should be as high as possible.

Onset voltage could be obtained directly from transfer curve defined as the gate voltage needed to switch the transistor from off-state mode to on-state mode.

Subthreshold swing provides information on the amount of V_{gs} needed to make I_{ds} increase by an order of magnitude. The performance of the transistor is better with lower subthreshold swing values. It can be defined by:

$S = \frac{\partial V_{gs}}{\partial log_{10}(I_{ds})}(mV/dec)$.

Another characteristic of TFTs is the threshold voltage V_{th}, corresponding to the V_g where a formation of conductive channel or an accumulation layer close to the semiconductor-dielectric interface is achieved. The threshold voltage V_{th} is influenced by many factors, such as the type of dielectric, the semiconductor material, defect states, impurities and device geometry, as well as semiconductor-dielectric interface. There are two main methodologies to determine this parameter: one is to use a linear extrapolation of I_{ds}/V_{gs} at low V_{ds} (transfer curve in linear regime); the second one is to adopt a linear extrapolation of $\sqrt{I_{ds}}/V_{gs}$ at high V_{ds} (transfer curves in saturation regime).

The transconductance, g_m, used to describe how gate voltage modulates the I_{ds}, is defined as:

$$\left[\mathrm{g_m} = \frac{\partial \mathrm{I_{ds}}}{\partial \mathrm{V_g}}\right]_{\mathrm{V_{ds}}=const},$$

The g_m is obtained through equation (1) in linear regime:

$$\left[g_m = \frac{\partial I_{ds}}{\partial V_g}\right]_{V_{ds}=const} = \frac{W\mu C}{L} V_{ds}$$

The g_m is obtained through equation (2) in saturation regime:

$$\left[\mathrm{g_m} = \frac{\partial \mathrm{I_{ds}}}{\partial \mathrm{V_g}}\right]_{\mathrm{V_{ds}}=const} = \frac{W\mu C}{L}(\mathrm{V_{ds}} - \mathrm{V_{th}})$$

In TFTs, a large number of organic photosensitive materials have been employed as channel materials. Thus, exposure to light has been introduced as an additional parameter to evaluate the performance of the devices. In addition, photosensitivity (P) and photoresponsivity (R) are used for characterization and defined by the following equations:

$$P = \frac{I_{light} - I_{dark}}{I_{dark}}$$

where I_{light} is the I_{ds} under light conditions and I_{dark} is the I_{ds} under dark conditions.

$$R=\frac{I_{light}-I_{dark}}{AP_{light}}$$

where A is the active region area under illumination and P_{light} is the illumination power intensity.

1.3 From TFTs to ion-gated transistors (IGTs)

Operating conventional TFTs requires high operation-voltage (up to tens of volts for e.g. 100-200 nm SiO_2) that is attributed to low gate dielectric capacitance, which sets a barrier to their integration in wearable, printable and low power consumption electronics. To solve this problem, lowering the operating voltage by employing a high permittivity dielectric material or reducing the thickness of the gate dielectric are commonly and effectively used methods. However, disadvantages, including decreased charge carrier mobility or high leaking current, occur with the former or latter choice.

Ion-gating turns out to be an alternative to conventional dielectrics for obtaining high capacitance (1-10 μF/cm^2). It makes use of the electrical double layer formed at an ionic liquid-channel interface when a bias is applied to the gate electrode. Due to the high capacitance, achievable at low-voltages (< 2V), it is feasible for ion-gated transistors to provide large charge carrier densities (~10^{15} cm^{-2}) in the channel. Ion-gating also facilitates novel applications to a broad range of flexible, printable and bio-electronics. The two-dimensional charge carrier density can be determined by:

$$\rho = \frac{Q'}{eA} \quad (11)$$

Where e is the elementary charge, A is the area of the films and Q' is the total gate-induced charge given by:

$$Q' = \frac{\int I_{gs} dV_{gs}}{r_v} \quad (12)$$

Where I_{gs} is the gate-source current, V_{gs} is the gate-source voltage and r_v is the sweeping rate given by

$r_v = \frac{step\ size\ (mV)}{sample\ period\ (s)}$ (13).

Combining (11) and (12) result in:

$\rho = \frac{\int I_{gs} dV_{gs}}{eAr_v}$ (14),

The mobility in ion-gated transistor linear regime could be calculated via (14) along with (10):

$\mu = \frac{L}{W} \frac{I_{ds}}{V_{ds} e \rho}$ (15).

Regarding the operating mechanisms of IGTs, there are two basic cases, depending on the permeability of the transistor channel materials (Figure 1-4)[18]. If the semiconductor is impermeable, and a bias is applied to the gate electrode, ions accumulate at the liquid-solid interfaces. This leads to an accumulation of carriers in the semiconductor and charge screening at the gate electrode, with an electric double layer at each interface (*electrostatic doping*).[18] When the semiconductor is permeable, an electrical double layer forms at the liquid/gate interface upon the application of gate voltage. Ions move towards the semiconductor and diffuse into it (*electrochemical doping*). Transistors with permeable channel materials are called electrochemical transistors (ECTs). The semiconductor channel in ECTs can have a three-dimensional (3D) character due to the penetration of the ions, while channel materials operating in electrostatic mode have a 2D character.

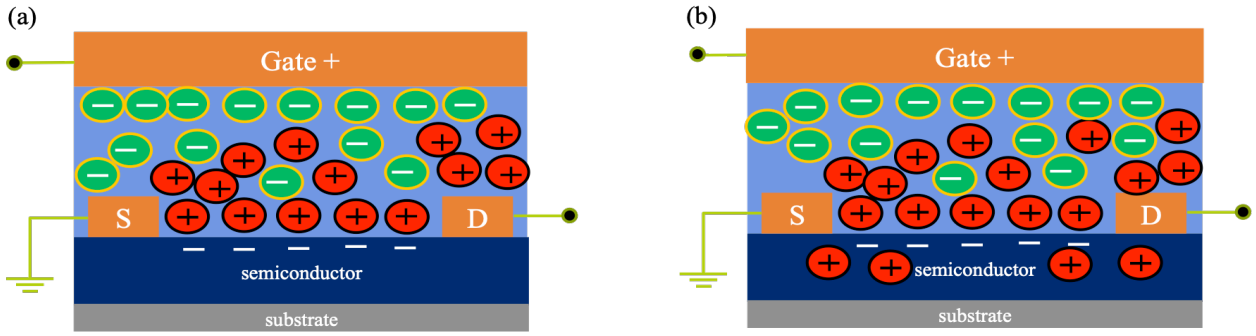

Figure 1-4 Carrier accumulation-mode operation of an ion-gated transistor for un-doped ion-impermeable (electrostatic mode of operation, a) and permeable semiconductors (electrochemical mode of operation, b).

1.4 Room temperature ionic liquids (RTILs)

Room temperature ionic liquids may be simply seen as liquid salts at room temperature. They are composed of mobile ions (usually asymmetric bulky organic cations and inorganic or organic anions). Due to their non-volatility and negligible vapor pressure, RTILs are sometimes labeled as environmentally attractive "green solvents". This makes them an alternative replacement for conventional organic solvents.

In electrochemical studies, most used compounds contain 1-alkyl-3-methylimidazolium, N-methyl-N-alkylpyrrolidinium, and tetraalkylammonium cations (Figure 1-5).[22] As for anions, hexafluorophosphate (PF_6^-), tetrafluoroborate (BF_4^-), and bis(trifluoromethylsulfonyl)imide ([TFSI]) are the most popular candidates (Figure 1-5).[22] In addition, [TFSI] is a notable type of hydrophobic anion that is also referred to as the imide ion. The shielded and delocalized negative charge on [TFSI] hinders ionic interaction with nearby cations, which in turn facilitates the high conductivities of the salts.

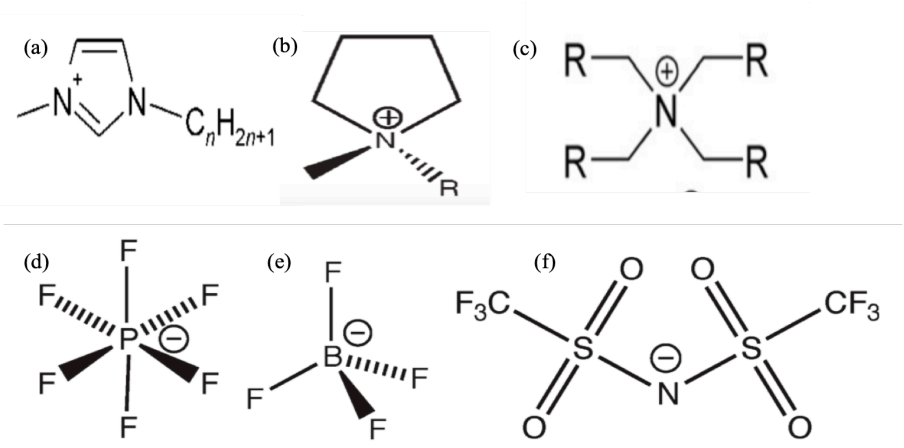

Figure 1-5 Molecular structures of cations: (a) 1-alkyl-3-methylimidazolium, (b) N-methyl-N-alkylpyrrolidinium, (c) tetraalkylammonium and anions: (d) hexafluorophosphate, (e) tetrafluoroborate, (f) bis(trifluoromethylsulfonyl)imide.[22,27]

The viscosity of a fluid is a measure of its resistance to deformation under force.[23] It strongly affects the mass transport rate in a solution. Size, shape and molar mass of the anions in a solution have an impact on its viscosity[22,24,26] as does its ability to form hydrogen bonds or allow for van der Waals interactions. As for cations, size is the main factor affecting viscosity, i.e., increasing the length of alkyl chain or its substituents is generally effective. Viscosity is temperature-dependent, decreasing with an increase in temperature.[22-25]

The melting point of RTILs is controlled by many factors. These include van der Waals interactions, symmetry of the cations, hydrogen bonding ability and ionic charge. [22,24]

RTIL density values are mostly between 1 g cm^{-3} and 1.6 g cm^{-3}. Ionic size affects density: the density of ionic liquid $[C_n mim][NTf_2]$ shows a decrease when the length of alkyl chain increases.[22,24]

In the electrochemical process, the conductivity of RTILs is of great importance. As RTILs solely contain ions, there exist a large number of charge carriers. High conductivities can be achieved when the charge carriers are mobile. Conductivity values of RTILs range from 0.1 to 20 mS cm^{-1}.[24] There is a general relationship between conductivity and viscosity, that is, lower viscosity leads to higher conductivity.[22,24] The conductivities RTILs exhibit are high enough to permit their use in electrochemical experiments carried out in conventional electrolyte. Thus, the intrinsic property of RTILs obviate the need for salt when performing experiments.[22,24]

Generally speaking, the electrochemical window of a solvent is important in the research, design and development of electrochemical applications. The window, which is the difference between the potential at the anodic (oxidation) and cathodic (reduction) limits, is of paramount importance when conducting an electrochemical experiment on a given species as it confines the oxidation and reduction processes to the species itself.[22 -23] The electrochemical window for RTILs can reach 5 V.[24]

1.5 Organic semiconductors as channel materials

Organic semiconductors are very popular candidates for channel materials in transistors because of their outstanding solution processability, flexibility and stretchability, which are key for next generation electronics. There are two flavors in organic semiconductors: conjugated small molecules and conjugated polymers. In organic electronic compounds, electronic conjugation is the fundamental property of being electronically conductive, i.e. possessing alternating single (σ) and double (σ and π) bonds between covalently bound carbon atoms. Charge carriers move at both the intermolecular and intramolecular level in solid organic electronic materials. The energy levels of the single molecules and polymers contribute to determining the electronic properties of the materials (usually in thin film form). In this case, the highest occupied molecular orbital (HOMO) and lowest unoccupied molecular orbital (LUMO) bands consist of HUMO and HUMO levels of individual molecules. However, if the intermolecular interactions are strong enough, long-range order will be built, affecting the electronic properties of the organic solids. The HOMO and LUMO bands would merge into conduction and valence band. In the transistor configuration, a large number of conjugated molecules in a thin film format were utilized.

In this thesis, we studied the organic small molecule material phenyl-C_{61}-butyric acid methyl ester (PCBM) and polymers poly [N-9'-heptadecanyl-2,7-carbazole-alt-5,5-(4',7'-di-2-thienyl-2',1',3'-benzothiadiazole)] (PCDTBT), and poly (3-hexylthiophene) (P3HT). The chemical structure of the organic semiconductors is shown in Figure 1-6.

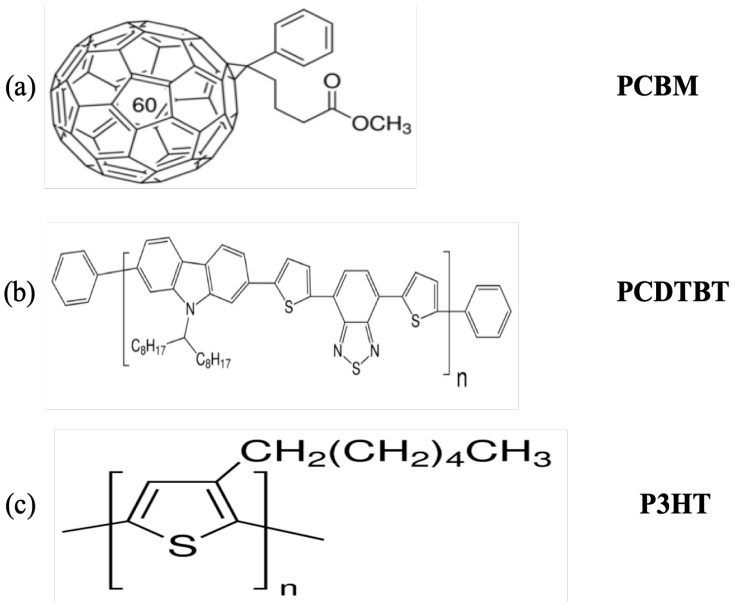

Figure 1-6 Molecular structures of molecules and polymers investigated in this PhD thesis (PCBM, PCDTBT and P3HT).

1.6 Research questions

Despite the large number of studies being carried out on ion-gated transistors (IGTs), more related studies still need to be done to determine the nature of the electrical double layer at the organic semiconductor-ionic media interface, as the ions could participate in the doping process, which is complex. Thus a deeper understanding of doping and charge carrier transport processes in conjunction with the doping process is necessary for achieving better device performance.

Various factors govern the performance of IGTs: the effective potential on gate electrode, the doping level of the semiconductor channel, and the device structure. In the transistor configuration, the semiconductor is contacted with the metal electrodes and interfaced to the ionic liquids, which might cause an issue for the charge injection process.

Organic semiconductors, such as small molecules or polymers, are employed in these processes. Redox process and electrochemical properties of these materials play an important role in the charge carrier transport. This would raise the question of how much the correlation of these

different processes would influence the performance of IGTs. Another question that would occur is: “how will the integration of intrinsic properties of organic semiconducting materials, such as air-stability and photo-sensitivity, with ion-gating functionality work?” At the same time, the molecular weight of organic semiconducting materials is also creating a question regarding the effectiveness of ion-gating, especially based on flexible substrates.

1.7 Motivation

Organic semiconductors such as conjugated small molecules (PCBM) and polymers (PCDTBT and P3HT), are promising materials for a wide range of applications in electronics, e.g. flexible displays, electronic skin and robotics. The integration of ion-gating with transistors is highly demanding as it paves the way to low-voltage operation mode (< 2 V) with high charge carrier density (up to 10^{15} cm^2) and opens the possibilities for novel electronic phases.

My main motivation for this work is provided by research issues and is consistent with the objective of this thesis, which is to explore how ionic liquids working as gating media contribute to current modulation in flexible ion-gated transistors and photo-transistors. This has involved more specifics as each organic semiconductor adopted as channel material interfaced with ionic liquids (ILs) and included: 1) the interaction of redox processes of PCBM with charge carrier transport considering the different physicochemical properties of different ILs; 2) air-stability and photosensitivity properties of PCDTBT embedded in ion-gated transistors; 3) the participation of different molecular weights of P3HT in the modulation of ion-gating based on rigid and flexible substrates. Because of their good ionic conductivity, large electrochemical stability window and high thermal stability, room temperature ionic liquids (RTILs) were the ideal candidates for these studies.

CHAPTER 2 LITERATURE REVIEW

A good understanding of IGTs is crucial for the development of printable, flexible and bio-electronics. Elucidating the electrochemical and electronic properties of organic semiconducting channel materials in situ can help to shed light on IGT working principles.[28]

This chapter starts with a report on state-of-the-art ionic gating media and IGTs. We next provide a brief introduction to the electrochemistry of fullerene derivatives used as channel materials in IGTs and to the phenomenon of the finite window of high conductivity. After which, the light-absorbing and environmentally stable organic semiconductor PCDTBT will be reviewed. Here we will also include a discussion on organic phototransistors. We will conclude the literature chapter with a report on studies regarding poly(3-hexylthiophene (P3HT) and the influence of different molecular weights on the structure of corresponding polymer films and doping mode of the devices.

2.1 Ionic gating media

Electrolytes are substances generally composed of salt and solvent. They contain disassociated ions: cations and anions. Due to the existence of mobile ions, they are “electrically conductive”. Water and other polar non-aqueous solvents can be employed as the medium but they are unstable and volatile in air. This makes it difficult to maintain a constant salt concentration. So, stable and low volatility solvents can be an alternative but a compromise in the conductivity has to be made.[28-30]

Ion gels can be obtained through the gelation of a block co-polymer building a network swollen by an ionic liquid. They possess a solid-like mechanical integrity. The solvent used to fabricate the ion-gels can destabilize the channel materials limiting the range of their applications.[28-30]

Polyelectrolytes are polymers with either positively or negatively charged ionizable groups. In polar solvents, these groups can dissociate. In a solid state, a thin film, polyelectrolytes can dominantly transport ions of only one polarity.

Polymer electrolytes are a type of quasi-solid electrolyte containing no conventional solvent. The blend of poly (ethylene oxide) (PEO) and lithium salts is the most commonly used form of polymer electrolytes.

Ionic liquids are a type of "solvent-free" liquid electrolyte. They have high ionic diffusivity and ionic conductivity because of relatively weak electrostatic interactions between ions. Room-temperature ionic liquids (RTILs) have attracted a lot of interest over the last decade. ILs exhibit high thermal stability (up to 300 ^{o}C), wide electrochemical windows (up to 5 V), high ionic conductivity and viscosity (10-1000 mPa s).[28-30] Table 2-1 lists the conductivity of different ionic media used to gate transistors.

Table 2-1 Conductivity of different ionic media used to gate transistors.

Category	Conductivity (mS cm^{-1})
Electrolyte solution	10-200
Ion gels	10^{-4} -10^{-2}
Polyelectrolytes	10^{-6} -10^{-3}
Polymer electrolytes	~1
Ionic liquids	0.1-20

2.2 IGTs

Electric double layers (EDLs) are the keys to storing electrochemical energy (as in batteries and supercapacitors).[28-30] EDLs are also relevant in describing the operation of IGTs.

Figure 2-1 illustrates an example of IGT making use of the ionic liquid [EMIM][TFSI] as the gating medium as well as an organic rubrene single crystal as the channel material, with a bottom-gate/bottom-contact structure, reported by J. Takeya et al.[31] This type of IGT can reach an ON/OFF ratio up to ~10^4 and a mobility of 5 $cm^2\ V^{-1}s^{-1}$ at room temperature. Before introducing the room-temperature IL into the devices, the air-gap rubrene single-crystal transistors were characterized for their transfer and output characteristics at voltages up to -100 V (giving a mobility of 11 $cm^2\ V^{-1}s^{-1}$). Using [EMIM][TFSI], due to the high capacitance of the electrical double layer, the devices could be operated at about 1 V, bringing about a charge carrier density of ~10^{13} cm^{-2}. The capacitance increased with the decrease in frequency and had a value of 4 $\mu F/cm^{-2}$ at 10 Hz.

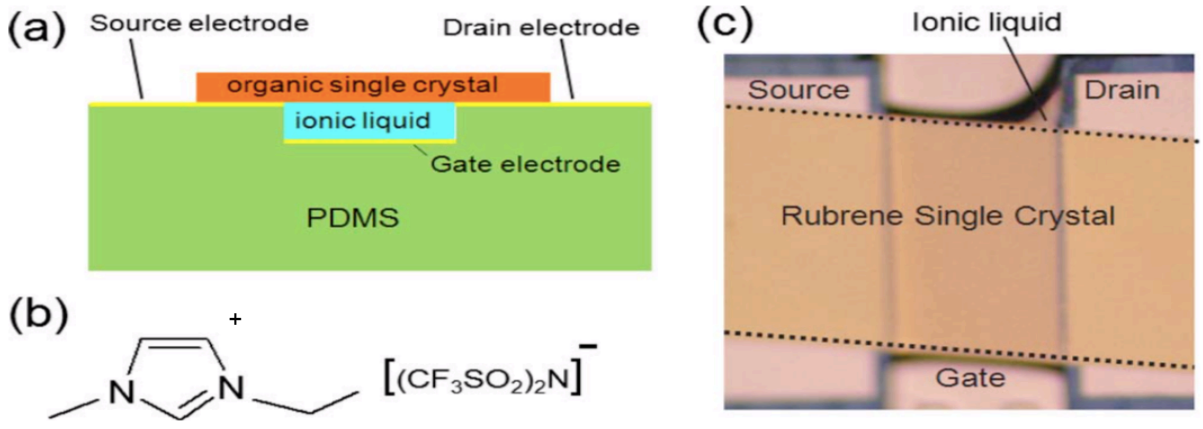

Figure 2-1 (a) Structure of organic crystal/ionic liquid transistors. (b) [EMIM][TFSI]. (c) Optical image of a rubrene crystal/[EMIM][TFSI] transistor. (Reprinted with permission from Ref. 31, Copyright © 2008 American Institute of Physics)

Frisbie et al. carried out research on ion-gated single crystal and polymer transistors and compared such transistors with counterparts gated with conventional dielectrics.[32] In one study, the ion gating medium was [EMIM][TFSI] (dielectric constant: ~24 at a frequency of 315 Hz), compared to silicone oil (dielectric constant: 2.9) and vacuum. They studied the relationship between mobility and charge carrier density in ionic liquid, silicone oil and vacuum gating media. Table 2 presents the maximum mobility value obtained via different gate dielectrics, showing opposite trends in single-crystal OFETs and polymer TFTs. For single crystals, the carrier mobility was dependent on the dielectric constant without strongly depending on the charge density. The highest charge mobility was obtained using vacuum as dielectric. In contrast, for polymer IGTs, charge mobility was a function of charge carrier density.

Table 2-2 Maximum mobility of transistors based on single crystals or polymers, gated with three different gating media. (Reprinted with permission from Ref. 32, Copyright © 2009 WILEY-VCH Verlag GmbH & Co. KGaA, Weinheim)

Gate dielectrics	Single crystal OFETs		Polymer TFTs	
	Rubrene	Pentacene	PQT-12	P3HT
Vacuum [0.18 nF cm^{-2}]	13 ± 1	1.5 ± 0.4	0.006 ± 0.003	0.005 ± 0.002
DC 704 oil [0.55 nF cm^{-2}]	8.8 ± 1.7	0.6 ± 0.2	0.04 ± 0.01	0.03 ± 0.02
[EMIM][TFSI] [15 μF cm^{-2}]	0.31 ± 0.06	0.020 ± 0.004	1.7 ± 0.8	1.2 ± 0.7

Although much research focused on p-type organic materials, some investigations on n-type organic materials were carried out as well. Takeya et al. reported on low-voltage operation of ion-gated n-type organic transistors based on 7,7,8,8-tetracyanoquinodimethane (TCNQ) single-crystals as the channel material and the [EMIM][TFSI] as the gating media (Figure 2-2).[33] They showed that the devices could operate at 0.5 V, a remarkably low drive voltage. The mobility could reach ~10^{-3} cm^2 V^{-1} s^{-1}.

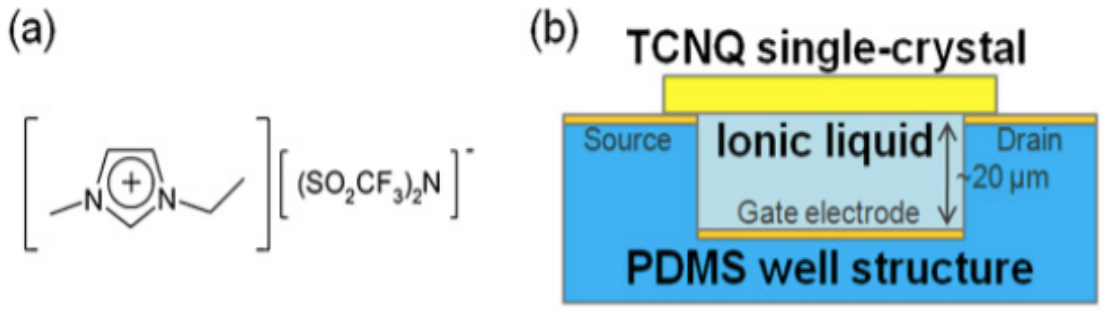

Figure 2-2 (a) Chemical structure of [EMIM][TFSI]. (b) Schematic illustration of ionic liquid-gated organic single crystal transistors. (Reprinted with permission from Ref. 33, Copyright © 2010 The Japan Society of Applied Physics)

The n-type organic semiconductor C_{60} fullerene was also studied after having been interfaced with the ionic liquid [EMIM][TFSI] (Figure 2-3).[33] V_{th} was ~0.4 V. The mobility was around 0.04 $cm^2 V^{-1} s^{-1}$.

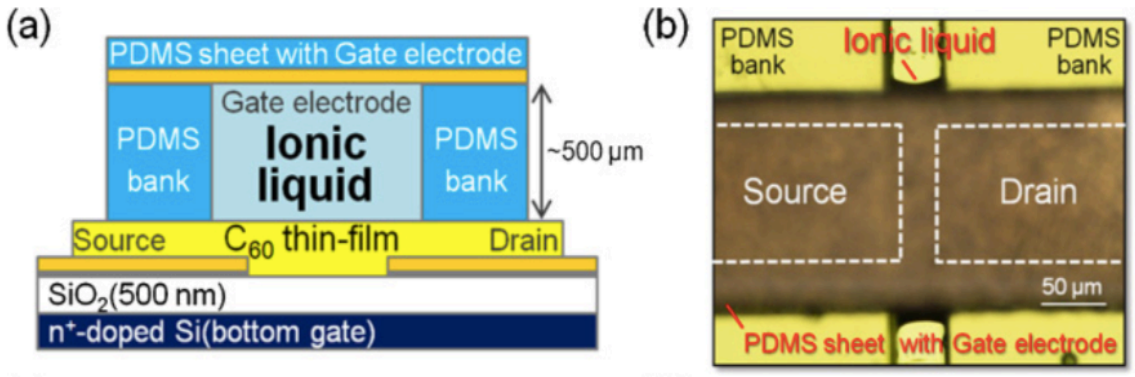

Figure 2-3 (a) Schematic illustration of ionic liquid-gated C60 thin-film transistors. (b) Optical view of a C_{60} thin film/[EMIM][TFSI] transistor. (Reprinted with permission from Ref. 33, Copyright © 2010 The Japan Society of Applied Physics)

2.3 Electrochemistry of fullerene and its derivatives

Electrochemical behavior of organic electronic semiconductors in transistor configuration is of interest because it relates charge transfer and charge carrier transport processes. C_{60} can undergo

up to six redox processes (Figure 2-4).[34,35] If the anions of the ionic gating medium barely influence the electrochemical behavior of C_{60} films, the nature of the cations is of the utmost importance.[34] Depending on the cyclic voltammetry (CV) behavior of the C_{60} films, the cations in the electrolyte can be categorized into two groups: large and small. The large cation group includes tetrabutylammonium (TBA^+), tetrahexylammonium (THA^+) and tetraoctylammonium (TOA^+), etc. In the case of small cations, the group includes small alkaline metal and alkali earth metal cations and tetraethylammonium (TEA^+). For large cations, a significant splitting is observed between the reduction and oxidation processes of C_{60} films. However, after a few scans, relatively stable CV behaviors are observable (Figure 2-5). [34,35]

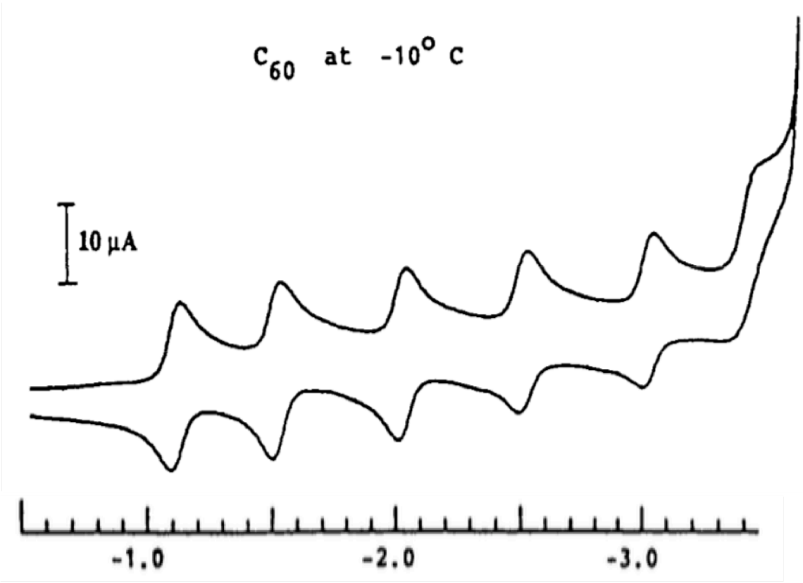

Figure 2-4 Reduction of C_{60} in CH_3CN/toluene at -10 °C using cyclic voltammetry, at 100 mV/s scan rate.[35] (Reprinted with permission from Ref. 35, Copyright © 1995 Published by Elsevier B.V.)

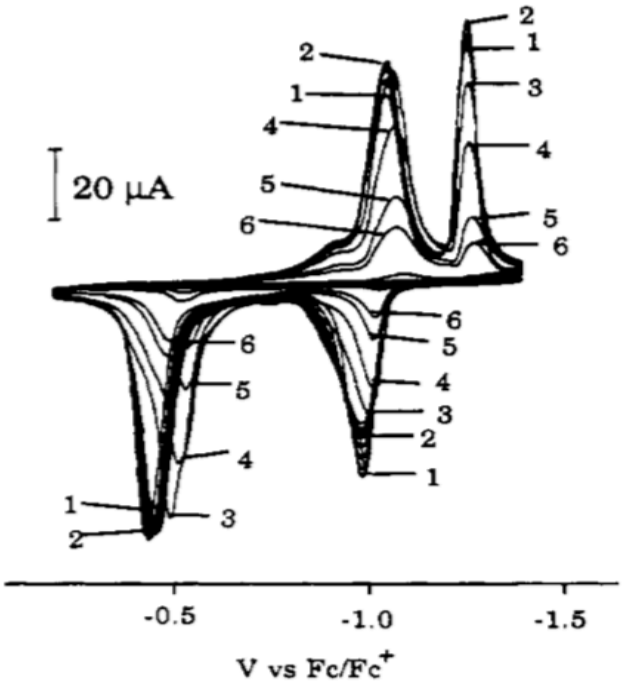

Figure 2-5 Effect of continuous cycling on C60 films on a 1 mm-diameter platinum wire electrode. Supporting electrolyte, 0.1 M TBAAsF6, scan rate 200 mV/s. Cycling over the first reduction process: 1, first cycle; 2, after 10 cycles; 3, after 5 min; 4, after 10 min; 5, after 20 min; 6, after 25 min. [35] (Reprinted with permission from Ref. 35, Copyright © 1995 Published by Elsevier B.V.)

Electrochemical behavior stability is not as good in the small cation group as that obtained in the large cation group. Convolution of reduction peaks into a large cathodic wave was observed (Figure 2-6). [35]

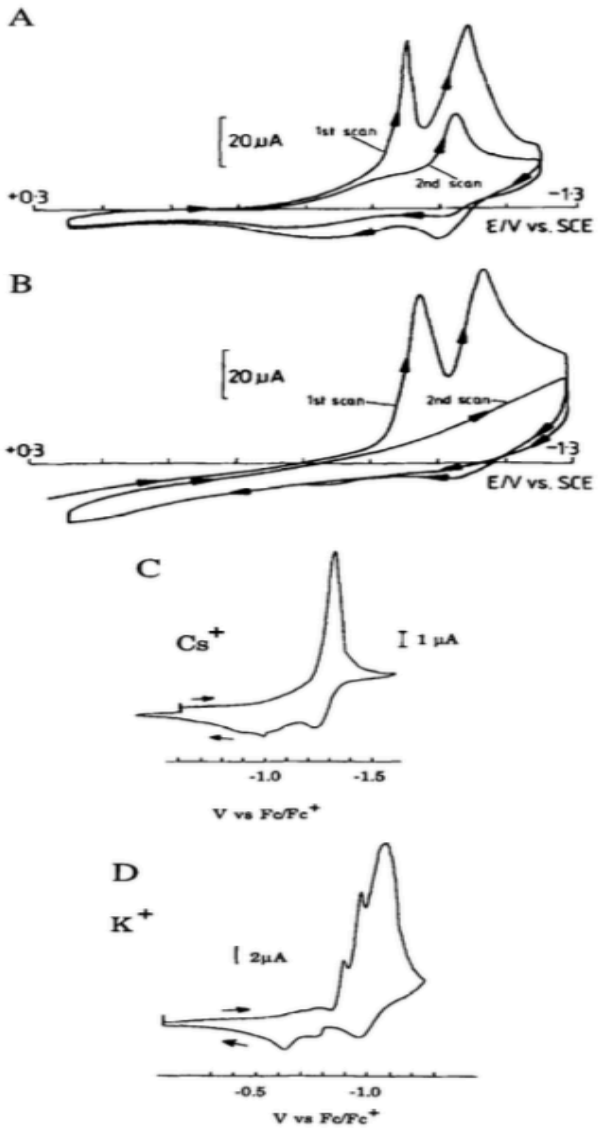

Figure 2-6 CVs of C_{60} films run in 0.1 M electrolytes: (A) $Ba(ClO_4)_2$, (B) $NaClO_4$, (C) $CsAsF_6$, (D) KPF_6.[8] (A) and (B): 100 mVs^{-1}; (C) and (D) at 200 mVs^{-1}. (Reprinted with permission from Ref. 35, Copyright © 1995 Published by Elsevier B.V.)

Because of the interesting multi-electronic processes of C_{60} films, studies on the solution processable fullerene derivative Phenyl-C_{61}-Butyric Acid Methyl Ester (PCBM) were carried out in IGT configuration. PCBM is one of the best performing electron acceptor materials used in devices such as organic photovoltaic cells (OPVs), organic light-emitting diodes (OLEDs) and

organic field-effect transistors (OFETs).[36,37] PCBM overweighs C_{60} in terms of solubility of organic solvents, relevant for the fabrication of PCBM films by solution-processing.[38]

2.4 Finite potential windows of high conductivity

A finite window of high conductivity is a general feature of organic conjugated polymers, consistent with theoretical expectations.[39-43] Wrighton et al. reported on the observation of the finite window of high conductivity with conducting polymer-based transistors (Figure 2-7).[39] CV measurements[44-47] were done using a Pt microelectrode array in 0.1 M (n-Bu)$_4$N]BF_6/SO2 at -40° C. Additionally, the I_D-V_G characteristics of the same microelectrode array in transistor configuration shows that I_D decreases when V_G goes beyond ~0.8 V vs Ag reference electrode, which also applies to the conductivity. This indicates that a finite potential-dependent window of conductivity is a property of the polymer.[39] Conductivity of the polymer could be deduced from the resistivity. This was obtained via the resistance measurement and calculation ($resistivity = resistance \times \frac{cross\ section\ area}{length}$). The resistance of the polymer was measured through I_D vs V_D at a given V_G ($resistance = \frac{drain-source\ voltage}{drain-source\ current}$).[40] Frisbie et al. reported on windows of finite conductivity with an ion-gated polymer transistor configuration with the polymer (poly(3-hexylthiophene) (P3HT) (Figure 2-8).[43] The mobility rose with the increase of charge carrier density to a peak value; eventually, a steady increase in charge carrier density resulted in conductivity peak.[43]

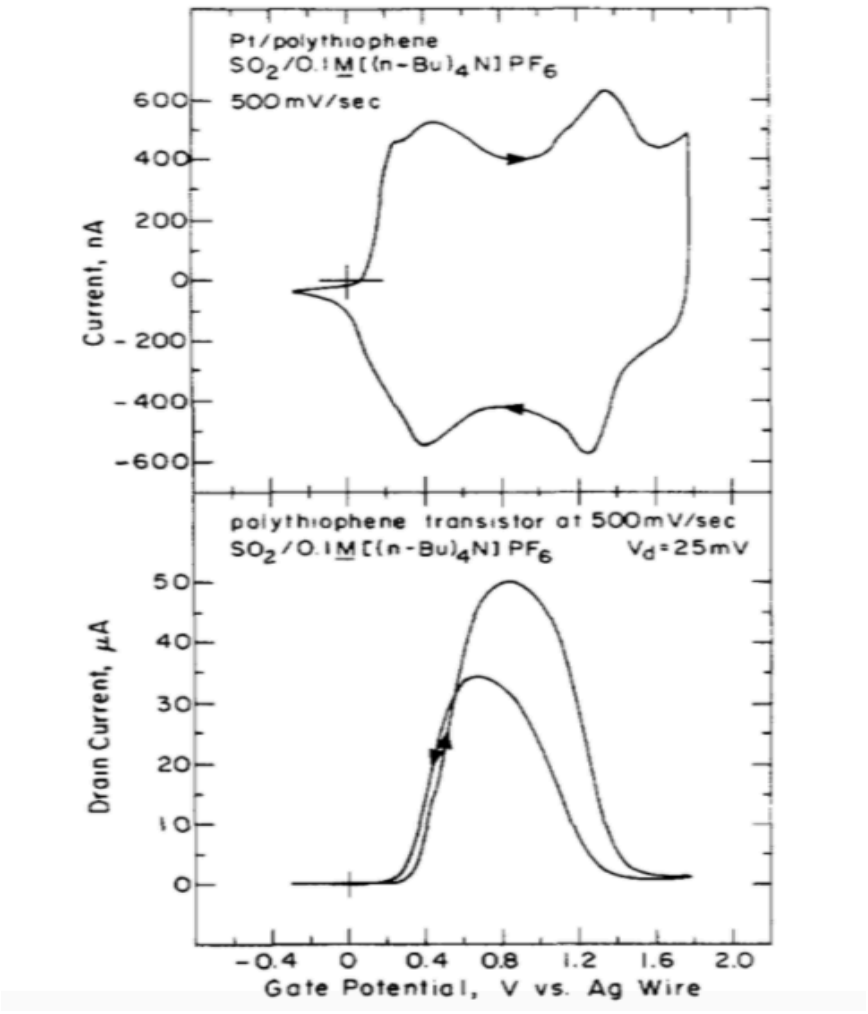

Figure 2-7 (Top) Cyclic voltammetry of thiophene connecting three adjacent Pt microelectrodes in SO_2/0.1 M $[(n\text{-}Bu)_4N]BF_6$ at -40 °C. (Bottom) I_D-V_G characteristic in the same medium for an adjacent pair of microelectrodes. Maximum conductivity on the positive sweep is ~10^{-1} Ω^{-1} cm^{-1}, and the window in which conductivity is at least 20% of maximum is 0.77V wide.[39] (Reprinted with permission from Ref. 39, Copyright © 1990 American Chemical Society)

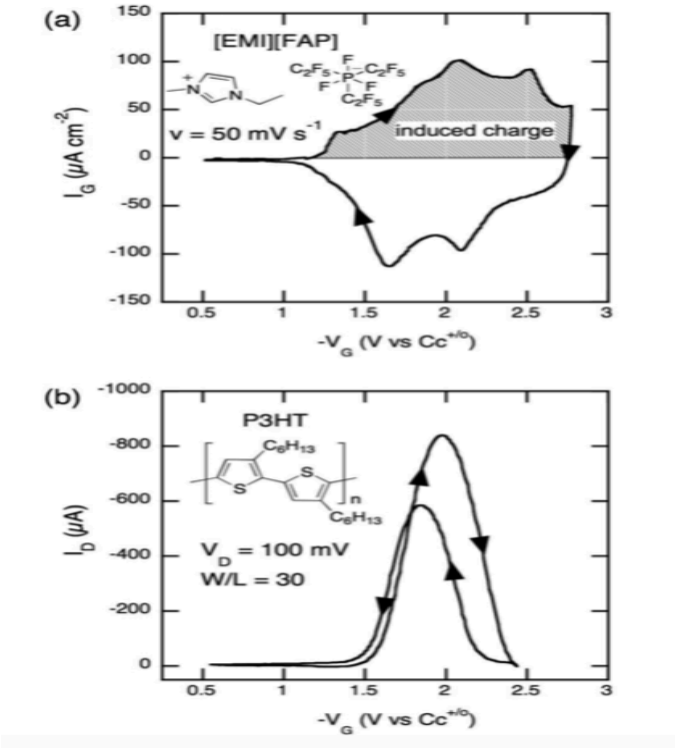

Figure 2-8 (a) Cyclic voltammogram in transistor configuration (I_G - V_G) of an [EMI][FAP] gated ~50 nm thick P3HT film; V_G is swept at 50 mV s^{-1}. (b) Drain current as a function of gate voltage for an [EMI][FAP] gated ~30 nm-thick P3HT film with a W/L aspect ratio of 30 and a 100 mV drain to source bias.[43] (Reprinted with permission from Ref. 43, Copyright © 2011 American Chemical Society)

2.5 Ambient-stable poly[N-9'-heptadecanyl-2,7-carbazole-alt-5,5-(4',7'-di-2-thienyl-2 ',1',3'-benzothiadiazole)] (PCDTBT)

Leclerc et al. reported on the synthesis process of a p-type semiconductor PCDTBT while revealing its outstanding thermal stability.[48] In ambient conditions, the oxidation of water dominates the stability of p-type polymers.[49] PCDTBT has a large ionization potential which also means a relatively deep HOMO energy level (-5.5 eV below the vacuum) making PCDTBT stable against oxidation and achieving a remarkable air and thermal stability.[50] Heeger et al.

reported on air-stable PCDTBT FETs still featuring high performance after being stored in air for 30 days (Figure 2-9).[50]

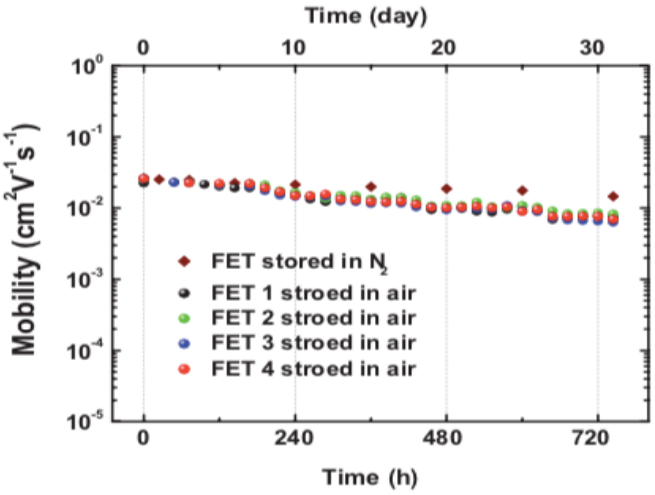

Figure 2-9 Hole mobilities obtained from PCDTBT FETs as a function of storage time in air. The measurements were made without any encapsulation/passivation layer. Results obtained from the FET device stored in air are shown for comparison.[50] (Reprinted with permission from Ref. 50, Copyright © 2010 WILEY-VCH Verlag GmbH & Co. KGaA, Weinheim)

Research on air-stability of transistors based on PCDTBT on flexible substrates such as biaxially oriented ethyleneterephthalate (BOPET) were reported by Gupta et al.[51] They adopted a bottom-gate, top source-drain contact structure to fabricate the device, using poly(methyl methacrylate) (PMMA) as the gate dielectric. The output and transfer characteristics were characterized at room temperature under ambient conditions (Figure 2-10). From the output characteristic, very little or no hysteresis was observed due to the low density of deep traps caused by the chemisorbed oxygen in the organic semiconductor. A mobility as high as 10^{-4} cm^2 V^{-1} s^{-1} was achieved under ambient conditions.

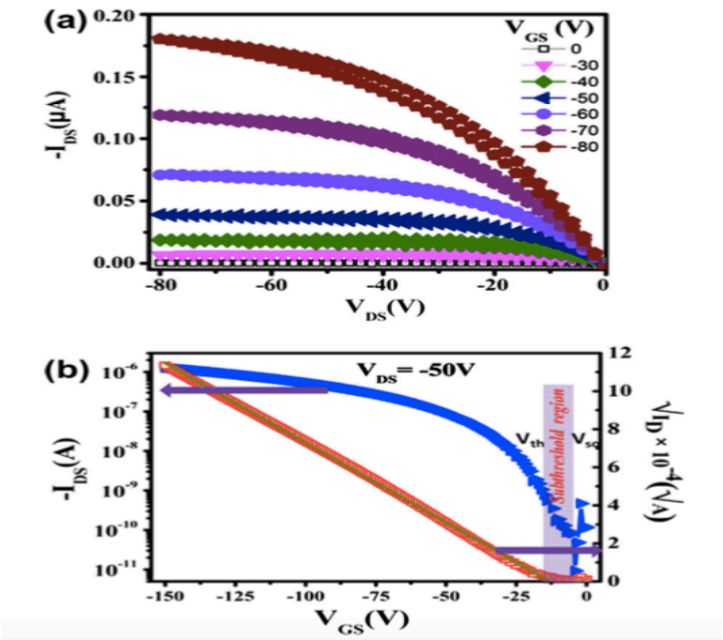

Figure 2-10 Device characteristics of a typical PCDTBT OFET with channel length of 12 μm and channel width of 1 mm. (a) Output characteristics i.e., variation of drain-source current (I_{DS}) with the drain-source voltage (V_{DS}) from 0 to -80V at different gate–source voltages (V_{GS}); (b) left scale: transfer characteristics in saturation region measured by varying the V_{GS} from 0 to -150V while keeping V_{DS} constant at -50V. Right scale: $\sqrt{|I_{DS}|}$ vs. V_{GS} plot. The shaded area shows subthreshold region that lies between threshold voltage (V_{th}) and switch-on voltage (V_{so}). (Reprinted with permission from Ref. 51, Copyright © 2013 Published by Elsevier B.V.)

Long-term stability measurements under ambient conditions were also carried out. The plot of relative mobility (μ_t/μ_o where μ_t is the mobility at time t and μ_o is the mobility of the fresh sample) and I_{DS} in the off state as a function of exposure time (up to 118 days) under ambient conditions showed a plateau (Figure 2-11).[51] Up to a period of 70 days, the relative mobility showed no effect of the air conditions and I_{DS} in the off state behaved stably, indicating PCDTBT's capability to resist moisture or oxygen. Moreover, devices with different channel lengths were also fabricated. No big changes were observed in the trend of relative mobility (μ_t/μ_o) and I_{DS} in the off state.

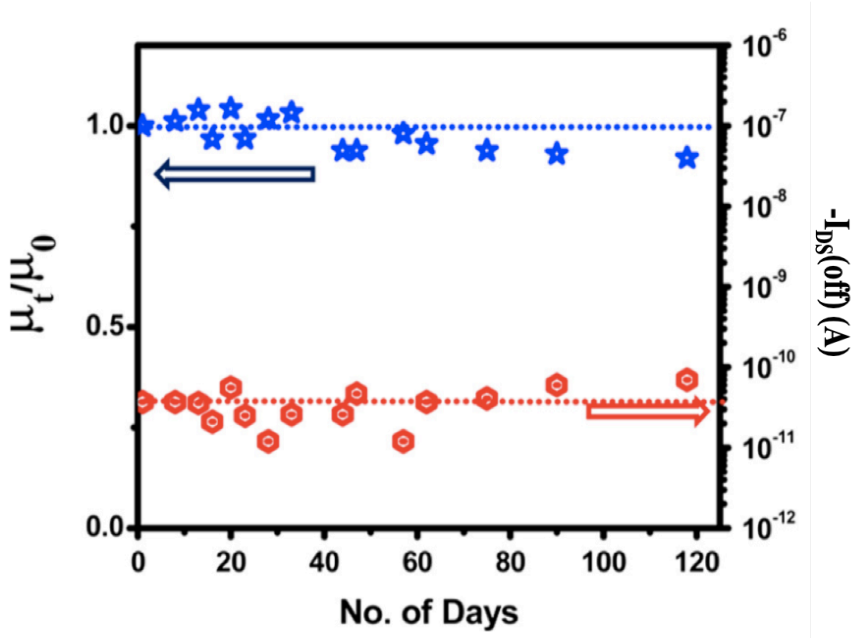

Figure 2-11 Plots of the relative mobility (μ_t/μ_o, where μ_t and μ_o are the mobility at time t and that of the fresh sample, respectively) and I_{DS} (off) as a function of air exposure time in days (temperature: 20–35 °C and relative humidity: 70–85%). (Reprinted with permission from Ref. 51, Copyright © 2013 Published by Elsevier B.V.)

2.6 Phototransistors

FETs adopting organic electronic materials as channel material are appealing for the opportunity they offer to fabricate lightweight, flexible and solution-processed devices. Combining FET with optical properties creates a new class of multifunctional transistors: organic phototransistors (OPTs).[52-58] The optoelectronic properties of organic phototransistors can be tuned through the chemical synthesis of the molecular structure of the organic semiconductor. This is an intrinsic advantage with respect to inorganic counterparts. Organic phototransistors can be applied in a wide range of fields, such as imaging, biomedical sensing and optical communications.[52-54] To date, a variety of organic materials for OPTs have been studied, including n-type, p-type, ambipolar and organic blends. Zhao et al. reported a phototransistor based on organic bulk heterojunction (Figure 2-12).[52] A bulk heterojunction (BHJ) (interpenetrating networks of the donor and acceptor components) is mostly used in organic solar cells. Bringing this structure

from the solar cell to the transistor configuration makes it possible to achieve a high sensitivity at a particular spectral range.[53]

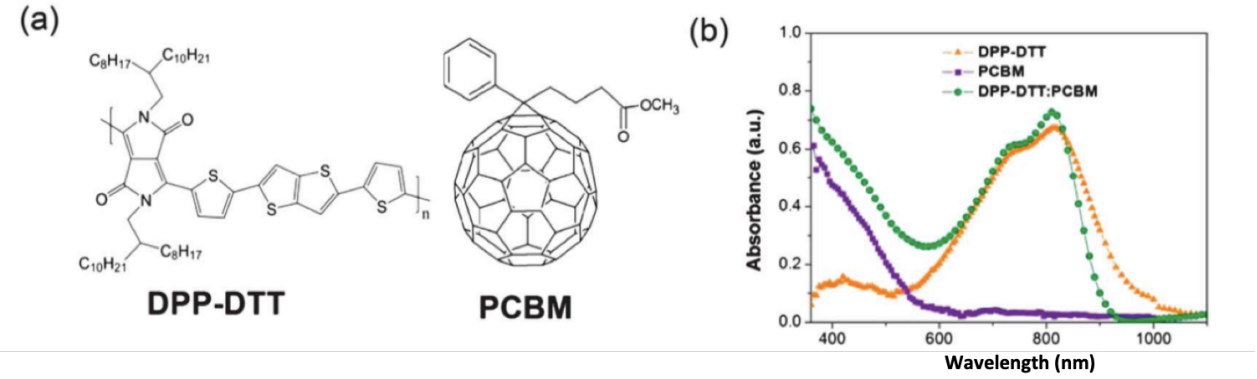

Figure 2-12 (a) Molecular structures of DPP-DTT and PCBM; (b) Absorption spectra of pure DPP-DTT, PCBM and DPP-DTT:PCBM blend (mass ratio 1 : 1).[52] (Reprinted with permission from Ref. 51, Copyright © 2013 The Royal Society of Chemistry)

In 2013, Jung et al. reported a new mussel-inspired polydopamine (PDA) (from a biological adhesive protein of marine mussels) phototransistor exhibiting typical p-type transistor behavior (Figure 2-13).[53] The PDA thin films exhibited a strong and broad absorption in UV and visible regions. V_{th} was estimated to be -6V, the ON/OFF ratio was 1.2×10^5, and the mobility was 0.96 $cm^2\ V^{-1}\ s^{-1}$ under dark conditions. However, under light conditions, a large increase in transistor current was observed. With the increase in light intensity, the photocurrent of the device increased, exhibiting PDA's excellent optical property. The maximum value of photoresponsivity (R) deduced was 9 A W^{-1} and the maximum photosensitivity (P) deduced was 6.9×10^4.

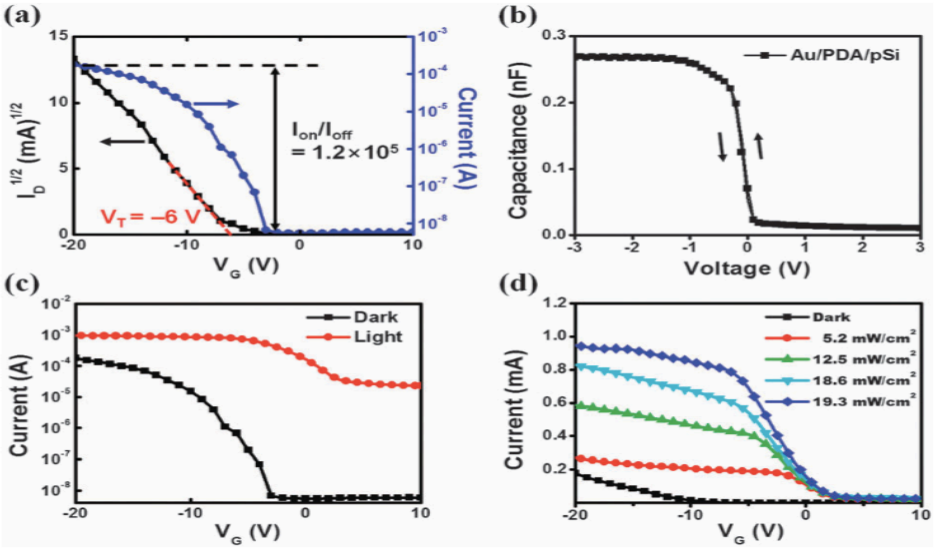

Figure 2-13 (a) Transfer characteristics of PDA phototransistor at V_D = -10V in the dark. (b) Current-Voltage hysteresis loop measured in air for the Au/PDA (30 nm)/p-Si device. (c and d) Plots of current vs. voltage (V_G) at V_D = -10V under dark and light irradiation conditions, and different input light intensities, respectively.[53] (Reprinted with permission from Ref. 52, Copyright © 2014 The Royal Society of Chemistry)

Wu et al. reported a high-performance, near-infrared phototransistor based on solution-processed air-stable n-type organic small molecule material 4,4-difluoro-4-bora-3a, 4a-diaza-s-indacene (BODIPY-BF2) in a bottom-gate, top-contact geometry.[54] The BODIPY-BF2 thin films having a strong absorbance at around 850 nm were deposited under different annealing conditions. They were characterized using UV-VIS-NIR absorption spectra measurements. The UV-VIS-NIR absorption results showed an enhancement in the NIR range (600-1000 nm) in annealed thin films compared with that of as-grown thin films. Moreover, the annealed thin films presented a different orientation of stripped crystalline domains with respect to the channel. Charge carrier mobility increased with the increase in the orientation angle (the angle between the long axis of the stripped domains and the edges of the top contacts that define the physical width of the accumulation channel). The organic phototransistors could reach an electron mobility of 1.13×10^{-1} cm^2 V^{-1} s^{-1} and an ON/OFF ratio as high as 10^6 with thin films annealed at 80 °C. The

maximum values of photoresponsivity and photosensitivity obtained were 1.14×10^4 A W^{-1} and 1.04×10^4, under NIR light irradiation.

2.7 Poly(3-hexylthiophene) (P3HT) with different molecular weights

One important parameter affecting the relationship between the solid-state structure and the functional properties of the polymers for organic electronic polymers is their molecular weight. Shaheen et al. published a paper on the effect of different molecular weights of P3HT (14 kDa, 20 kDa, 25 kDa, 48 kDa, 55 kDa, 60 kDa and 331 kDa) on carrier mobility.[59] At low molecular weight, P3HT would form a one-phase, paraffinic (a characteristic of paraffin wax or a paraffin hydrocarbon) structure containing unconnected, chain-extended crystallites. With an increase of the molecular weight, a semicrystalline structure was achieved (Figure 2-14).[59]

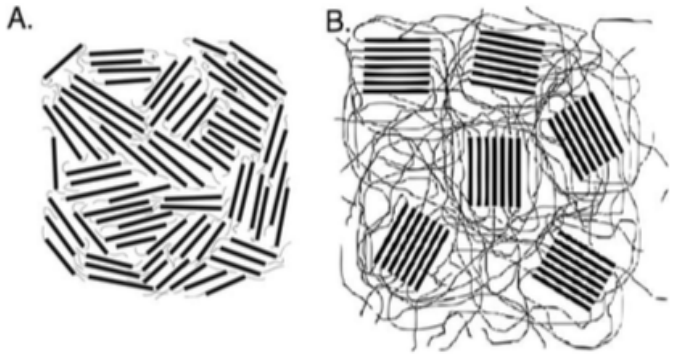

Figure 2-14 Schematic illustration of the microstructure of (A) low molecular weight P3HT forming a paraffinic microstructure and (B) high molecular weight P3HT that leads to a semicrystalline structure. Illustrations are approximate and not intended to show actual dimensions of crystallites.[59] (Reprinted with permission from Ref. 59, Copyright © 2017 Wiley Periodicals, Inc.)

Various molecular weights could also be accompanied by other changes in aspects such as morphology and solubility. Studies from different research groups showed wide differences in mobility values. Fréchet et al. reported the studies conducted on P3HT samples synthesized via a

modified McCullough route and commercial (Aldrich) P3HT semiconductors obtained via a Rieke (Figure 2-15).[60] They fabricated bottom-gate, bottom-contact thin film FETs using different molecular weight P3HT. The ON/OFF ratios obtained fell in a range between 10^3 and 10^5 bearing no relation to the molecular weight. They divided their samples into three groups, Group A: bromine-terminated polymers made by the modified McCullough route, Group B: the commercial Rieke route polymers, and Group C: the methylthiophene-terminated polymers. The molecular weight of each group varied from 3.2 kDa to 36.5 kDa. They observed that, with the increase in molecular weight, mobility increased due to chain packing. The researchers inferred this after ruling out other possible factors, such as chemical defects.

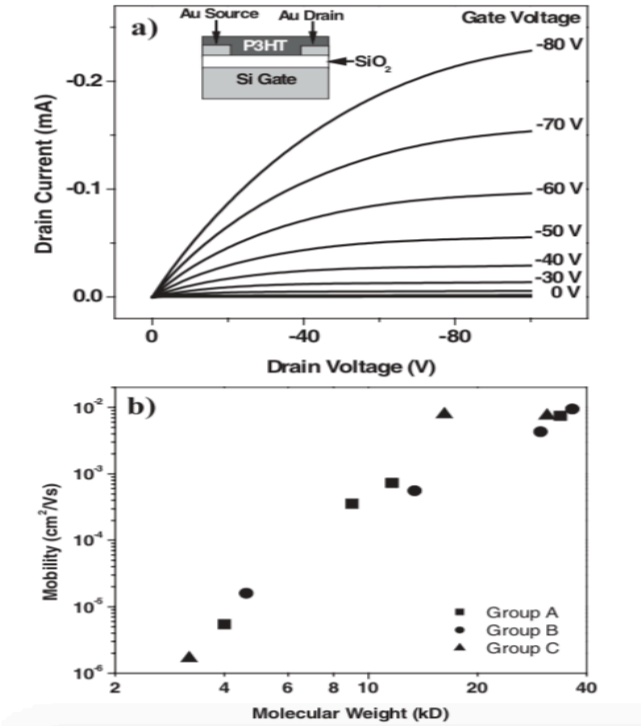

Figure 2-15 a) Current-voltage curves of a 10 µm long by 40 mm wide transistor with a molecular weight of 33.8 kD. The inset shows a diagram of the device structure. b) Plot of field-effect mobility versus the average molecular weight. (Reprinted with permission from Ref. 60, Copyright © 2017 Wiley Periodicals, Inc.)

Neher et al. reported investigations on nanoscopic charge transport in P3HT films through pulse-radiolysis time-resolved microwave conductivity (PR-TRMC) measurements.[61] In addition, macroscopic transport properties via bottom-gate, top-contact thin film FET configuration were studied. The P3HT molecular weights used in their studies ranged from 2.5 kDa to 35 kDa. Values achieved by PR-TRMC measurements showed a slight increase in the mobility trend as molecular weight increased. Compared to this, the macroscopic OFET mobility values exhibited a pronounced increase.

The molecular weight is also a key parameter governing other characteristics of thin films. These include modulus (the ratio of stress to the corresponding strain), viscoelasticity (i.e. viscous and elastic characteristics under deformation), glass transition point (the point or narrow region of the temperature scale where the thermal expansion coefficient undergoes a discontinuity and below which configuration rearrangements of the polymer backbones are extremely slow).[62,63]

With the increase in molecular weight, the viscosity of the semiconducting solution increases, thereby having an impact on the thickness and morphology of thin films. Park et al. reported on a systematic study on the correlation of P3HT molecular weight with the characteristics of the thin films fabricated via time-controlled spin-coating methods.[64] These included morphology, optical and electrical characteristics in a bottom-gate, top-contact thin film transistor geometry. In their study, three different molecular weights were used: 36 kDa, 69 kDa and 90 kDa. The AFM results showed that the root mean square surface roughness of the P3HT thin films increased as the spinning time decreased, independently on the molecular weight (Figure 2-16). However, the thickness of 3-second cast thin films increased with the increase of the molecular weight. For the 60-second cast thin films, the intermediate molecular weight reached a higher thickness than its two counterparts (Figure 2-17). As for charge carrier mobility, the value obtained in P3HT films spin-cast for 3 seconds overweighed the value of the mobility obtained with spin-cast for 60 seconds. This was observed for the three different molecular weights.

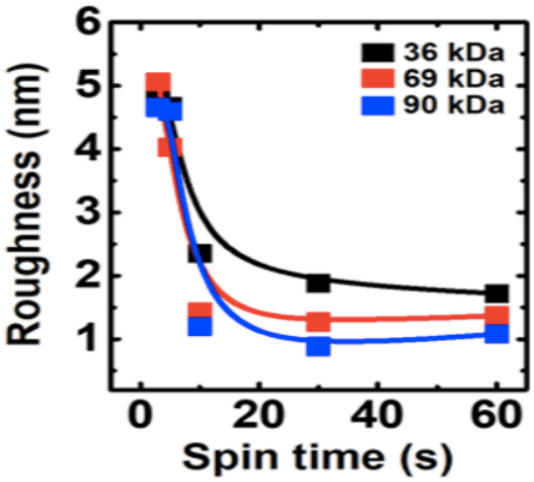

Figure 2-16 The RMS roughness of the film surface as a function of the spinning time. (Reprinted with permission from Ref. 64, Copyright © 2019 American Chemical Society)

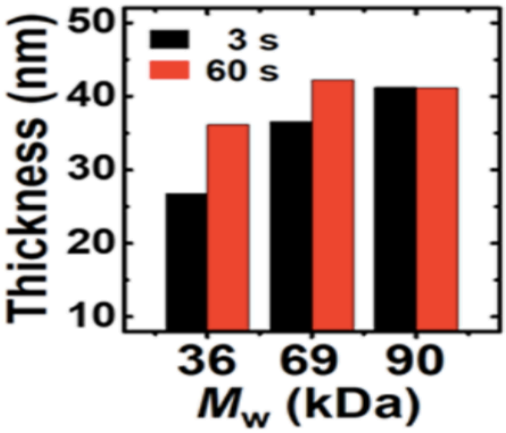

Figure 2-17 Final film thickness values of the P3HT thin films that had been spin-cast over the indicated spinning times from P3HTs with different molecular weights. (Reprinted with permission from Ref. 64, Copyright © 2019 American Chemical Society)

CHAPTER 3 OBJECTIVES

Tremendous efforts are ongoing in materials science and engineering to explore new solutions to energy-, health- and environment-related problems challenging our modern society. For instance, outstanding research on materials and devices combining ionic (cations and anions) and electronic (electrons and holes) transport has been conducted to develop technologies and devices for electrochemical energy storage, bioelectronics, printable & flexible electronics.[28,65-73]

Ion-gated transistors (IGTs), making use of ionic gating media, are a typical example of devices exploiting combined ionic and electronic transport. Besides their intrinsic technological interest, IGTs are relevant platforms to study a number of fundamental issues. For instance, one issue is the relationship between the redox state of the transistor channel material interfaced with the ionic medium and the electronic conductivity in the channel.

Fullerene-based materials are known to undergo several (up to 6) reversible electron transfer processes and as such they are ideal materials to study the above-mentioned relationship. PCBM is a member of the fullerene derivative family. It is commonly used in organic bulk heterojunction solar cells as n-type semiconductor. Moreover it has been studied as channel material in solution-processed organic field-effect transistors.[74]

Regarding the ionic gating media, room temperature ionic liquids stand out for their wide electrochemical stability window (up to ca. 5V), good ionic conductivity (0.1-18 mS cm^{-1}) at room temperature and negligible volatility up to 300 °C.[24,75] Room temperature ionic liquids made of imidazolium cations and [TFSI] anions possess high ionic conductivity and low viscosity, due to a limited degree of interionic interaction.[24,75]

The correlation between the electronic conductance of ion-gated field-effect transistors with ion-pairing effects in the gating medium has been studied by D. D. Tullio et al.[76] However, this still leaves massive space to investigate the doping process in IGTs as a function of the redox

state of the transistor channel material and the nature of the ion-gating medium, e.g. in terms of ion size and ion pairing.

The operational stability of IGTs in ambient conditions is key to realizing unencapsulated air-stable organic transistors. PCDTBT is an air-stable and low band gap (ca 1.8 eV) carbazole-based copolymer, successfully employed and exploited in bulk heterojunction solar cells and field-effect transistors. PCDTBT is an ideal candidate to study air-stable IGTs. Moreover, its optical properties offer the opportunity to extend our research to ion-gated phototransistors, focusing on how photo-gating affects modulation of transistor current.

The mechanical properties (e.g. flexibility) of organic semiconductors open a new range of applications, such as flexible transistors, displays and biosensors.[28,65-73] Organic semiconductor films with a thickness in the nanometric range do not necessarily feature the same mechanical properties as bulk (single crystal) samples. In addition, the molecular weight of organic electronic polymers somehow influences the mechanical properties of organic semiconductors such as P3HT (a popular conjugated polythiophene derivative engineered with alkyl side chains): in general, the ductility (ability of a material to be drawn or plastically deformed without fracture) and toughness (ability of a material to resist both fracture and deformation) increase with an increase in molecular weight.[77] The charge carrier (hole) mobility of P3HT films is largely affected by the molecular weight, too. What will happen with the incorporation of ions in the films to the mechanical properties such as flexibility and the figures of merit of P3HT-based devices is of primary interest.

Taking all factors into consideration, the objectives of this PhD thesis are to:

(1) Study ion-gated film transistors based on molecular materials (PCBM) capable of undergoing several redox processes, to assess the effect of the electron transfer (redox) state of the molecules on their charge carrier transport behavior. Within objective 1, we will focus on the following aspects:

a) Measure, for every redox process, the corresponding transistor characteristics. The first and the following redox processes, paralleled by ion redistribution will be characterized. Pay particular attention to the behavior of the voltammetric current with the electrochemical potential sweep rate to evaluate charge transfer vs. mass transfer rates.

b) Investigate the effect of the physicochemical properties of ionic liquids on the PCBM redox and transport characteristics.

Make use of room temperature ionic liquids belonging to the same family – but differing as to cations – to elucidate the role of cations in doping n-type PCBM films. The molecular structure of the ions, their size and polarizability as well as the presence of ion pairing effects are expected to play an important role in the doping process.

Findings of this research are included in Article 1.

(2) Study the operational stability during doping-dedoping in ambient conditions for ion-gated transistors and the synergy between doping dependence on the electrical bias and photo-gating in organic transistors. In fulfilling objective 2, we will focus on:

a) Exploring the ambient air operational stability of [EMIM][TFSI]-gated PCDTBT transistors.

PCDTBT has low highest occupied molecular orbital (HOMO, located at ca -5.5 eV vs. vacuum), which makes it chemically stable in ambient conditions. In ion-gated transistors, PCDTBT films are interfaced to the ionic liquids involving the doping process of the ions, making it difficult to predict the device stability.

b) Exploiting the multifunctionality of PCDTBT in an ion-gated phototransistor configuration.

PCDTBT possesses quite low optical band-gap (ca 1.8 eV) providing increased absorption at longer wavelengths (two distinct absorption bands: ca 350 nm - 450 nm and 450 nm - 650 nm), which in turn improves the efficiency of the sunlight harvest.[50] In

ion-gated phototransistor configuration, PCDTBT works as the photosensitive channel material combining electrochemical and photo responses. We have investigated, with simulated solar light, how photo-gating participates in modulating charge carrier density and current, see Article 2.

(3) Exploring the effect of polymer molecular weight on the effectiveness of ion-gating on P3HT films, on rigid and flexible substrates.

a) Investigating how the ion-gating approach works with P3HT films of different molecular weights.

The molecular weight of P3HT has an impact on the structure and the charge carrier transport properties of the thin films. When the molecular weight is low, the microstructure of P3HT films would be one-phase, paraffinic (high molecular weight hydrocarbon) comprised of chain-extended and unconnected crystallites.[50] However, at high molecular weight, the chain entanglement density increases which in turn causes the increase of amorphous regions.[50,78] Furthermore, the morphological properties of the channel materials would have an effect on the electrochemical phenomena at the ionic liquid-channel material interface, as the electrochemical transformations are surface- and morphology-dependent, which in turn would facilitate or hinder the transport of ionic and electronic charge carriers during the electrochemical process.[79-80] Bringing ions into the research on the relationship with molecular weight will improve our understanding of how ion-gating affects the performance of a device and probes how different molecular weight films accommodate ions. This is investigated in Article 3.

b) Exploring the mechanical properties of ion-gated transistors based on P3HT with different molecular weights.

With the adoption of ionic gating media, flexibility is feasible in integration with polymer substrates such as polyimide. Bending cycle tests conducted on devices based on P3HT

films with different molecular weights shows how device performance corresponds to a particular molecular weight. Results are included in Article 3.

CHAPTER 4 EXPERIMENTAL METHODS AND TECHNIQUES

In this chapter, we describe the microfabrication process used to pattern substrates (section 4.1), methods to deposit the thin films (section 4.2) and process materials (section 4.3) as well as the characterization techniques used in the thesis (section 4.4).

4.1 Microfabrication

The microfabrication process flow used in this PhD work is shown in Figure 4-1.

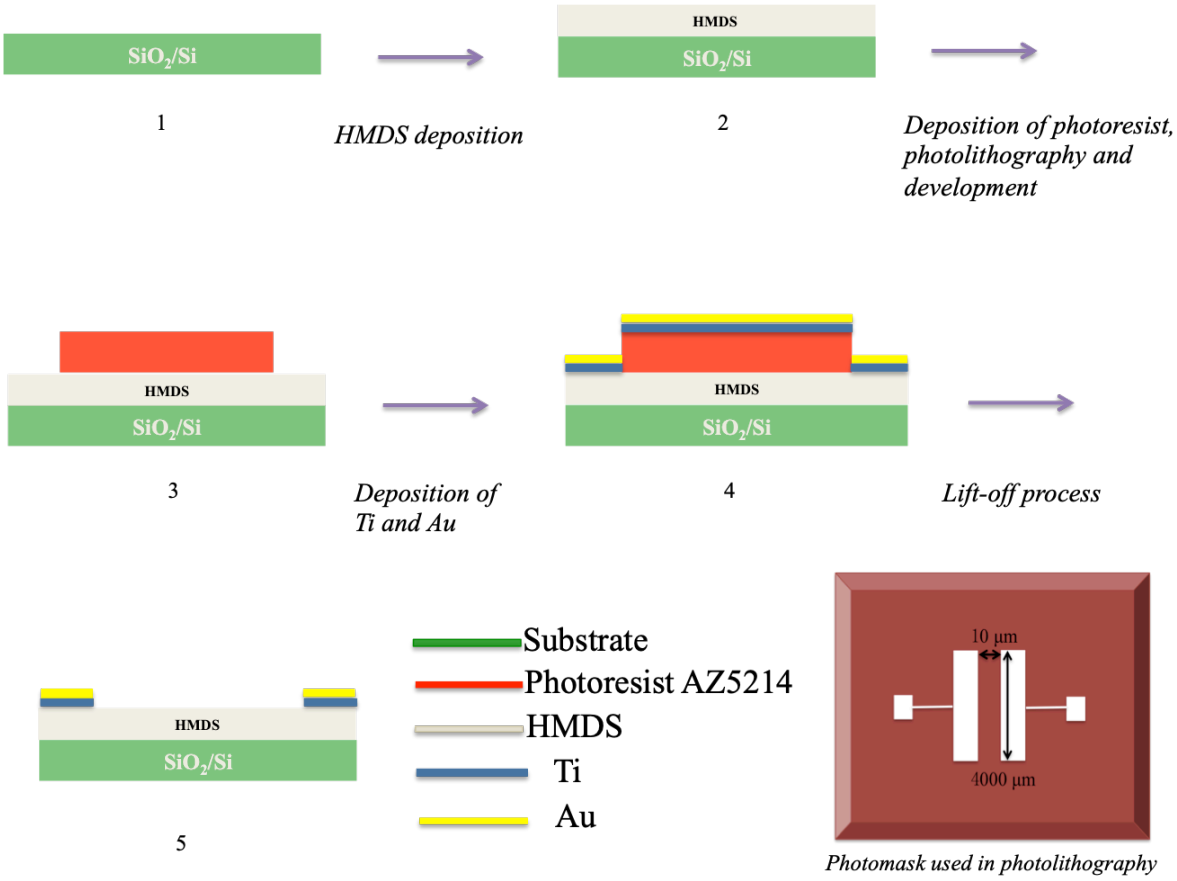

Figure 4-1 Microfabrication process flow used in this PhD thesis (thickness of HMDS and SiO_2 is not in scale).

In the photolithography process, HMDS helps to build a hydrophobic surface to improve wetting and adhesion of the subsequent layers. Ti acts as an adhesion layer for the deposition of Au.

4.2 Thin films deposition

In order to deposit highly uniform thin films (a few nanometers to several micrometers thick) at low cost, solution processing is the ideal method.[81] In this PhD work, we used two common solution processing techniques: spin-coating (Figure 4-2) and drop-casting (Figure 4-3).

For spin-coating, a certain amount of solution containing the target material (in our case the semiconductor) in a solvent is applied to the substrate surface (1), following a rotation of the substrate at a set speed which allows the majority of the solution to spin off the edge (2). Meanwhile, the airflow dries the majority of the solvent during the rotation process (3) before the film fully dries depositing the target material(s) on the surface of the substrate (4).[81]

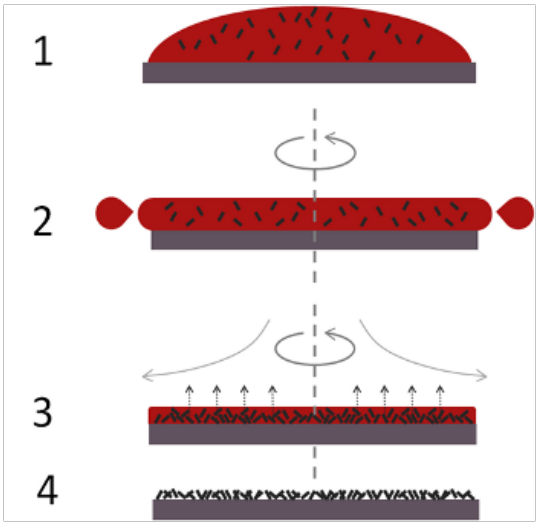

Figure 4-2 Example of spin-coating a solution using a static dispense.[81] (Reprinted with permission from Ossila Ltd, Copyright © 2015 Ossila)

On the other hand, during drop-casting, an organic semiconductor solution is dropped on the flat substrate followed with the evaporation of the solvent to obtain the target films.[82]

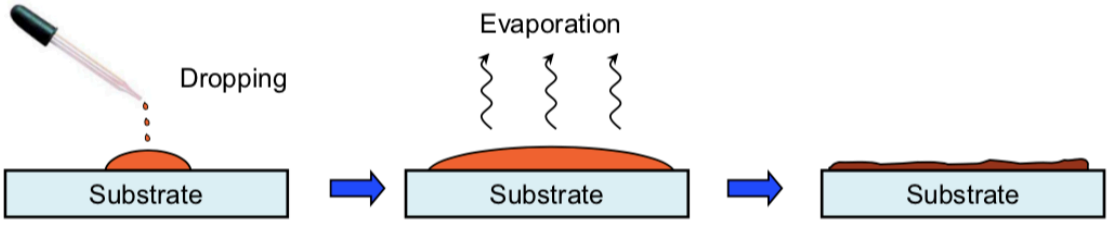

Figure 4-3 Steps during drop-casting.[83] (Reprinted with permission from Ref. 64, Copyright © 2015 IEEE)

4.3 Processing of materials

4.3.1 Ionic liquids purification

Water is considered to be the main impurity to affect RTILs when applied in organic electronics.[22] Thus purification procedures are necessary prior to the use of RTILs. In this work, the RTILs we used, [EMIM][TFSI] and [PYR_{14}][TFSI], were purchased from IoLiTec (purity > 99%). Their properties and molecular structures are shown in Table 4-1 and Figure 4-4, respectively.[84] RTILs were purified under vacuum conditions (ca 10^{-5} Torr) for 24 hours at 80 °C before use.

Table 4-1 Physicochemical properties of the ionic liquids considered in this PhD work.[84]

	[EMIM][TFSI]	**[PYR_{14}][TFSI]**
Melting Point (°C)	***-3***	***-18***
Density (g/cm^3)	***1.52 (20°C)***	***1.40 (20°C)***
Ionic Conductivity (mS/cm)	***6.63 (20°C)***	***2.12 (20°C)***
Viscosity (mPa s)	***39.4 (20°C)***	***94 (20°C)***
Anodic and Cathodic limits (V)*	***2.6; -2.1***	***2.8; -2.5***

*vs Ag/AgCl reference electrode.

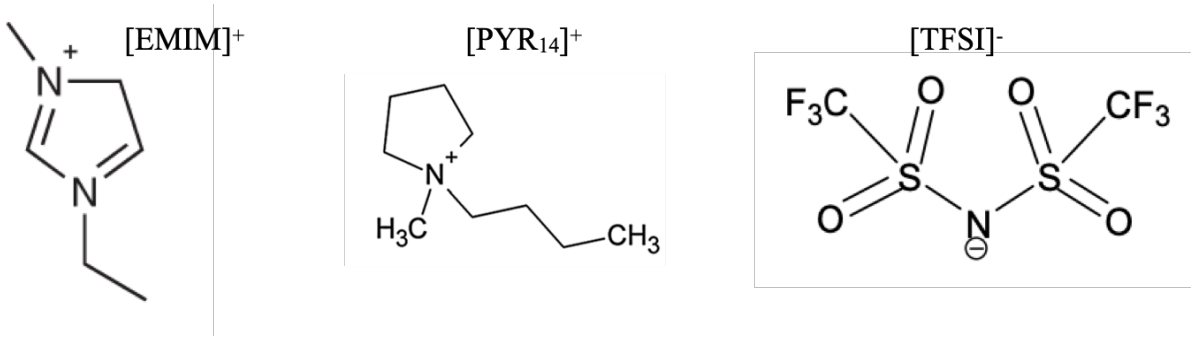

Figure 4-4 Molecular structures of ions: $[EMIM]^+$, $[PYR_{14}]^+$ and $[TFSI]^-$.

4.4 Techniques

4.4.1 Cyclic voltammetry

Cyclic voltammetry (CV) is a widely used technique to acquire information on electrochemically active materials and electrochemical reactions.[44-46] The most common configuration for electrochemical measurements consists of three electrodes. These include working, counter and reference electrodes. They are all connected to a potentiostat which controls the applied potential between the working and the reference electrodes. The current flows between the working electrode and the counter electrode. At the working electrode, the electrochemical event of interest takes place.[44,45] The current is sustained at the counter electrode. In addition, the reference electrode maintains a well-defined and stable potential.[45] A typical experimental set-up is shown in Figure 4-5.

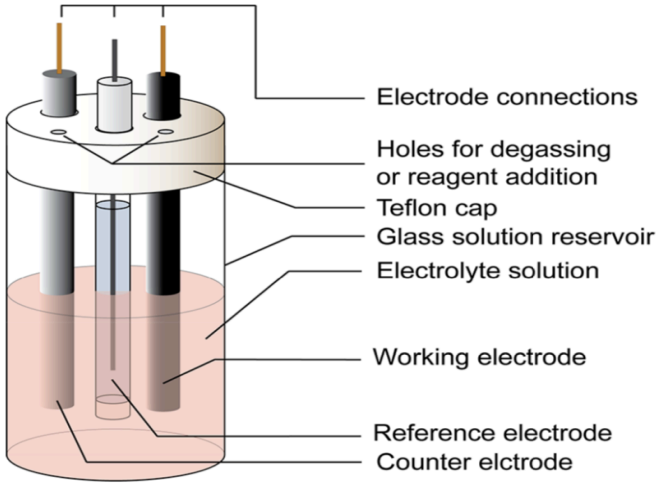

Figure 4-5 Schematic representation of an electrochemical cell for CV experiments.[45] (Reprinted with permission from Ref 45, Copyright © 2017 The American Chemical Society and Division of Chemical Education, Inc.)

A reduction process at the working electrode can be described as A + e^- ⇌ B. A typical cyclic voltammetry experiment consists of a linear scan of the potential during which current is measured (Figure 4-6).[44] The scan starts from a potential E_1; going towards E_2, a more negative potential, electron transfer events from the electrode to the species A take place, and species B is formed. The re-formation of A can take place if the potential is swept back to E_1 from E_2.

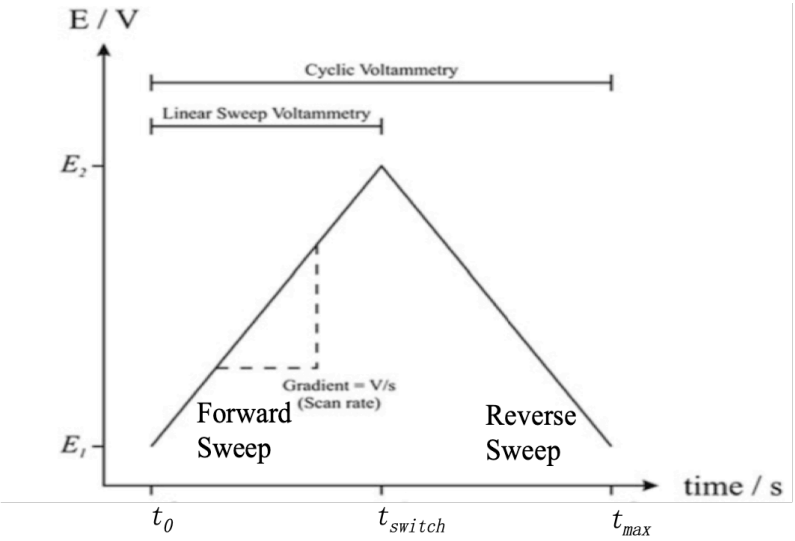

Figure 4-6 The waveform of the potential applied during a typical cyclic voltammetry experiment.[44] (Reprinted with permission from Ref 44, Copyright © 2014 Springer London Heidelberg New York Dordrecht)

In a cyclic voltammetry experiment, the scan rate (the gradient of the line) is a constant parameter from the initial potential to the vertex potential and back again. In Figure 4-6, on the forward sweep, the potential can be given via equation $\mathrm{E} = \mathrm{E}_1 - \mathrm{vt}$ at any time. The sweeping sense will reverse at $\mathrm{t} = \mathrm{t}_{\mathrm{switch}}$. When $\mathrm{t} > \mathrm{t}_{\mathrm{switch}}$, the potential can be obtained through the equation $\mathrm{E} = \mathrm{E}_2 + \mathrm{v}(\mathrm{t} - \mathrm{t}_{\mathrm{switch}})$.

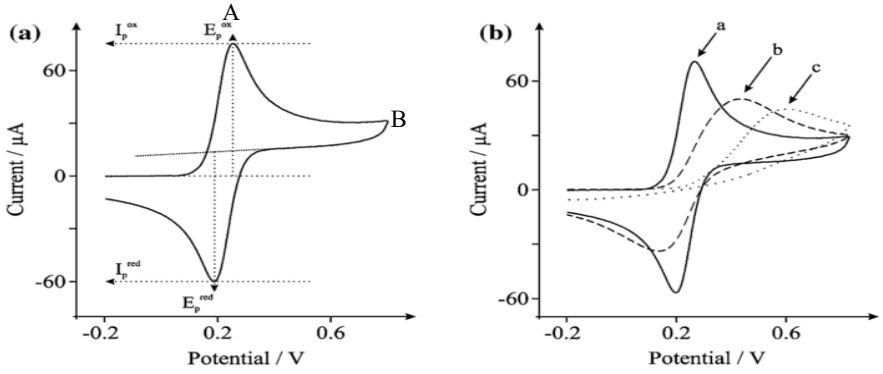

Figure 4-7 **a**) Typical cyclic voltammogram depicting the peak position E_P and peak height I_P. **b**) Cyclic voltammograms for reversible (a), quasi-reversible (b) and irreversible (c) electron transfer.[44] (Reprinted with permission from Ref 44, Copyright © 2014 Springer London Heidelberg New York Dordrecht)

A cyclic voltammogram is a plot of current versus potential. Figure 4-7 shows the typical cyclic voltammetric curve for the case of the electrochemical process as described in the equation A+e^- ⇌ B.[44,46,85] Figure 4-7 (b) presents three cases: reversible, quasi-reversible and irreversible cyclic voltammetries. In the reversible case, the rate of the mass transport is slower than the rate of electron transfer. At the same time, the position of the peak potential is not dependent on the voltammetric scan rate. In the quasi-reversible case, the rates of mass transport and electron transfer are quite comparable. In this regime, the peak potential will change with the applied voltammetric scan rate. In the irreversible case, the mass transport rate is greater than the electron transfer rate.[46]

*T*he peak current for reversible electron transfers is given via equation (1)

$$i_p = 0.4663(\frac{F^3}{RT})^{1/2}\ n^{3/2}\, AD^{1/2}\, Cv^{1/2} \quad (1),^{44,85}$$

where *A* is the electrode area, *C* is the bulk concentration of the redox species, *v* is the scan rate. The peak current will increase with an increase in the scan rate as shown in Figure 4-8.

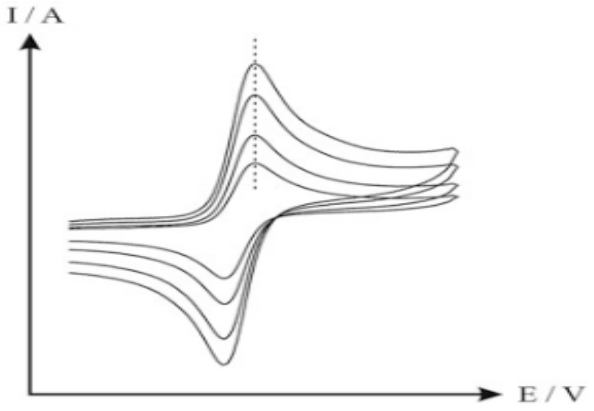

Figure 4-8 Reversible cyclic voltammetric response. Note the shift of the peak maxima with scan rate.[44] (Reprinted with permission from Ref 44, Copyright © 2014 Springer London Heidelberg New York Dordrecht)

In this PhD thesis, we performed electrochemical measurements on organic semiconductor films (PCBM, PCDTBT and P3HT) interfaced to ionic liquids with the cyclic voltammetry technique.

Information on counter and reference electrodes as well as equipment is accessible in the articles part of this thesis.

4.4.2 Electric characterization

For the electric characterization of transistors, there are two main sets of current-voltage curves to be acquired: transfer and output (Figure 4-9). Transfer curves are plots of source-drain current (I_{ds}) versus gate-source voltage (V_{gs}).[47] Moreover, output characteristics are plots of I_{ds} versus V_{ds} with a constant gate voltage.[47] For this PhD work, they were obtained employing an Agilent B1500A semiconductor parameter analyzer connected to a micromanipulated electrical probe station.

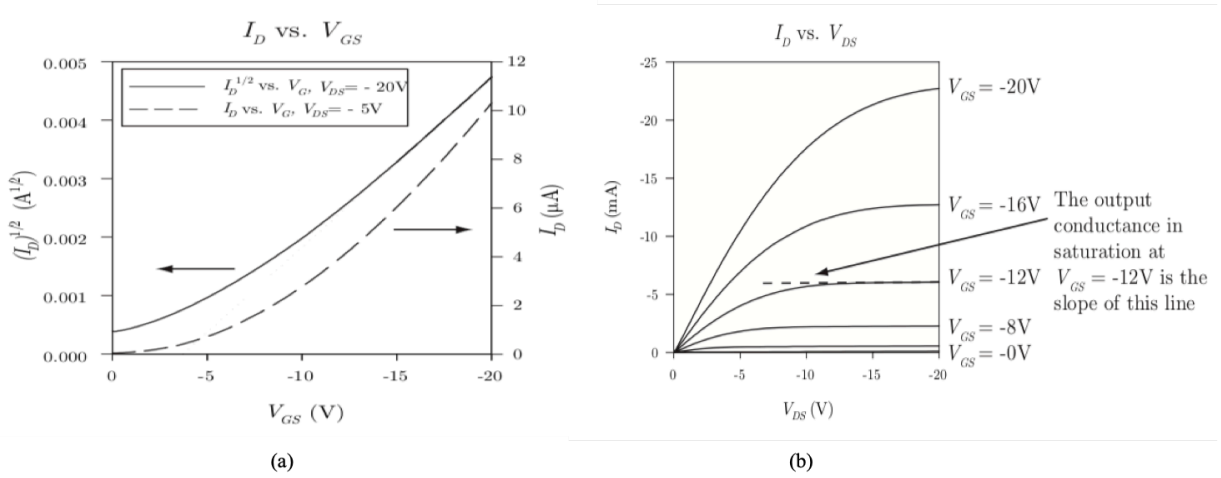

Figure 4-9 Examples of transfer and output characteristics of field-effect transistors. (a) Transfer measurements showing both sqrt (I_{ds}) and I_{ds} vs V_{gs}. (b) The output characteristic for an organic OFET. The *output conductance* can be determined from this curve at each V_{gs} value (i.e. conductance deduced from the output characteristics as a function of V_{gs}, i.e. at different degrees of doping).[47] (Reprinted with permission from Ref 47, Copyright © 2009 Springer Science+Business Media, LLC)

4.4.3 Structure and morphology characterization

Atomic force microscopy (AFM) is a scanning probe microscopy technique to image the topography of surfaces (Figure 4-10).[86] There are two main AFM operation modes: static and dynamic. The latter can be divided into tapping and non-contact modes.[87,88]

In static mode, the tip is in contact with the scanned surface (sample); the cantilever tip is dragged across the sample. Depending on the detected variation of the bending of the cantilever, the force can be estimated based on Hooke's law.[87,88] In dynamic mode, the cantilever mounted on an actuator deliberately vibrates close to or at its resonance frequency. AFM is a three-dimensional characterization technique and the resolution has different values for horizontal (XY) and vertical (Z) axes. On the horizontal axis, the resolution is the shortest distance between two points that can be differentiated on the sample. For the vertical axis, the AFM noise floor (measured via capturing probe motion on the surface while AFM is not scanning) is defined as the resolution.

Tapping mode is used to study the nanoscale morphology and roughness of organic semiconductor films. This is to obtain non-destructive imaging and to prevent the tip from being trapped.[89]

In this PhD work, the samples were scanned in ambient conditions, in tapping mode, with a Digital Instruments Dimension 3100 (Santa Barbara, CA) combined with a Veeco Nanoscope V controller (Bruker). Tapping mode was performed at a scan rate of 1 Hz using etched silicon cantilevers (ACTA from Applied Nanostructures, Inc.) with a resonance frequency around 300 KHz, a spring constant of 40 N/m and tip radius < 10 nm. All images were acquired with medium tip oscillation damping (20% – 30%).

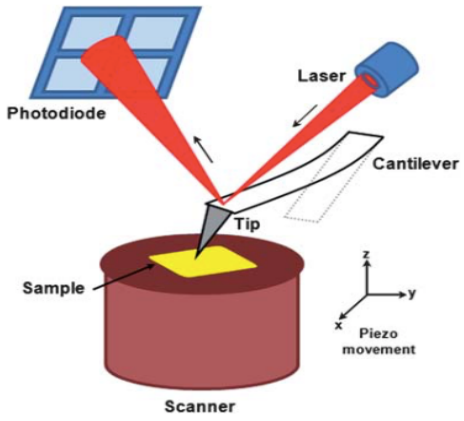

Figure 4-10 Scheme of an atomic force microscope including main components.[89] (Reprinted with permission from Ref. 89, Copyright © 2010 The Royal Society of Chemistry)

X-Ray Diffraction (XRD) (Figure 4-11) is a powerful non-destructive technique to characterize crystalline materials. This can also provide information regarding preferred crystal orientation (texture), phase as well as other structural parameters. These include strain, crystal defects, crystallinity and average grain size.[90,91] For a sample, at a specific angle from each set of lattice planes, the constructive interference of a monochromatic beam of X-rays diffracted by the atoms of the materials can produce X-ray diffraction peaks.[91] Distribution of atoms within the lattice can determine the peak intensity. For a given material, the X-ray diffraction pattern is called the fingerprint of the periodic atomic arrangements.[91] Bragg's law is the basis of XRD analysis that relates to the spacing between the angle of diffraction, the atomic planes (d) and the wavelength (λ). This can be written as $2dsin\theta = n\lambda$, where θ is the incident angle and n is any integral. Diffractions can take place when Bragg's law is satisfied.[91]

The structure of the organic semiconductor films was investigated by XRD with a Bruker D8 diffractometer using a (Cu Kα) beam. X-ray scans were measured every $2\theta = 0.01$ and the time per step was 0.6 s.

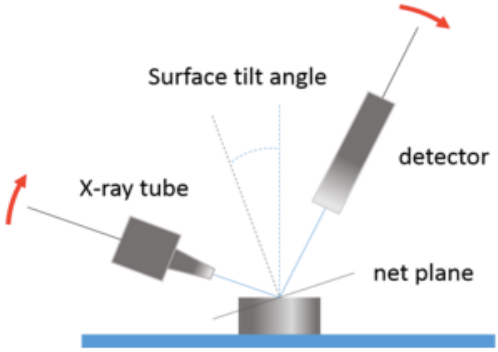

Figure 4-11 Scheme of X-ray diffractometer.[90] (Reprinted with permission from Ref. 90, Copyright © Freiberg Instruments)

4.4.4 Thickness characterization

Profilometer is a technique used to extract topographical data from a surface. These include surface roughness and step heights. Profilometers are equipped with at least two major parts: a detector (to determine where the points on the samples are) and a sample stage (where to hold the sample). There are two types of profilometers: stylus and optical.

In this PhD work, Dektak 150 Profilometer, a stylus profilometry based technique, was used to determine the thickness of organic semiconductor films. In the measurement, the probe was physically moved along the film surface in order to acquire the surface height.

CHAPTER 5 ARTICLE 1: ELECTROLYTE-GATED TRANSISTORS BASED ON PHENYL-C61-BUTYRIC ACID METHYL ESTER (PCBM) FILMS: BRIDGING REDOX PROPERTIES, CHARGE CARRIER TRANSPORT AND DEVICE PERFORMANCE

Article 1 has been published in the *Chemical Communications* on May 2nd, 2018. The Supplementary Information and Experimental are provided in Appendix A. This article reports on the effectiveness of ion-gating on the modulation of charge carrier density in line with what will be further discussed in Chapter 6 and Chapter 7. Specifically, it reports on the doping, paralleled by ionic redistribution, of the n-type semiconductor PCBM.

5.1 Authors

Tian Lan, [a] Francesca Soavi, [b] Massimo Marcaccio, [b] Pierre-Louis Brunner, [c] Jonathan Sayago [d]* and Clara Santato [a]*

[a.] *Polytechnique Montréal, Département de Génie physique, Montréal, Québec H3C 3A7, Canada*

[b.] *Department of Chemistry, Università di Bologna, 40126, Italy*

[c.] *Solaris Chem Inc., 598 Chaline St., Saint-Lazare, Quebec, J7T 3E8, Canada*

[d.] *Instituto de Energías Renovables, Universidad Nacional Autónoma de México, Temixco, Morelos 62588, Mexico*

5.2 Abstract

The n-type organic semiconductor phenyl-C_{61}-butyric acid methyl ester (PCBM), a soluble fullerene derivative well investigated for organic solar cells and transistors, can undergo several successive reversible, diffusion-controlled, one-electron reduction processes. We exploited such processes to shed light on the correlation between electron transfer properties, ionic and electronic transport as well as device performance in ionic liquid (IL)-gated transistors. Two ILs were considered, based on bis(trifluoromethylsulfonyl)imide [TFSI] as the anion and 1-ethyl-3-methylimidazolium [EMIM] or 1-butyl-1-methylpyrrolidinium [PYR_{14}] as the cation. The aromatic structure of EMIM and its lower hindrance with respect to [PYR_{14}] favor a 3D (bulk) electrochemical doping. As opposed to that, for PYR_{14} the doping seems to be 2D (surface-confined). If the n-doping of the PCBM is pursued beyond the first electrochemical process, the transistor current vs gate-source voltage plots in [PYR_{14}][TFSI] feature a maximum that points to the presence of finite windows of high conductivity in IL-gated PCBM transistors.

5.3 Introduction

Electrolyte-gated transistors (EGTs) exploit electrical double layers, forming at the interface between an ion-including medium and a semiconductor, to modulate the electrical conductance in the transistor channel.[28,92] The high capacitance (typically 10~40 μF cm^{-2}) of thin electrical double layers (ca 2-4 nm-thick) permits to reach high charge carrier density in semiconducting channels (ca 10^{15} cm^{-2}), at low operating voltages (as low as 0.1-0.5 V). EGTs based on channels of 2D materials, metal oxides and organic molecular semiconductors, making use of different gating media, such as ionic liquids (ILs), ion gels and saline aqueous solutions, have been reported in the literature. Among such channel materials, organic semiconductors are interesting for applications in bioelectronics as well as flexible and printable electronics.[93-95] The working principle of EGTs depends on several factors, such as the nature of the transistor channel material and the gating medium. It is reasonable to hypothesize that the softness and the redox activity

featured by organic semiconductors render them prone to a bulk (3 dimensional, 3D) electrochemical doping, where charge carrier injection/extraction from metal electrodes (source and drain) to the semiconductor is assisted by the incorporation/removal of ions in the channel. Nevertheless, specific contributions pertaining to intermolecular interactions between the ions of the gating medium and the organic semiconducting molecules of the transistors channel, as well as the size of the ions, can dramatically affect the effectiveness of the doping and its extension in the film (3D vs 2D). Therefore, such specific contributions have to be considered to properly describe the operation of organic EGTs.

Organic semiconductors based on fullerenes and their derivatives have been employed in organic bulk heterojunction solar cells and organic transistors.[96-99] Fullerene-based materials have been widely investigated in the past decades for their electrochemical properties, both in solution and thin film form.[35,100] C_{60} in tetrahydrofurane (THF) solutions, with supporting electrolyte tetrabutylammonium hexafluorophosphate $(C_4H_9)_4NPF_6$, at -60 °C, can undergo six successive reversible, diffusion-controlled, one-electron reduction processes, whereas the same number of reductions had been previously observed only in solvent mixtures.[34,101] Cyclic voltammetry has been recently used, in parallel with low-temperature photoelectron spectroscopy, to estimate the location of the lowest unoccupied molecular orbital (LUMO) levels of phenyl-C61-butyric acid methyl ester (PCBM) in film form, a fullerene derivative soluble in common organic solvents and, as such, interesting for solution-based thin film technologies. Three quasi reversible reduction processes were observed in the solvent o-dichlorobenzene including the support electrolyte tetrabutylammonium tetrafluoroborate $(TBA)BF_4$.[37] Interestingly, literature reports that the electrochemical behavior of C_{60} in thin film form is more complex with respect to solution counterparts.[35] The nature of the supporting electrolyte cation affects the reduction processes, in terms of structure, free energy and solubility of the C_{60} phases formed by electrochemical doping. In general, it has been observed that the larger the doping cation, the larger is the peak splitting in the cyclic voltammograms. Scanning Electrochemical Microscopy (SECM) experiments conducted in acetonitrile containing $(TBA)BF_4$ revealed that the partial

reduction of the films is paralleled by an increase in their conductivity. Considering that PCBM can undergo several redox processes, we found particularly intriguing to explore, in IL-gated transistor configuration, possible correlations between the redox state of the PCBM, the nature of the ions of the IL gating medium and the charge carrier transport and device properties of the PCBM transistor channel material. Our interest was fortified by the possibility to observe the presence of a finite window of high conductivity upon reducing electrochemically the PCBM films beyond the first reduction process. Such windows of high conductivity have been already reported in the literature for p-type organic polymer semiconductors.[39,43]

5.4 Results and discussion

In this work, we report on PCBM transistors gated by two ILs based on bis(trifluoromethylsulfonyl)imide [TFSI] as the anion and 1-ethyl-3-methylimidazolium [EMIM] or 1-butyl-1-methylpyrrolidinium [PYR_{14}] as the cation. We used atomic force microscopy (AFM) and X-ray Diffraction (XRD) to gain insight on the structure of the PCBM films. We studied the film charge transfer properties by cyclic voltammetry. Afterwards, IL-gated PCBM transistors were characterized at different sweep rates and different intervals of the gate-source voltage, to gain insight on the interplay of ionic and electronic transport and the effect of the advancement of the electrochemical doping on charge transport.

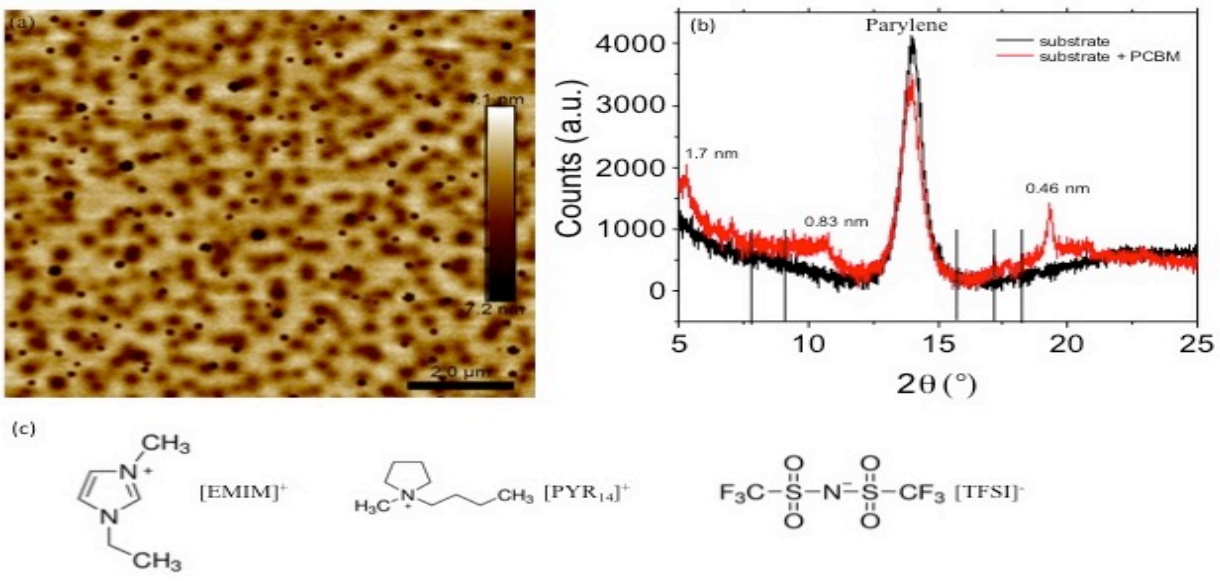

Figure 5-1. (a) 10 μm×10 μm AFM image of PCBM films deposited on SiO_2, height scale: -7.2 nm to 4.1 nm; (b) XRD patterns of the PCBM films including parylene wells confining the ionic liquid gating medium (see Electronic Supplementary Information, ESI). [105]

AFM images show that PCBM films spin-coated on SiO_2 completely cover the substrate and have root mean square roughness (rms) of ca 2.0 nm (Figure 5-1a). The XRD patterns of the films (Figure 5-1b) show 3 peaks located at 5.3° (corresponding to an interplanar distance of 1.7 nm), 10.7° (0.83 nm) and 19.3° (0.46 nm), in agreement with the XRD patterns of polycrystalline PCBM films.[102] After characterization, we exposed the films to the ILs [EMIM][TFSI] and [PYR_{14}][TFSI] to study their charge transfer properties in these media, by cyclic voltammetry. [EMIM][TFSI] and [PYR_{14}][TFSI] feature ionic conductivities of 8.8 mS cm^{-1} and 2.6 mS cm^{-1}, viscosities of 36 mPa s and 84 mPa s at room temperature and wide electrochemical stability windows (4.1 V and 5.7 V).[103] The cyclic voltammetry experiments were carried out in transistor configuration. Here, the PCBM film included between source and drain electrodes constituted the working electrode and a high surface area activated carbon gate electrode acted as both the counter and the reference electrode.[104] Within the interval of the electrochemical potential included between 0.5 V and -1.9 V vs carbon reference, we observed several redox processes in the cyclic voltammograms (Figure 5-2). In [EMIM][TFSI], PCBM electrodes featured 3 reduction processes during the forward (cathodic) scan. Using a sweep rate of 100 $mV \cdot s^{-1}$ (Figure 5-2a), the cathodic peaks (for the 3rd cycle) were located at ca. -1 V (shoulder), -1.4 V (peak) and -1.65 V (peak). Three corresponding anodic peaks, located at ca. -1.45 V, -1.1 V and -0.6 V together with a broad shoulder at ca. -0.2 V, were observed in the backward (anodic) scan. In [PYR_{14}][TFSI] (Figure 5-2d), the 3 reduction processes have cathodic peaks located at ca. -1 V (shoulder), -1.4 V (peak) and -1.65 V (peak) whereas 3 corresponding anodic peaks were observed, in the backward scan, at ca. -1.5 V, -1.05 V and -0.7 V. The small and broad shoulder at -0.2 V, reported for [EMIM][TFSI], was completely absent in [PYR_{14}][TFSI], thus suggesting that such a shoulder can be attributed to the re-oxidation of some kind of reduced form of PCBM product, most probably identified as a partially protonated reduced PCBM, considering the acidic

protons belonging to [EMIM]. It is worth noticing that the oxidation peak at -0.7 V in [PYR_{14}][TFSI] has a *triangular* shape, typical of surface redox processes. The hindrance of [PYR_{14}] with respect to [EMIM] could lead to the significant presence of surface-confined redox processes in [PYR_{14}][TFSI] with respect to [EMIM][TFSI]. Theoretical calculations, assuming a spherical shape for the ions, permitted an estimation of the volume of the cations of the ILs: 182 $Å^3$ for [EMIM] (leading to a radius of ca. 3.5 Å) and 253 $Å^3$ for [PYR_{14}] (radius ca. 3.9 Å).[106] Different sweep rates were explored to gain insight on the electron transfer processes in the two media. The voltammetric currents are, for a fixed rate, higher in [EMIM][TFSI] than [PYR_{14}][TFSI], likely due tothe better ionic conductivity of [EMIM][TFSI]. Other contributions could also explain the higher current in [EMIM][TFSI], e.g. the lower steric hindrance of [EMIM] (and its acidic proton) vs [PYR_{14}], which translates into an easier access/removal of the ion to the reduction/oxidation of PCBM. The decrease of the sweep rate led to minor changes in the peak positions and a decrease in the current (Table S1).[93,107]

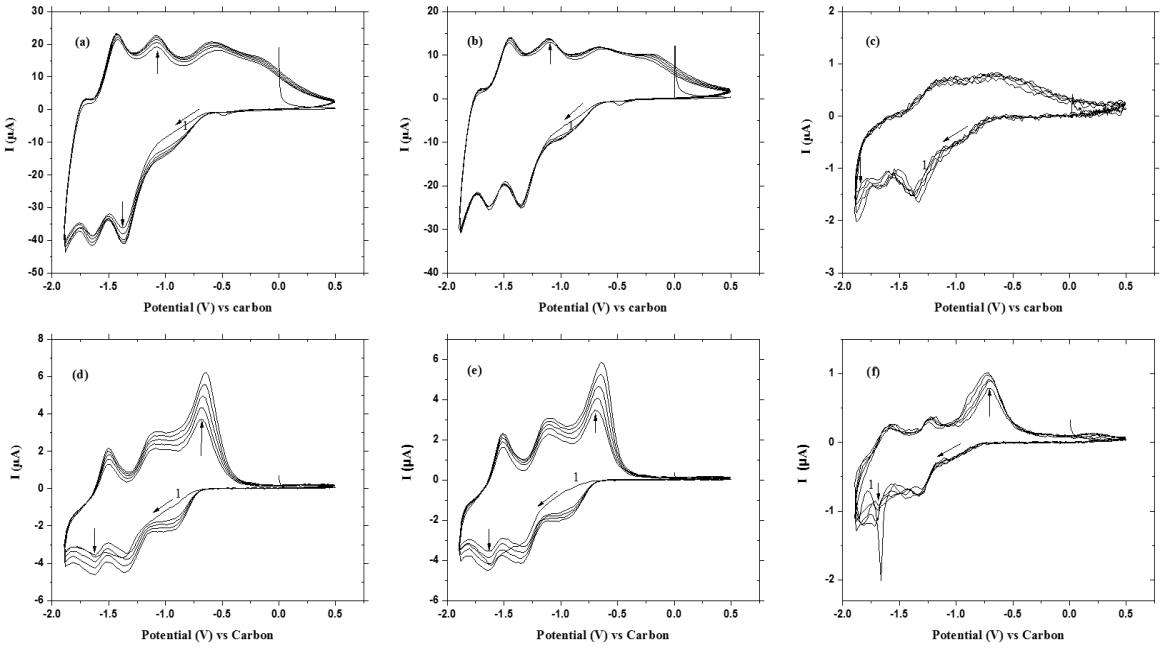

Figure 5-2. Cyclic voltammograms obtained in transistor configuration for PCBM films in [EMIM][TFSI] (a, b, c) and [PYR_{14}][TFSI] (d, e, f), with sweep rates of 100 $mV \cdot s^{-1}$ (a, d), 50

$mV \cdot s^{-1}$(b, e) and 1 $mV \cdot s^{-1}$ (c, f). The quasi reference electrode is made of high surface area activated carbon. Only the first five cycles are shown.

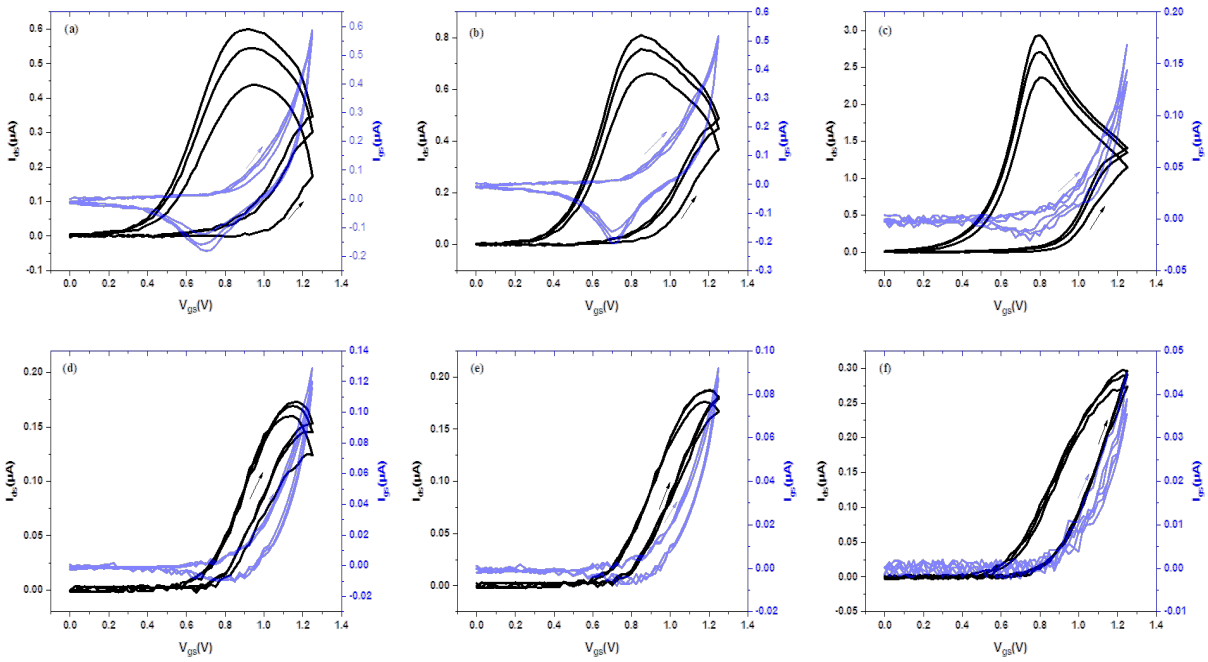

Figure 5-3. Transfer characteristics of PCBM transistors making use of (a, b, c) [EMIM][TFSI] and (d, e, f) [PYR_{14}][TFSI] as the gating medium, obtained for V_{gs} between 0 V and 1.25 V at different sweep rates: (a, d) 100 $mV \cdot s^{-1}$, (b, e) 50 $mV \cdot s^{-1}$,(c, f) 1 $mV \cdot s^{-1}$. V_{ds}=0.1 V.

The knowledge gained about the electrochemical behavior of the PCBM films constituted the underpinning to design electrolyte-gated transistors using [EMIM][TFSI] and [PYR_{14}][TFSI] as the gating media. The use of the high surface area activated carbon gate enabled low voltage (sub-1 V) transistor operation and permitted to avoid the use of an external reference electrode, thus simplifying the device structure.[104] We initially characterized transistors for values of V_{gs} included between 0 V and 1.25 V. The devices showed *n*-type transistor behavior and worked in accumulation mode (Figure 5-3, Fig. S2). It is apparent from the transfer characteristics that the threshold voltages of the transistors have values of about 0.8 V. The linear transfer characteristics of PCBM transistors, at different sweep rates, show that the decrease of the rate leads to higher transistor current (I_{ds}). At lower sweep rates, doping ions better accommodate in the channel. At 1 $mV\ s^{-1}$, I_{ds} is ca. 4 times higher than at 100 $mV \cdot s^{-1}$ for [EMIM][TFSI] whereas it is slightly less

than 2 times higher for [PYR_{14}][TFSI]. A higher I_{ds} is observed in [EMIM][TFSI]-gated transistors compared to [PYR_{14}][TFSI], indicating a higher doping effectiveness with [EMIM] compared to [PYR_{14}], in agreement with the cyclic voltammetry. The higher I_{ds}, together with the significant hysteresis observed with [EMIM][TFSI], points to a 3D (bulk) doping mechanism for PCBM in [EMIM][TFSI]. The doping in [PYR_{14}][TFSI] is still electrochemical but it likely involves only the surface of the PCBM film (surface-confined doping, two dimensional, 2D). The difference in the doping mechanisms can be attributed to the different steric hindrance of the two IL cations (higher for [PYR_{14}]) but also to their different molecular structure (the aromatic [EMIM] is expected to have a higher affinity with PCBM with respect to [PYR_{14}], i.e. to be more easily intercalated in the PCBM films to give a 3D doping, instead of a 2D one). The presence of the acidic proton in [EMIM] should also be considered, for [EMIM]. The aromatic nature of [EMIM] can establish a cooperative and strong π-π stacking interactions with the reduced caps of the fullerene, leading to a higher number of counterions in comparison to the case of [PYR_{14}].[108] The *thinner* structure of [EMIM], in comparison to that of [PYR_{14}], permits [EMIM] to slide easily in the PCBM network. The charge carrier density, p, in our PCBM channels was deduced from the equation $\mathrm{p} = \frac{\mathrm{Q}}{\mathrm{eA}} = \frac{\int \mathrm{I_{ds}} \mathrm{dV_{gs}}}{\mathrm{r_v eA}}$ where Q is the accumulated charge during the forward scan in the transfer curve (obtained through the integration of I_{gs} with V_{gs}), A is the geometric area of the PCBM film interfaced to the electrolyte, e is the elementary charge and r_v is the sweep rate. The charge carrier densities we obtained at sweep rates of 1, 50 and 100 mV·s^{-1} were 3×10^{15}, 2×10^{14} and 10^{14} cm^{-2} in [EMIM][TFSI] and 8×10^{14}, 3×10^{13} and 2×10^{13} cm^{-2} in [PYR_{14}][TFSI]. The electron mobility, μ, was obtained through $\mu = \frac{\mathrm{L}}{\mathrm{W}} \frac{\mathrm{I_{ds}}}{\mathrm{V_{dsep}}}$ where L is the source and drain interelectrode distance, 10 μm, and W is the width, 4 mm. The values of the mobility for transistors making use of [EMIM][TFSI] at sweep rates of 1, 50 and 100 mV s^{-1} were ca. 7×10^{-6}, 3×10^{-4} and 7×10^{-4} cm^2 V^{-1} s^{-1} whereas they were 8×10^{-6}, 4×10^{-4} and 8×10^{-4} cm^2 V^{-1} s^{-1} in [PYR_{14}][TFSI]. The values of the mobility are similar for the 2 gating media, but lower with respect to PCBM transistors making use of SiO_2 or organic gate dielectrics.[109] The relatively low mobility is attributable to the disruption of the π-π packing taking place at different extents,

depending on the nature of the doping mechanism (a more pronounced disruption being expected for the bulk doping). On the other hand, the values of the mobility are strongly affected by the sweep rate of V_{gs}. We observe that, increasing the sweeping rate from 1 mV s^{-1} to 50 mV s^{-1}, the charge density accumulated in the PCBM films decreases of roughly one order of magnitude, whereas the mobility increases of about two orders of magnitude. We could deduce that high sweep rates lead to lower charge carrier density, in turn leading to high charge carrier mobility. Looking carefully at the results, we can also see that the charge carrier densities, for the same sweep rate, are lower for [PYR_{14}][TFSI] than for [EMIM][TFSI], although the values of the mobility are similar. This deduction seems to point to the 2D vs 3D doping observable in the two cases, respectively. The transistor ON (1 V)/OFF (0 V) ratio was about 70-100, for both [EMIM][TFSI] and [PYR_{14}][TFSI]-gated transistors.

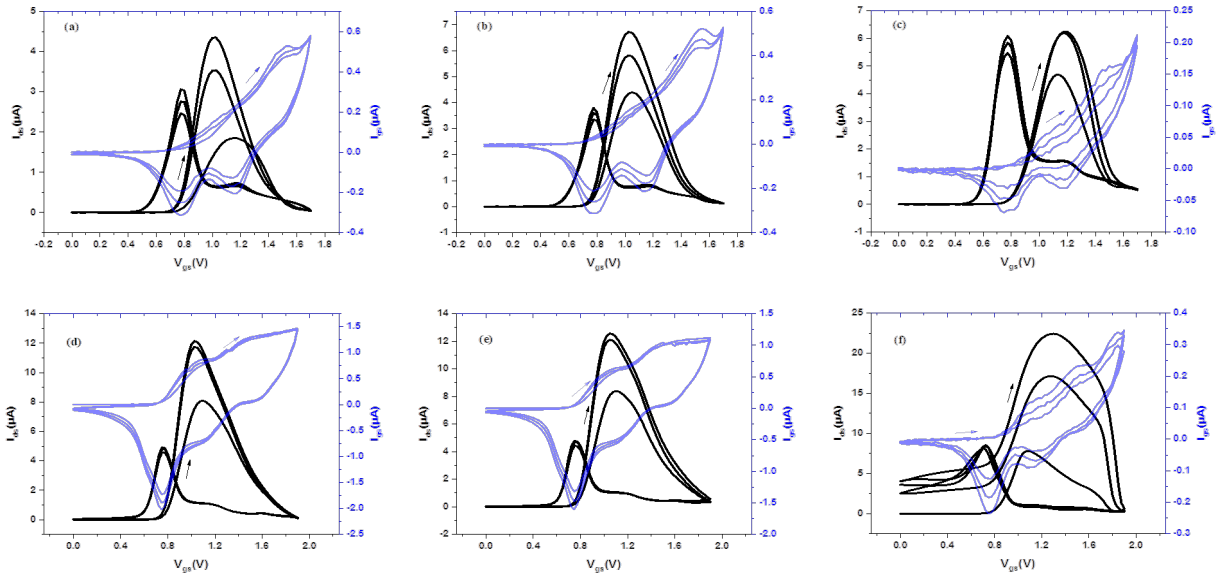

Figure 5-4. Transfer characteristics of PCBM transistors making use of [PYR_{14}][TFSI] as the gating medium, at different V_{gs} sweep rates: (a, d) 100 mVs^{-1}, (b, e) 50 mVs^{-1}, (c, f) 1 mVs^{-1}. The range of V_{gs} values (compare with Figure 5-3) permits to study the behavior of the transistors beyond the first electrochemical doping process. For (a), (b) and (c) the interval of V_{gs} is included between 0 V-1.7 V; for (d), (e) and (f), between 0 V-1.9 V.

We later extended the characterization of the transistors to higher values of V_{gs}, namely 1.7 V and 1.9 V (Figure 5-4 and Fig. S3). For the [PYR_{14}][TFSI] case, Figure 5-4 shows dramatic differences with respect to when V_{gs} limited to 1.25 V (Figure 5-3). In [PYR_{14}][TFSI], for V_{gs} up to 1.7 V, during the first I_{ds} vs V_{gs} forward scan, one peak is observable during the 1st cycle (3 cycles are shown in Figure 5-4), located at ca 1.2 V for 100 mV s^{-1}, 1.1 V for 50 mV s^{-1} and ca 1.2 V at 1 mV s^{-1}. The peaks at ca 1.2 V and 1.1 V are more intense during the 2nd and 3rd cycle, with respect the first. There is a shift of the peak position from the 1st to the last 2 cycles. In the backward scan, two peaks are observable; the peak positions do not change significantly from the 1st to the last 2 cycles. The decrease of the rate from 100 to 50 and 1 mV s^{-1} leads, as expected, to an increase of I_{ds}. I_{gs} vs V_{gs} plots recorded at 100, 50 and 1 mV s^{-1} show, during the forward scan of the 1st cycle, one shoulder at ca 1.1 V and a peak at ca 1.5 V, and, on the backward scan, 3 peaks at high sweep rates and only 2 peaks at 1 mV s^{-1}, in agreement with the voltammetric results. The shape of the curves is similar for V_{gs} up to 1.9 V, apart from the case of 1 mV s^{-1}, where the effect of the 3rd injection in the PCBM seems observable in the transfer plots. We propose that the kinetics of the 3rd injection is affected by the interaction with the IL cations themselves, thus making the process more sluggish than the 1st or the 2nd ones, as it is observable only at 1 mV s^{-1}. The maximum in the transfer curves when the doping takes place beyond the 1st redox process ($V_{gs} \geq 1.25$ V), is analogous to that of p-type polymers featuring finite windows of high conductivity.[39,43] Band filling and bipolaron formation (fullerene C_{60} itself forms bipolarons at sufficiently negative potentials[110]) at high densities can explain the decrease in conductivity.

5.5 Conclusion

In conclusion, to gain insight into possible correlations between the electrochemical and the charge carrier transport properties of organic semiconductors, we investigated the doping process in n-type PCBM transistors making use of [EMIM][TFSI] and [PYR_{14}][TFSI] as the gating media and high surface area carbon as the gate electrode. Cyclic voltammetry permitted to observe 3 reduction processes in the films, thus opening the possibility to follow the film doping for

different reduction states. Our transistor characterization points to a predominant 2D, surface-confined electrochemical doping with the [PYR_{14}][TFSI] and a predominant 3D (bulk) doping with [EMIM][TFSI]. Preliminary results obtained using 4 M [Li][TFSI] in tetraethylene glycol dimethyl-ether (TEGDME) as the gating medium ("solvent in salt", radius of the solvated Li ion ca. 2.5 Å) confirm our hypothesis on the dramatic effect of the steric hindrance of the cation on the doping mode of the PCBM films.[111-113] Indeed, the characteristics of the transistors making use of 4 M [Li][TFSI] in TEGDME resemble those observed with [EMIM][TFSI], interpreted as bulk doping (Fig. S4 and Fig. S5). Interestingly, in [PYR_{14}][TFSI], the shape of I_{ds} reminds that of p-type organic semiconductors featuring finite windows of high conductivity, thus suggesting that these windows are a general feature of organic semiconductors.

5.6 Acknowledgements

T.L. acknowledges CSC for a PhD scholarship, J.S. DGAPA-UNAM, and C.S. NSERC (DG) and MESI (PSR-SIIRI-936) for financial support. F.S. and C.S. acknowledge the Bilateral Progr. Italy-Quebec 2017-19.

CHAPTER 6 ARTICLE 2: AMBIENT-STABLE, ION-GATED POLY[N-9'-HEPTADECANYL-2,7-CARBAZOLE-ALT-5,5-(4',7'-DI-2-THIENYL-2',1',3'-BENZOTHIADIAZOLE)] (PCDTBT) TRANSISTORS AND PHOTOTRANSISTORS

Article 2 was published in *Organic Electronics* on July 4th, 2019. The Supplementary Information is provided in Appendix B. In this article, the effectiveness of ion-gating on the modulation of charge carrier density was investigated. Moreover, air-stability and photo-sensitivity of ion-gated PCDTBT transistors were studied.

6.1 Authors

Tian Lan[1], Francis Bélanger[2], Francesca Soavi[3] and Clara Santato[1]*

1. Polytechnique Montreal, Engineering Physics Department, Montréal, Quebec, H3C 3A7, Canada
2. Seqens, 725 rue Trotter, St-Jean-sur-Richelieu, Quebec, J3B 8J8, Canada
3. Department of Chemistry, Università di Bologna, 40126, Italy

6.2 Abstract

Poly[N-9'-heptadecanyl-2,7-carbazole-alt-5,5-(4',7'-di-2-thienyl-2',1',3'-benzothiadiazole)] (PCDTBT) is a low bandgap carbazole-based copolymer, successfully employed in bulk heterojunction solar cells and field-effect transistors. In this work, we report on the possibility to dramatically lower the operating voltage of PCDTBT transistors by using an ion gating medium, instead of conventional gating media, such as SiO_2. Using the ionic liquid [EMIM][TFSI] [1-ethyl-3-methylimidazolium bis(trifluoromethylsulfonyl)imide] as the ion gating medium, we

characterized the device performance of [EMIM][TFSI]-gated PCDTBT transistors, in inert atmosphere and in air. Furthermore, we report on [EMIM][TFSI]-gated PCDTBT phototransistors, where the transistor current is not only controlled by the electrical bias applied to the gate electrode but also by exposure to simulated solar light.

Key words: ion-gating, organic transistors, environmental stability, Poly[N-9'-heptadecanyl-2,7-carbazole-alt-5,5-(4',7'-di-2-thienyl-2',1',3'-benzothiadiazole)] (PCDTBT), phototransistors.

6.3 Introduction

Ion-gated transistors (IGTs) employ ionic gating media (e.g. electrolyte solutions, ionic liquids, ion gels and polymer electrolytes) to modulate the charge carrier density of the transistor channel material. These transistors feature low operating voltages (< 1 V) due to the high capacitance (ca 1-10 μF/cm^2) of the electrical double layers forming at the ion gating medium/transistor channel interface.[28,30,65,67,68,104,114-117] Attractive features of IGTs, besides their low operating voltage, are their printability, mechanical flexibility and facility of integration with bio- and chemo-sensors.[28,65,67,68,104,114] A number of organic electronic materials have been utilized as channel materials in IGTs, such as pentacene, poly-3-hexylthiophene (P3HT) and poly[2-methoxy-5-(2-ethylhexyloxy)-1,4-phenylenevinylene] (MEH-PPV). [28,65,67,68]

Poly[N-9′-heptadecanyl-2,7-carbazole-alt-5,5-(4′,7′-di-2-thienyl-2′,1′,3′-benzothiadiazole)] (PCDTBT) is an air-stable low bandgap (ca 1.8 eV) organic electronic polymer successfully used, together with phenyl-C61-butyric acid methyl ester (PCBM), in bulk heterojunction (BHJ) solar cells.[48,118] PCDTBT has been also used as transistor channel material in field-effect transistors making use of SiO_2 as gate dielectric; such transistors featured hole mobility of ca ~10^{-3} cm^2 V^{-1}s^{-1}.[50]

Organic phototransistors are multifunctional devices combining the switching and amplifying functions typical of transistors with light response (photocurrent).[119] PCDTBT ion-gated

transistors are ideal candidates to demonstrate low-voltage, stable organic transistors and phototransistors.

In this work, we report on ion-gated PCDTBT transistors and phototransistors. As the ion gating medium we used the ionic liquid 1-ethyl-3-methylimidazolium bis(trifluoromethylsulfonyl)imide, [EMIM][TFSI], featuring ionic conductivity of 8.8 mS cm^{-1} and viscosity of 36 mPa s, at room temperature as well as an electrochemical stability window of ca 4.1 V.[103] We used atomic force microscopy (AFM) and X-ray Diffraction (XRD) to study the morphology and structure of the films, prior to their interfacing with the ionic liquid. An electrochemical study of the behavior of the PCDTBT films in [EMIM][TFSI] was used to guide the film characterization in ion-gated transistor and phototransistor configurations. The transistor characterizations were successfully performed both in inert and ambient atmosphere.

6.4 Results and discussion

AFM topographic images show that PCDTBT films, fabricated via two different solution-based deposition methods (drop-casting and spin-coating), completely cover the SiO_2 substrate, featuring smooth surfaces (root mean square roughness (rms) of ca 0.5 nm for both methods), ideal to be interfaced with ionic liquids (Figure 6-1 and Fig. S1). We did not observe any crystalline peak in the XRD pattern of the films, i.e. films are amorphous (Fig. S2).[50] The optical absorption spectra of PCDTBT thin films are included in Fig. S3.

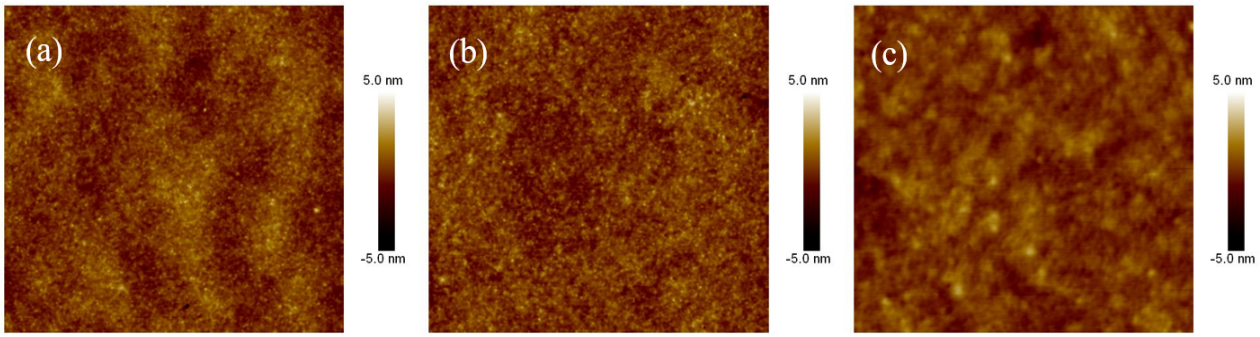

Figure 6-1. AFM images of PCDTBT films deposited on SiO_2 by drop-casting: (a) 10 µm×10 µm, (b) 5 µm×5 µm and (c) 2 µm×2 µm (for spin-coated films, see Fig. S1).

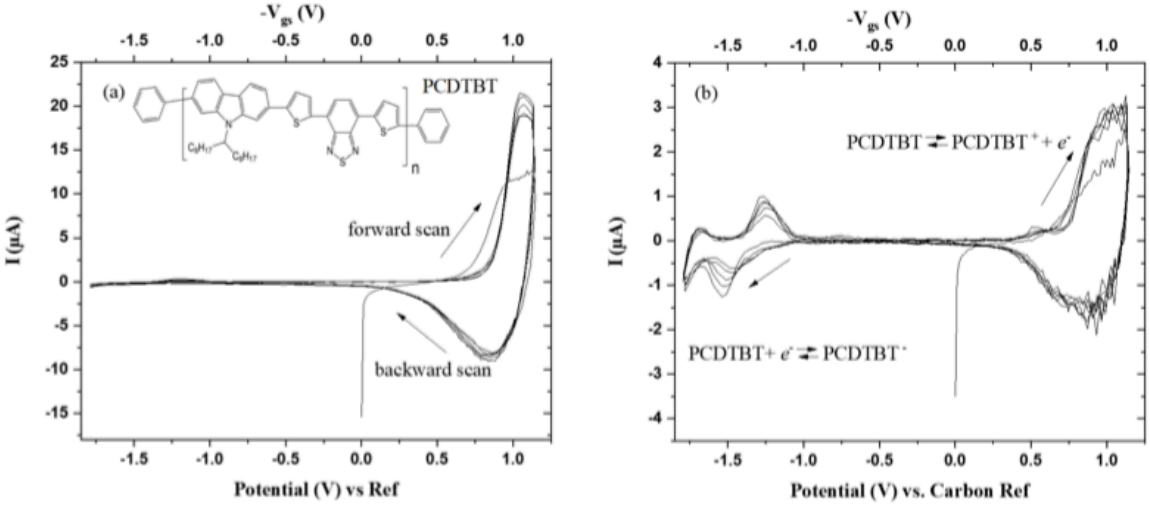

Figure 6-2. Cyclic voltammograms obtained in transistor configuration for PCDTBT films fabricated via drop-casting in [EMIM][TFSI], at scan rates of 10 $mV \cdot s^{-1}$ (a) 1 $mV \cdot s^{-1}$ (b). The quasi reference electrode is made of high surface area activated carbon. The first five cycles are shown.

The cyclic voltammetry characterization of the drop-cast and spin-coated films was carried out in transistor configuration, at scan rates of 10 and 1 mV/s, within the interval of electrochemical potential included between -1.8 V and 1.15 V vs quasi carbon reference (i.e. within the electrochemical stability window of the ionic liquid, Figure 6-2 and Fig. S4). The experimental configuration is such that the PCDTBT film, included between the source and drain electrodes, is the working electrode and a high surface area activated carbon gate electrode acts both as counter and reference electrode.[114] Within the interval 0 V and +1.15 V, at 10 mV/s, we observe a shoulder at 0.9 V followed by a gentle increase of the voltammetric current in the forward (anodic) scan, during the 1st cycle. With the increase of the cycle number, a peak is observable at around 1.1 V; in the backward scan, there is a peak located at ca 0.8 V. In the interval of 0 V and -1.8 V, no significant redox signature is observable.

At 1 mV/s, in the interval 0 V and +1.15 V, there is a peak at 1.15 V in the forward scan, in the 1st cycle; in the backward scan, a broad peak is observable at around 0.9 V. At the same scan rate, in the interval 0 V and -1.8 V, during the forward scan of the 1st cycle, there is a peak at ca -1.5 V, whose position shifts slightly positively with the increase of the cycle number. In the backward scan, there is an oxidation peak located at ca -1.25 V, featuring a slight positive shift with the increase of the cycle number. After the electrochemical measurements, we successfully carried out the characterization of [EMIM][TFSI]-gated PCDTBT transistors, in N_2 glovebox. Results pointed to the p-type behavior of the transistors as well as to the higher transistor currents measured for PCDTBT transistors based on drop-cast films, with respect to their spin-coated counterparts (Fig. S5). This observation brought us to choose transistors based on drop-cast films to study the ion-gating and photogating aspects of PCDTBT transistors (Figure 6-3 and Fig. S6; for a comparison with analogous films gated with the conventional SiO_2 dielectric please refer to S7 and S8). We characterized our transistors both in dark and illumination conditions (simulated solar light), in vacuum. Under illumination conditions, the output and transfer characteristics of [EMIM][TFSI]-gated PCDTBT transistors show a clear increase of the transistor current.

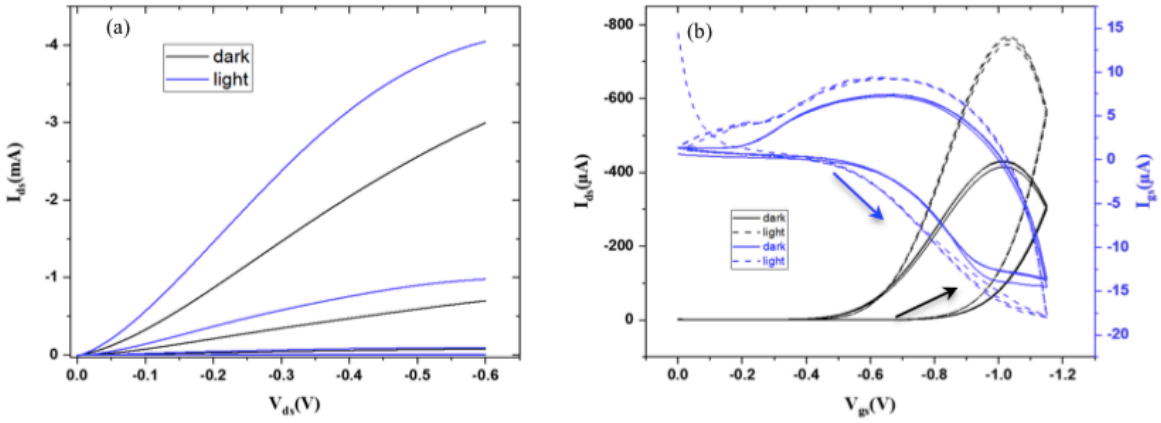

Figure 6-3. [EMIM][TFSI]-gated PCDTBT transistors fabricated via drop-casting characterized under dark and illumination conditions, in vacuum. (a) Output characteristics for V_{gs} =0, -0.55, -0.7, -0.85, -1, -1.15 V. (b) Transfer characteristics in the linear regime (V_{ds}=-0.2 V). Voltage scan rate 10 mVs^{-1}.

The charge carrier density, *p*, in our PCDTBT channels, was deduced from the equation:

$$p = \frac{Q}{eA} = \frac{\int I_{dis} dV_{gs}}{r_v eA} \quad (1),$$

where Q is the accumulated charge during the forward scan in the transfer curve (obtained through the integration of the gate-source current, I_{gs}, vs the gate-source voltage, V_{gs}), A is the geometric area of the PCDTBT film interfaced to the ionic liquid (4 mm×9 mm), *e* is the elementary charge and r_v is the scan rate of V_{gs}.[43,104,121] The charge carrier density obtained at 10 $mV \cdot s^{-1}$ was 8×10^{15} cm^{-2} under dark conditions (Fig. S9 (a)). The hole charge carrier mobility, μ, obtained through:

$$\mu = \frac{L}{W} \frac{I_{ds}}{V_{ds} ep} \quad (2),$$

where L is the drain-source interelectrode distance, 10 μm, W is the electrode width, 4 mm, I_{ds} is the drain-source current, and V_{ds} is the drain-source voltage (V_{ds}=-0.2 V), is about 3×10^{-3} cm^2 V^{-1} s^{-1}. The values of the mobility are somehow slightly higher with respect to PCDTBT transistors making use of conventional dielectrics, such as SiO_2 (ca 10^{-3} cm^2 $V^{-1}s^{-1}$).[50] The charge carrier density obtained under light conditions was 1×10^{16} cm^{-2} whereas the mobility did not significantly change (Fig. S9 (b)). Photoresponsivity and photosensitivity are relevant figures of merit for phototransistors. The photoresponsivity is:

$$R = (I_{d,light} - I_{d,dark})/P_{in}A \quad (3),$$

in which $I_{d,light}$ is the drain-source current under illumination conditions, $I_{d,dark}$ is the drain-source current in the dark, *A* is the active region area of a transistor under illumination (10 μm × 4 mm) and P_{in} is the illumination power intensity. The photosensitivity is:

$$P_s = (I_{d,light} - I_{d,dark})/I_{d,dark} \quad (4).$$

The maximum values we deduced for R and P_s were 1 and 7.3 AW^{-1} (Fig. S10). Despite the low values of the photosensitivity obtained with our phototransistors, the values of the

photoresponsiviy are comparable to those reported in the literature of organic phototransistors (Table S2). It is worth noticing that the operation voltages for our IG phototransistors are about one order of magnitude lower if compared to counterparts based on conventional gating media (e.g. SiO_2 or Al_2O_3). Given the stability in ambient conditions of PCDTBT, explained by the position of the low highest occupied molecular orbital (HOMO, located at ca -5.5 eV vs vacuum),[118,120] we explored the ambient air operational stability of [EMIM][TFSI]-gated PCDTBT transistors. The transistor current increased with the time spent by the device in ambient conditions from the second day and eventually stabilized during the following days of measurements (Figure 6-4). The hole mobility showed an analogous behavior with transistor current.

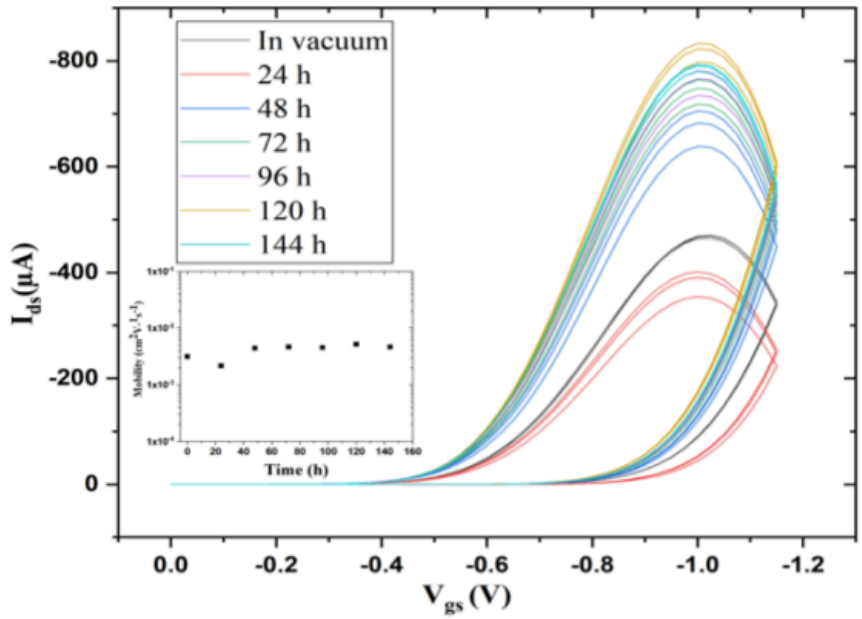

Figure 6-4. [EMIM][TFSI]-gated PCDTBT transistors fabricated via drop-casting, characterized in ambient conditions. Linear transfer characteristics (V_{ds}=-0.2 V) at 10 mV s^{-1} recorded at different shelf lifetime (24, 48, 72, 96, 120, 144 h) in ambient conditions. The inset shows the evolution of the hole mobility vs shelf lifetime in ambient conditions.

6.5 Conclusion

In conclusion, we reported on environmentally stable ion-gated transistors based on solution-processed films of PCDTBT, a low band-gap (1.8 eV) copolymer well investigated in organic photovoltaics. The smooth surface of PCDTBT films was interfaced with the [EMIM][TFSI] ionic liquid, which acted as the ion gating medium. The saturation region of the transistors was reached at about 0.4 V, a dramatically lower value with respect to transistors gated with conventional dielectrics (ca. SiO_2). Exposing the transistors to simulated solar light led to an increase of the charge carrier density with respect to dark conditions. The increase of the charge carrier density under illumination conditions was not paralleled by an increase of the hole mobility. The development of low-voltage transistors operating in ambient conditions represents a further step towards the demonstration of robust organic transistors for printable and flexible technologies, to be possibly coupled with printed batteries. On the other hand, our low-voltage phototransistors pave the way to autonomous, printed and flexible devices.

6.6 Experimental

SiO_2/Si substrates were photolithographically patterned with source and drain electrodes (40 nm-thick Au on 4 nm-thick Ti adhesion layer) with interelectrode distance, L, of 10 μm and width, W, of 4 mm. Prior to deposition of the PCDTBT semiconducting films, the substrates were cleaned with sequential steps of 5 min in isopropyl alcohol, 10 min in acetone and 5 min in isopropyl alcohol, in an ultrasonic bath. PCDTBT solutions consisting of 15 mg and 1.5 mg PCDTBT (Molecular weight 13 kDa, PCAS Canada) in 1 ml chlorobenzene were stirred overnight in a N_2 glove box (< 5 ppm O_2, H_2O). PCDTBT films were deposited by drop-casting (1.5 mg/ml) and spin-coating (15 mg/ml) on the SiO_2 substrates and set on a hot plate at 50 °C for 2 h, in the N_2 glove box. The typical thicknesses of the films measured by profilometry were ca 240 nm for drop-casted films and ca 77 nm for spin-coated. [EMIM][TFSI] (IoLiTec, >99%) was purified at 60 °C, 10^{-5} Torr, overnight. The ionic liquid was included in a Durapore® membrane,

4 mm×9 mm-sized, 125 μm-thick, laminated on top of the PCDTBT channel. The gate electrode consisted of high surface area carbon paper (Spectracarb 2050), 6 mm×3 mm, 170 μm-thick, coated with an ink made of activated carbon (PICACTIF SUPERCAP BP10, Pica, 28 mg ml-1) and polyvinylidene fluoride (PVDF, KYNAR HSV900, 1.4 mg ml^{-1}) binder, in N-methyl pyrrolidone (NMP, Fluka). The gate electrode was offset with respect to the transistor channel. Transistor characteristics were acquired employing an Agilent B1500A semiconductor parameter analyzer connected to a house-made micromanipulated electrical probe station in N_2 glove box and vacuum (ca 10^{-4} Torr). Electrochemical characterizations were obtained in situ, in transistor configuration, with a VersaSTAT 4 potentiostat. Atomic Force Microscopy (AFM) images were taken in air, at room temperature, on a Digital Instruments Dimension 3100, in tapping mode, with Al-coated silicon cantilevers. X-ray diffraction (XRD) spectra of the PCDTBT films was taken using a Bruker D8 diffractometer with a wavelength (CuK_a) of 1.54 Å. A solar light simulator (SLB-300A Compact Solar Simulator Class AAA) was used as the illumination source (1 KW/m^2, AM 1.5, wavelength range of 400 nm to 1100 nm). UV-Vis absorption spectra measurement were recorded using a Cary 7000 Universal Measurement Spectrophotometer (Agilent, UMS).

6.7 Acknowledgements

T.L. and C.S. respectively acknowledge the China Scholarship Council (PhD scholarship) and NSERC (Engage grant) for financial support.

CHAPTER 7 ARTICLE 3: FLEXIBLE ION-GATED TRANSISTORS MAKING USE OF POLY-3-HEXYLTHIOPHENE (P3HT): EFFECT OF THE MOLECULAR WEIGHT ON THE EFFECTIVENESS OF GATING AND DEVICE PERFORMANCE

Article 3 was published in the *Journal of Electronic Materials* on June 17th, 2020. The Supplementary Information is provided in Appendix C. In this article, the effectiveness of ion-gating on the modulation of charge carrier density was proved for P3HT films with different molecular weights. Additionally, mechanical flexibility of ion-gated transistors was investigated.

7.1 Authors

Tian Lan[1], Zhaojing Gao[1], Martin S Barbosa[1,2], Clara Santato[1]*

1—Polytechnique Montreal, Engineering Physics Department, Montréal, Quebec, H3C 3A7, Canada. 2—São Paulo State University, Departamento de Fisico-Química, São Paulo, 14800-060, Brazil. 3—e-mail: clara.santato@polymtl.ca.

7.2 Abstract

Poly-3-hexylthiophene (P3HT) is a benchmark semiconducting polymer in organic electronics. Ion- gated transistors (IGTs), making use of ionic gating media, are particularly interesting for flexible and printable organic electronic applications. The molecular weight of P3HT is known to affect the morphology and structure of the corresponding films and, ultimately, the performance of devices based thereon. Here we report on IGTs based on films of P3HT with different molecular weights (~20 kDa, 30-50 kDa and 80-90 kDa) and, as the gating medium, the well-investigated ionic liquid [EMIM][TFSI], to investigate the effects of the film morphological

and structural properties on charge carrier transport and, eventually, IGT performance. P3HT films were deposited over rigid (SiO_2/Si) and flexible (polyimide) substrates. All the P3HT IGTs could be operated at low-voltage (about 1 V) and achieved a hole mobility larger than 0.1 $cm^2 V^{-1} s^{-1}$, pointing to the extremely favorable [EMIM][TFSI]/P3HT interface for IGT applications, for all the molecular weights investigated. We finally investigated the stability of flexible devices considering two different bending radii (R=10 mm and R=5 mm).

Keywords: Poly-3-hexylthiophene (P3HT), bendable polymer substrates, ion-gated transistors, ionic liquids.

Abbreviations

P3HT Poly-3-hexylthiophene

IGTs Ion-gated transistors

MW Molecular weight

AFM Atomic force microscopy

XRD X-ray Diffraction

IPA Isopropyl alcohol

PDMS Polydimethylsiloxane

7.3 Introduction

Conjugated organic small molecules and polymers have been investigated as channel materials in thin film transistors based on ion-gating technologies for printable, flexible and (bio)electronic applications.[28,65-73] Ion-gated transistors (IGTs) exploit the high capacitance (ca 1-10 $\mu F/cm^2$) of thin electrical double layers (ca 2-4 nm-thick) forming at the interface between the channel

material and the ion gating medium to achieve low-voltage operation modes (typically about 0.1-1 V). [28,65,67-69,104,114]

Poly-3-hexylthiophene (P3HT) is a well-studied organic semiconductor, possessing an optical band gap of about 1.9 eV,[122-123] good solubility in organic solvents for solution processing over large areas and good charge carrier mobility.[124] The molecular weight (MW) of P3HT affects the structure of the P3HT films, in turn affecting their charge carrier transport properties and, ultimately, the performance of corresponding devices.[58,78,103,125] Indeed, the increase of MW brings about an increase of the entanglement density of the polymer chains, in turn leading to the increase of the amorphous portion (as opposed to polycrystalline) of the films.[58,78,126] This is expected to strongly affect ion permeability, and therefore the advancement of doping, in P3HT IGTs. Therefore, to develop high performance flexible and printable P3HT IGTs, it is important to shed light on the effect of the MW of P3HT on the effectiveness of the ion gating.

In this work, we report on transistors based on films of P3HT with different MWs gated by the ionic liquid 1-ethyl-3-methylimidazolium bis(trifluoromethylsulfonyl)imide, [EMIM][TFSI], making use of rigid (SiO_2/Si) and flexible (polyimide) substrates.[124] Prior to transistor characterization, we used atomic force microscopy (AFM) and X-ray Diffraction (XRD) to study the morphology and structure of the P3HT films, as a function of the MW. Electrical measurements on flexible devices were carried at different bending radii, over multiple bending cycles.

7.4 Experimental

Substrates pre-treatment

Glass substrates (75 mm×50 mm×1 mm) were cleaned with running isopropyl alcohol (IPA) and dried with nitrogen gas. Polyimide films (75 mm×50 mm×125 μm) were cleaned with acetone, isopropyl alcohol and DI water, respectively for 10 min, in an ultrasonic bath. A polydimethylsiloxane (PDMS) solution was prepared using elastomer and curing agent with the

ratio of 10:1. The solution was mixed in planetary mixer at 2000 rpm for 3 min. The PDMS solution was spin-coated on the clean glass substrates at 500 rpm for 30 s following with a heat treatment at 100 ºC for 20 min. The polyimide films were stacked onto the pre-baked PDMS/glass substrates then placed on the hotplate at 100 ºC for 20 min.

Transistor fabrication

SiO_2/Si and Polyimide/Glass substrates were photolithographically patterned with source and drain electrodes (40 nm-thick Au on 5 nm-thick Ti adhesion layer) with interelectrode distance, L, of 10 μm and width, W, of 4 mm. Afterwards, polyimide films were peeled off from the glass substrates. Prior to deposition of the P3HT semiconducting films, the SiO_2/Si substrates and polyimide films were cleaned with sequential steps of 5 min in isopropyl alcohol, 10 min in acetone and 5 min in isopropyl alcohol, in an ultrasonic bath. P3HT solutions consisting of 10 mg (molecular weight ca 20 kDa, ca 30-50 kDa, and ca 80-90 kDa, Solaris Chem, Canada) in 1 ml chlorobenzene were stirred overnight in a N_2 glove box (< 0.1 ppm O_2, H_2O). P3HT films were deposited by spin-coating (10 mg/ml) on the SiO_2 substrates and polyimide films and set on a hot plate at 140 °C for 2 h, in the N_2 glove box. The thicknesses of the P3HT films deposited over SiO_2/Si, as measured by profilometry, were: 58±3 nm for low MW, 48±1 nm for intermediate MW and 65±5 nm for high MW. [EMIM][TFSI] (ionic conductivity of 8.8 mS cm^{-1} and viscosity of 36 mPa s and electrochemical stability window of ca 4.1 V, at room temperature) (IoLiTec, >99%) was purified at 60 °C, 1.33×10^{-6} kPa, overnight.[103] The ionic liquid was placed in a Durapore® membrane, 4 mm×9 mm-sized, 125 μm-thick, laminated on top of the P3HT channel. The gate electrode consisted of high surface area carbon paper (Spectracarb 2050), 6 mm×3 mm, 170 μm-thick, coated with an ink made of activated carbon (PICACTIF SUPERCAP BP10, Pica, 28 mg ml^{-1}) and polyvinylidene fluoride (PVDF, KYNAR HSV900, 1.4 mg ml^{-1}) binder, in N-methyl pyrrolidone (NMP, Fluka).

Structural and electrical characterizations

Transistor characteristics were acquired employing an Agilent B1500A semiconductor parameter analyzer connected to a house-made micromanipulated electrical probe station in N_2 glove box. Atomic Force Microscopy (AFM) images were taken in air, at room temperature, on a Digital Instruments Dimension 3100, in tapping mode, with Al-coated silicon cantilevers. X-ray diffraction (XRD) spectra of the P3HT films was taken using a Bruker D8 diffractometer with a wavelength (CuK_a) of 1.54 Å.

7.5 Results and discussion

We studied spin-coated films of P3HT with three different molecular weights (MWs), namely low MW (~20 kDa), intermediate MW (30-50 kDa) and high MW (80-90 kDa). XRD patterns obtained for P3HT films deposited on Si/SiO_2 revealed a (100) diffraction peak located at $2\theta=5.1°$, typical of the lamellar layer structure of crystalline P3HT (Figure 7-1).[126,127] The difference in peak intensity for the three types of films indicate that low MW films have a higher degree of crystallinity, in agreement with the literature.[126] AFM was used to characterize the surface topography of the P3HT films deposited on SiO_2/Si (Figure 7-2). The values of the root mean square roughness (rms) were 1.5 nm for low MW, 3.8 nm for intermediate MW and 5.6 nm for high MW (Figure 7-2 and Table 7-1). Low MW films are expected to possess a better solubility, leading to a lower roughness of the corresponding surface.[128-130] On the basis of the AFM and XRD results, we can expect that high MW films feature structural and morphological characteristics bringing about easy ion permeability, i.e. effectiveness of the doping through ion gating.

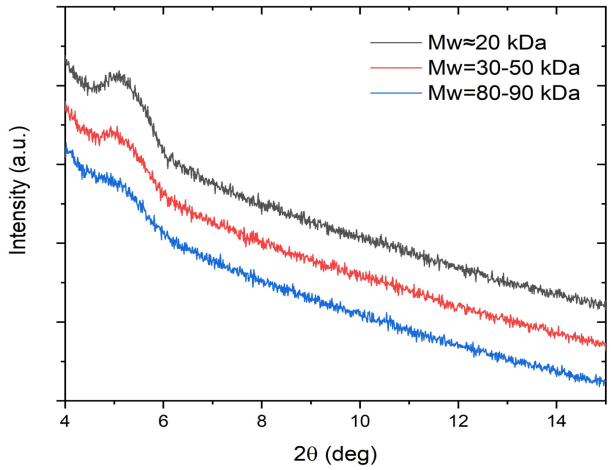

Figure 7-1. XRD patterns of films of P3HT with different MWs, spin-coated on SiO_2/Si.

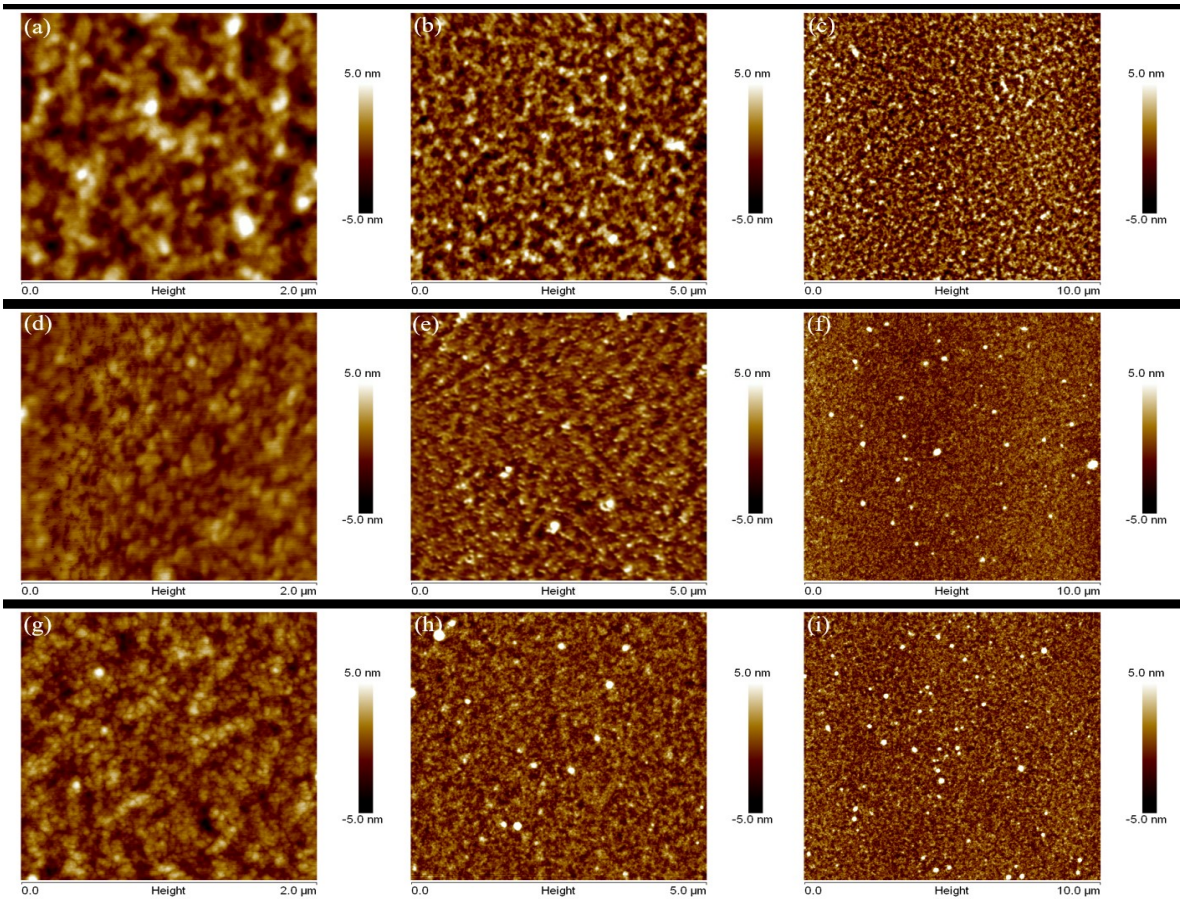

Figure 7-2. AFM images of P3HT films with different MWs (a-c: low MW; d-f: intermediate MW; g-f: high MW, please refer to main text for further details) spin-coated on SiO_2/Si.

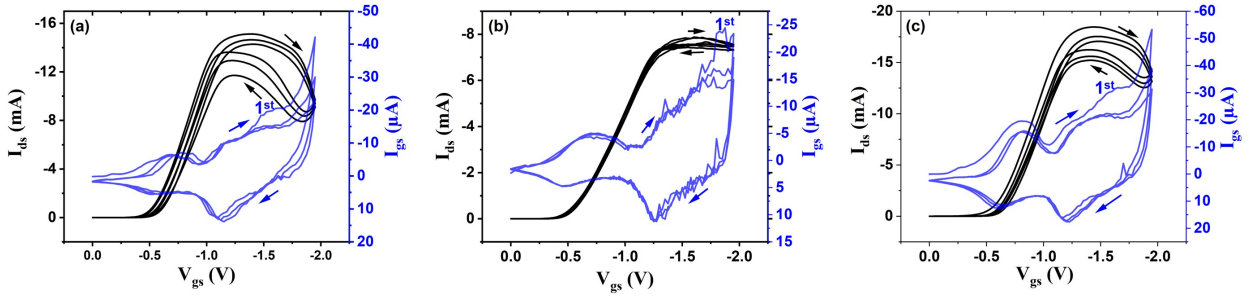

Figure 7-3. [EMIM][TFSI]-gated P3HT films transistors (a: low MW; b: intermediate MW; c: high MW) on rigid SiO_2/Si substrates via spin-coating characterized in N_2 glovebox. Transfer characteristics in the linear regime (V_{ds}=-0.2 V, 3 scans shown). Voltage scan rate 50 mVs^{-1}.

Table 7-1 Morphological and structural features of P3HT films deposited on SiO_2/Si studied in this work together with three-dimensional charge carrier density (2D and 3D) deduced from equation (1) and hole mobility deduced from corresponding IGTs. P3HT with different MWs have been investigated. Values of the thickness of the films given in Experimental.

Molecular Weight	Roughness (nm)	XRD Peak Position (2θ°)	Charge Carrier Density 2D (cm^{-2})	Charge Carrier Density 3D (cm^{-3})	Hole Mobility (cm^2/Vs)	ON/OFF Ratio
low MW	1.5	5.1 (highest intensity)	7×10^{15}	1.2×10^{21}	0.10	1.5×10^{5} ($-1.5\times10^{-2}/-1\times10^{-7}$)
intermediate MW	3.8	5.1	4×10^{15}	8×10^{20}	0.13	8.2×10^{3} ($-7.4\times10^{-3}/-9\times10^{-7}$)
high	5.6	5.1	1.2×10^{16}	1.8×10^{21}	0.09	9.0×10^{3}

MW		(lowest intensity)				(-1.8×10^{-2}/-2×10^{-6})

The device characterization of [EMIM][[TFSI]-gated P3HT transistors on SiO_2/Si was carried out in a N_2 glovebox. Transfer and output characteristics showed typical *p*-type transistors behavior (Figure 7-3 and supplementary Figure S1). The transfer characteristics for low and high MW show a maximum, a feature previously observed with IGTs based on films of small organic molecules and polymers.[43,116]

The gate-source current vs gate-source bias plots (I_{gs} *vs* V_{gs}, Figure 7-3, blue line and blue arrows) showed, during the first *forward* (anodic) scan (i.e. from the onset voltage, located at 0 V, towards negative values)[104], broad oxidation features. For the three MWs, a first feature is observable at about -0.6 V. A second feature is included between about -1.1 V and -1.6 V, for low and high MW films. On the *backward* (cathodic) scan, a peak located at about -1.2 V, with a shoulder at about -1.6 V, and a broad peak at about -0.5 V are observable.[126]

The charge carrier density, p, in our P3HT channels, was deduced from the equation:

$$p = \frac{Q}{eA} = \frac{\int I_{gs} dV_{gs}}{r_v e A} \quad (1)$$

where Q is the accumulated charge during the forward scan in the transfer curve (obtained through the integration of I_{gs} with V_{gs}), A is the geometric area of the P3HT film interfaced to the ionic liquid (4 mm×9 mm), e is the elementary charge and r_v is the scan rate of V_{gs}.[43,104,121] The values of the density for IGTs on SiO_2/Si substrate were about 7×10^{15} cm^{-2} for low MW, 4×10^{15} cm^{-2} for intermediate MW and 1.2×10^{16} cm^{-2} for high MW.

The hole charge carrier mobility, μ, was obtained through:

$$\mu = \frac{L}{W} \frac{I_{ds}}{V_{ds} e p} \quad (2)$$

where L is the drain-source interelectrode distance, 10 μm, W is the electrode width, 4 mm, I_{ds} is the drain-source current, and V_{ds} is the drain-source voltage (V_{ds}=-0.2 V). The hole mobility on SiO_2 substrate was ca 0.10 $cm^2 V^{-1} s^{-1}$, 0.13 $cm^2 V^{-1} s^{-1}$ and 0.09 $cm^2 V^{-1} s^{-1}$ for low, intermediate and high MW (Table I).

The transistor ON/OFF ratios were 1.0×10^5 for low MW, 8.5×10^3 for intermediate MW and 7.5×10^3 for high MW (transistors based on films prepared with low MW P3HT, featuring the highest crystallinity among the films investigated, had the lowest value of I_{off}).[131,132]

After the study of transistors on rigid substrates, devices based on flexible polyimide substrates were fabricated and characterized simultaneously for their electrical and mechanical properties (Figure 7-4, supplementary Figure S2, supplementary Figure S3 and supplementary Figure S4). The values of the density deduced for films spin-coated on polyimide were about 7.4×10^{15} cm^{-2} for low MW, 4.3×10^{15} cm^{-2} for intermediate MW and 7.5×10^{15} cm^{-2} for high MW. The values of the hole mobility observed on polyimide were ca 0.09 $cm^2 V^{-1} s^{-1}$, 0.12 $cm^2 V^{-1} s^{-1}$ and 0.10 $cm^2 V^{-1} s^{-1}$ for low, intermediate and high MW. Moreover, threshold voltages (V_{th}) show similar values for devices on SiO_2 substrate (ca -0.5 V) and polyimide substrate at rest (ca -0.55 V). Measurements were performed both with flat devices (at rest) as well as bent counterparts. In the latter case, the investigated curvature radii (R) were 10 mm and 5 mm. For the case of high MW, from the comparison between the characteristics of devices flat or bent, we deduced that devices bent with R=10 mm showed about 40% decrease of the transistor current at V_{gs}=-1.5 V (Figure 7-4 (c)). With further bending (R=5 mm), the performance of the devices presented a further 43% decrease in I_{ds}, i.e. the device performance got worse with the decrease of curvature radii.

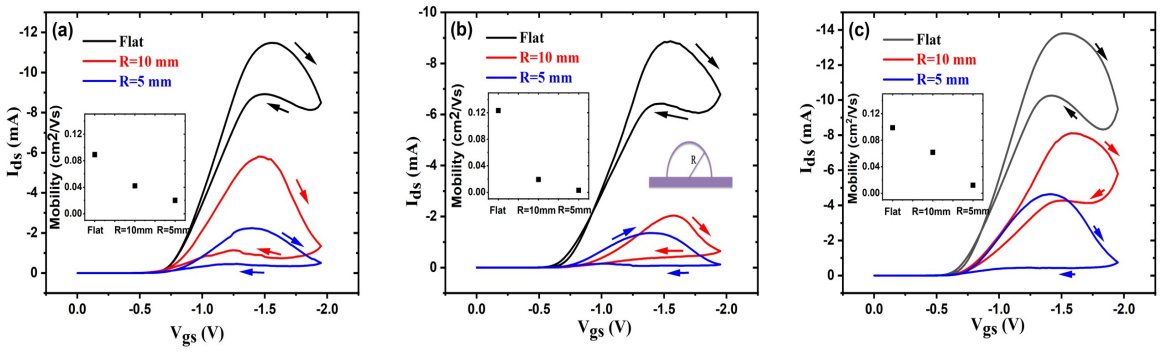

Figure 7-4. Transfer characteristics in the linear regime (V_{ds}=-0.2 V) for [EMIM][TFSI]-gated P3HT films transistors (a: low MW; b: intermediate MW; c: high MW) on flexible polyimide substrates, flat (at rest) or under bending conditions (R=10 mm and 5mm) (b). V_{gs} scan rate 50 mVs^{-1}. Inset shows hole mobility vs R.

To further investigate the stability of the bendable devices, we measured the change of the hole mobility as function of the number of bending cycles, with R=5 mm (Figure 7-5). The results pointed to an overall decrease of the mobility with the increase of the bending cycles. Compared to the initial mobility at rest, after 1500 cycles there was a 67%, 78% and 80% decrease in mobility for low, intermediate and high MW P3HT IGTs. The mobility of devices based on intermediate and high MW P3HT reached a *quasi plateau* after 1000 bending cycles (with a current of 46% of the initial value for low MW, 59% for intermediate MW and 35% for high MW P3HT, respectively).

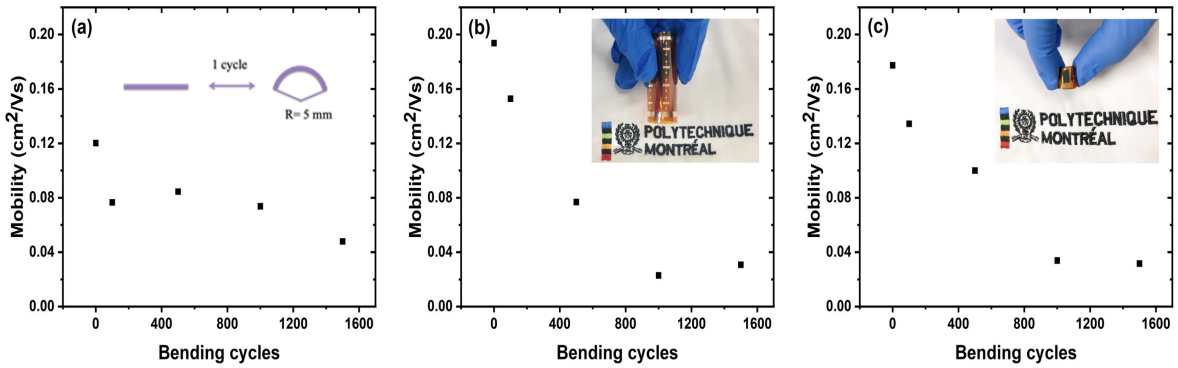

Figure 7-5. Hole mobility of [EMIM][TFSI]-gated P3HT transistors on flexible polyimide substrates (a: low MW, b: intermediate MW, c: high MW) as a function of bending cycles with R=5 mm.

7.6 Conclusions

In conclusion, we reported on ion-gated transistors based on films of P3HT at three different molecular weights (MWs), on rigid (SiO_2/Si) and bendable (polyimide) substrates. Using [EMIM][TFSI] as the ion-gating medium, high values of the charge carrier density (10^{20}-10^{21} cm^{-3}) were observed for the transistors. For low and high MW P3HTs, such high charge carrier density was accompanied by the presence of a maximum of the transistor current in the transfer characteristics, attributable to finite regions of high conductance.[43,116] The effectiveness of the doping does not seem to straightforwardly correlate with the MWs of the P3HT. This is likely due to the good permeability of the films to the ions of the ionic liquid considered. Indeed, such permeability seems to be independent on the differences observed in the film structure and morphology with the MW. Values of the hole mobility as high as 0.13 $cm^2 V^{-1} s^{-1}$ and 0.19 $cm^2 V^{-1} s^{-1}$ were obtained on SiO_2/Si and polyimide substrates, for films based on P3HT with intermediate MW. This confirms the fact that the P3HT/[EMIM][TFSI] interface is a favorable one for IGTs, bringing about effective doping at low operating voltages. Additionally, transistors on polyimide were tested for their bendability with two different bending radii (R=10 mm and 5 mm). Devices were characterized for 1500 bending cycles. Intermediate and high MW P3HT films, after an initial decrease of the mobility of about one order of magnitude during the first 1000 cycles, showed a stabilization of the hole mobility, between 1000 and 1500 cycles. Results are promising for the development of IGT flexible technologies. Capitalizing on the present results, we are currently extending our studies to ion gel (quasi solid state) gating media and stretchable substrates.[133]

7.7 Acknowledgements

T. L. and Z. J. G acknowledge the China Scholarship Council (PhD scholarships). C.S. acknowledges NSERC (DG) for financial support.

CHAPTER 8 GENERAL DISCUSSION

In this thesis, organic semiconductors, including PCBM, PCDTBT and P3HT, were adopted as channel materials and investigated for their electrochemical and charge carrier transport properties. Ionic liquids were employed as gating media to replace conventional dielectrics, such as SiO_2. The choice of organic semiconducting materials and ionic liquids in this thesis was made with various considerations and purposes. First, organic materials possess a unique number of features compared to their inorganic counterparts regarding applications involving electronic and biological domains. These include weak van der Waals intermolecular forces giving the materials a characteristic “softness” that could be adjusted through chemical synthesis. This allows for the uptake of ions when the organic materials are interfaced to the ionic media bringing about doping in ion-gated transistors (operating at remarkably low voltages). These characteristics align with the benefits of adopting room-temperature ionic liquids as gating media. These consist of pure ions. This differs from electrolytes, such as polymer electrolytes, gel electrolytes and aqueous electrolytes where solvents dissolve salts. Ionic liquids possess a wide range of advantages, such as excellent thermal stability, a wide electrochemical window, etc. Ionic liquids are the ideal candidates for applications in electronic and electrochemical devices such as solar cells, fuel cells, batteries and capacitors. In recent years, ionic liquids working as gating media in organic transistors have attracted a lot of attention. Enormous progress has been made in fundamental studies for practical applications of the devices.

Traditionally, chemical doping is used irreversibly to induce charge carriers in solids accompanied by serious side effects such as parasitic chemical reactions. However, the electrostatic (field-effect) doping method avoids these difficulties by reversibly achieving the modulation of the charge carrier density at the semiconductor-gating media interface. The choice of gating media materials plays a very important role in the performance of the devices. This needs to meet more than one critical requirement such as specific capacitance at the semiconductor-ionic medium interface, device transconductance, etc. The specific capacitance

determines the amount of the induced charge carriers at a given gate voltage in the semiconductor channel. The charge Q' (in Coulomb) that accumulates in a parallel-plate capacitor is:

$$Q' = CV \qquad (1)$$

where V is the applied voltage (in Volt) and C is the capacitance (in Farad). In addition, specific capacitance (Farad per unit area) can be obtained via (2)

$$C = \frac{\varepsilon_0 \varepsilon_r}{d} \qquad (2)$$

where ε_0 is the vacuum permittivity, ε_r is the relative permittivity and d is the distance between the two plates.

Making use of ionic liquids as gating media exploits the electrical double layers forming at the ion gating medium-channel semiconductor interface. This, in turn, exhibits a high capacitance in a typical range of 10~40 μF cm^{-2}. This leads to high charge carrier density (~10^{15} cm^{-2}) in the semiconducting channel of the transistor which then features low operating voltages (< 2V). It is worth mentioning that the charge carrier density achieved in transistor channels is higher than that obtained through a conventional dielectric such as SiO_2, by orders of magnitude.

Bringing ionic liquids into the organic transistor configuration bridges electronics and ionics. At the same time, it relates to other research fields such as electrochemistry. This opens possibilities and opportunities to explore different aspects of electrical double layers and also provides a basis for developing new characteristics in electronic applications, such as flexibility.

Depending on the properties of interfaced semiconductors and ionic liquids, there exists two basic operating mechanisms for ion-gated transistors. In the former case, the ions of ionic liquids cannot permeate the semiconductor. With a bias applied on the gate electrode, ions migrate and accumulate at the gate-ionic liquids and semiconductor-ionic liquids interfaces. In the latter case, ions of ionic liquids can permeate the semiconductor. The application of a bias on the gate electrode would cause the migration of ions into the semiconductor films.

8.1 The effectiveness of ion-gating on the modulation of charge carrier density

The aforementioned discussion regarding electrical double layers points out clearly that low operation voltage can be achieved by high charge carrier density in the semiconducting channel interfaced with ion-gating medium. However, the effectiveness of ion-gating can be influenced by other parameters, such as the properties of organic semiconductors and ionic liquids, electrochemical potential, and sweep rate.

In **Article 1**, we adopted n-type organic semiconductor PCBM as the channel material, and two room-temperature ionic liquids: [EMIM][TFSI] and [PYR_{14}][TFSI] as gating media. Different sweep rates: 100, 50 and 1 mVs^{-1} were employed to gain insight into the ion-gating of these two different media. The charge carrier densities obtained in [EMIM][TFSI] at sweep rates of 100, 50 and 1 mVs^{-1} were 10^{14} cm^{-2}, 2×10^{14} cm^{-2} and 3×10^{15} cm^{-2}. These results showed that the charge carrier density increased as the sweep rate decreased. As for [PYR_{14}][TFSI], the same phenomenon was observed. The charge carrier densities achieved in [PYR_{14}][TFSI] were 2×10^{13} cm^{-2}, 3×10^{13} cm^{-2} and 8×10^{14} cm^{-2} at sweep rates of 100, 50 and 1 mVs^{-1}, respectively. We can deduce from the results that high sweep rates lead to lower charge carrier density. Moreover, for the same sweep rate, charge carrier density in [EMIM][TFSI] is higher than that in [PYR_{14}][TFSI]. This implies the different effectiveness of these two ionic liquids sharing the same anion in the modulation of the charge carrier density.

In **Article 2**, we employed the p-type, air-stable low band gap organic semiconductor PCDTBT as the channel material and, as the ion-gating medium, we used the well-studied room temperature ionic liquid [EMIM][TFSI]. Based on the optical absorption properties of the semiconducting material, the electrical measurements were carried out under dark and light conditions allowing us to investigate the ion-gating effectiveness in different cases. The charge carrier densities obtained were 8×10^{15} cm^{-2} and 1×10^{16} cm^{-2} for dark and light conditions, respectively. Obviously, the value of charge carrier density achieved under light conditions is higher than that under dark conditions, but the difference is not significant.

In **Article 3**, we demonstrated ion-gated P3HT transistors with three different molecular weights (MWs) based on rigid (SiO_2/Si) and bendable (polyimide) substrates. The values of the charge carrier density obtained on rigid substrates were 7×10^{15} cm^{-2}, 4×10^{15} cm^{-2} and 1.2×10^{16} cm^{-2} for low MW, intermediate MW and high MW, respectively. As for bendable substrates, the values of the charge carrier density deduced were about 7×10^{15} cm^{-2} for low MW, 4×10^{15} cm^{-2} for intermediate MW and 8×10^{15} cm^{-2} for high MW. From these two sets of results on different substrates, we can deduce that intermediate MW is overshadowed by its two counterparts in charge carrier density; but the difference is not dramatic. The values of charge carrier density for low MW and high MW on bendable substrates are quite close to each other. The morphological structures of the P3HT films with different molecular weights are not the same, nor is the degree of crystallinity of the films.

8.2 Ions accompanying the doping process

As mentioned above, there are two general operating modes for ion-gated transistors: electrostatic and electrochemical. In electrostatic mode, ions are confined to the surface of the semiconducting channel; however, in electrochemical mode, ions permeate the semiconductor films and compensate for the induced charge carriers flowing between drain and source. Thus the semiconducting channel can be three-dimensional with the participation of ion penetration paired with electrochemical doping. At the same time, structural changes (e.g. swelling) are associated with the electrochemical doping process.

In **Article 1**, we investigated the doping process in ion-gated transistors making use of n-type organic semiconductor PCBM (a type of soluble fullerene derivative that can undergo several successive reversible one-electron reduction processes) interfaced with two different ionic liquids: [EMIM][TFSI] and [PYR_{14}][TFSI]. For decades the electrochemical properties of fullerene-based materials have been broadly studied in the form of thin films and in solution. As an example, C_{60} was explored in both solution and thin film forms, but results showed that the electrochemical behavior of C_{60} is more complex in thin films. Additionally, the supporting

cation in the electrolyte affects the reduction processes and generally the larger doping cation leads to larger peak splitting in the cyclic voltammograms. Taking into consideration that PCBM is capable of undergoing several redox processes, it is particularly intriguing to elucidate the role of the cations in the doping of n-type PCBM films.

The cyclic voltammetry measurements were carried out in the ion-gated PCBM transistor configuration within the interval of the electrochemical potential between 0.5V and -1.9V vs carbon reference. In [EMIM][TFSI] and [PYR_{14}][TFSI], three featured sets of reduction peaks and corresponding anodic peaks were observed and listed in Table 1. Comparing the cyclic voltammograms obtained through [EMIM][TFSI] and [PYR_{14}][TFSI], a triangular oxidation peak was observed in [PYR_{14}][TFSI] at -0.7 V, typical of surface redox processes. In addition, the linear transfer characteristics for [EMIM][TFSI]- and [PYR_{14}][TFSI]-gated transistors showed that drain-source current (I_{ds}) was higher in [EMIM][TFSI]. This indicates a higher doping effectiveness compared to [PYR_{14}][TFSI]. The significant hysteresis associated with higher transistor current in [EMIM][TFSI] revealed a bulk (three-dimensional) doping mechanism for PCBM films interfaced with [EMIM][TFSI]. However, for PCBM films interfaced with [PYR_{14}][TFSI], the doping process is likely surface-confined (two-dimensional). This is mainly due to differences in the steric hindrance and molecular structures of the two cations ($[EMIM]^+$, $[PYR_{14}]^+$).

Table 8-1 Cathodic and anodic peak positions extracted from cyclic voltammograms at a scan rate of 100 mVs^{-1}. Reference electrode: activated carbon paper.

[EMIM][TFSI]		[PYR_{14}][TFSI]	
Cathodic	Anodic	Cathodic	Anodic
-1.0 V	-1.45 V	-1.0 V	-1.5 V
-1.4 V	-1.1 V	-1.4 V	-1.05 V
-1.65 V	-0.6 V	-1.65 V	-0.7 V

8.3 Air-stability and flexibility incorporated in organic electronics

Nowadays, there are still many factors restricting the development of air-stable and flexible organic electronics. Thus, the characteristics of air-stability and flexibility open more possibilities for the potential applications of organic electronics. As for ion-gated transistors, being air-stable and flexible proves they are capable of being robust in both printable and flexible technologies.

In **Article 2**, we successfully fabricated ion-gated PCDTBT transistors and characterized the devices in ambient atmosphere. The air-operational stability of the devices was achieved, mainly due to the favorable position of the highest occupied molecular orbital of PCDTBT. From the I_{ds} *vs* V_{gs} plot at different shelf times, we observed an increase in the transistor current after 24 hours. We also obtained stability over the following days in the transistor current. The trend of the hole mobility was in agreement with the behavior of the transistor current.

In **Article 3**, we reported on P3HT ion-gated transistors with different molecular weights based on polyimide substrates. Variations of molecular weights can have an impact on the microstructure of P3HT films which, in turn, affects the charge carrier transport. Thus, the performance of the devices can correlate with the molecular weight of the semiconducting films.

In this article, the electrical and mechanical properties of the transistors with different molecular weight-P3HT films on flexible (polyimide) substrates were characterized at the same time on two different bending radii (R= 10 mm and R= 5 mm). Compared with the flat (non-bending) devices, we observed a 40% decrease in the transistor current in high molecular weight P3HT ion-gated transistors at bending condition R=10 mm. Moreover, a further 43% decrease in the transistor current was obtained at R=5 mm bending condition.

Bending cycle measurements at R=5 mm were conducted on the flexible devices with P3HT films of different molecular weights. From the mobility vs bending cycle plots, we observed an overall decrease in mobility with an increase in bending cycles compared to the initial one at rest. However, a quasi-plateau was reached for intermediate and high molecular weight P3HT films. A comparative stabilization in the mobility was obtained between 1000 and 1500 cycles, paving the way to build and develop the bridge to ion-gated transistors and flexible technologies.

CHAPTER 9 CONCLUSION AND PERSPECTIVES

In summary, this thesis is devoted to gaining insights into the compatibility between organic materials and ionic liquids in terms of electrochemical, electrical and mechanical properties established in ion-gated transistors. Also, we reviewed the working mechanism and advancements of ion-gated transistors that work under low voltage operation mode. The research demonstrated and confirmed the effectiveness of ion-gating on modulation of charge carrier density and revealed the challenges related to combining ionic liquids and organic semiconductors for air-stable and flexible applications. We performed in-depth exploration of the doping process (2D & 3D) and charge carrier transport in transistors. The focus placed on organic semiconductors (polymer and small molecule materials) adopted as transistor channel materials and ionic liquids used as gating media makes it appealing to investigate the interface among them under ion-gating.

The study of the potential applications in flexible technologies and ambient conditions for ion-gated transistors is of additional interest. It would broaden the vision and deepen the understanding of organic electronics. Moreover, photo-gating is an add-on under light conditions for ion-gated transistors, bringing added value to the research topic.

First, we observed three reduction processes in the PCBM films interfaced with ionic liquids, [EMIM][TFSI] and [PYR_{14}][TFSI], in the cyclic voltammetry experiments. A noticeable oxidation peak at -0.7V in [PYR_{14}][TFSI] with respect to its counterpart [EMIM][TFSI] was seen in a triangular shape, typical of surface redox processes. Furthermore, [PYR_{14}][TFSI] possesses higher hindrance compared to [EMIM][TFSI]. This can lead to the presence of surface-confined redox processes.

Assuming a spherical shape of the ions, the volume of cations of these two ionic liquids was estimated in theoretical calculations: 182 $Å^3$ for [EMIM] and 253 $Å^3$ for [PYR_{14}]. The size of

[PYR_{14}] is bigger than [EMIM], in turn limiting the permeation of [PYR_{14}] to travel in the fullerene films.

The transistor characterizations showed two-dimensional (2D) surface-confined doping in [PYR_{14}][TFSI] and three-dimensional (3D) doping in [EMIM][TFSI]. Additionally, we observed finite windows of high conductivity in PCBM films (*n*-type) interfaced with [PYR_{14}][TFSI], a common feature of *p*-type organic semiconductors.

We demonstrated the capability of ion-gated transistors making use of solution-processed PCDTBT films to operate stably in air conditions. The PCDTBT films obtained through different deposition methods achieved smooth surfaces (root mean square roughness (rms) of ca 0.5 nm) and completely covered the substrates. Compared with transistors based on conventional dielectrics (ca. SiO_2), ion-gated PCDTBT transistors can reach a much lower onset of the saturation region (0.4 V).

Under illumination conditions, we obtained an increase in transistor current with respect to that under dark conditions, while mobility did not change significantly. The maximum values of photoresponsivity and photosensitivity obtained were 1 and 7.3 AW^{-1}.

PCDTBT itself possesses intrinsic stability attributed to the low position of the highest occupied molecular orbital (HOMO, located at ca. -5.5 eV vs vacuum). Thus, we extended the air-stability study to ion-gated transistors, making use of PCDTBT films. The devices were placed in ambient conditions at different shelf times up to about 150 hours: a stable transistor current was obtained during subsequent measurements after the first day. An analogous behavior in hole mobility with the transistor current was also observed.

We fabricated ion-gated P3HT transistors of three different molecular weights (~20 kDa, 30-50 kDa and 80-90 kDa), compatible with processing on rigid (SiO_2/Si) and flexible (polyimide) substrates. The molecular weight of P3HT is correlated with the structure and morphology of the films, studied by X-ray diffraction and atomic force morphology. In turn, performance of the devices based on P3HT films is related to the molecular weight as well.

The values of the hole mobility obtained on SiO_2/Si substrates were ca 0.10 $cm^2 V^{-1} s^{-1}$, 0.13 $cm^2 V^{-1} s^{-1}$ and 0.09 $cm^2 V^{-1} s^{-1}$ for low, intermediate and high molecular weight. The ON/OFF ratios were 1×10^5 for low molecular weight, 8.5×10^3 for intermediate molecular weight and 7.5×10^3 for high molecular weight.

To shed light on the flexibility of the devices, we fabricated them on polyimide substrates and characterized their electrical and mechanical properties. The hole mobility values obtained on flexible substrates were 0.09 $cm^2 V^{-1} s^{-1}$, 0.12 $cm^2 V^{-1} s^{-1}$ and 0.10 $cm^2 V^{-1} s^{-1}$ for low, intermediate and high molecular weight, respectively. With further bending measurements (curvature radii (R) are 10 mm and 5 mm) performed on the devices for high molecular weight, a comparison between the flat and bent devices showed approximately a 40% decrease in the transistor current at V_{gs}=-1.5V at R=10 mm. Further bending measurements at R=5 mm presented another 43% decrease in I_{ds}.

The stability of bendable devices is paramount, so we chose a bending radius R=5 mm to carry on the bending cycle tests (up to 1500 cycles). The plots of hole mobility vs the number of bending cycles showed an overall decrease in hole mobility with an increase in the bending cycles. Nevertheless, after 1000 cycles, a quasi-plateau in hole mobility was achieved in intermediate and high molecular weights.

This thesis is primarily focused on the study of ion-gated transistors. It provides, as well, different aspects regarding the function of ion-gating and establishes basic guidelines for the application of ion-gating in thin film transistors. This work may be applied to the development of other electronic devices, thus laying the foundation for further research, such as:

(i) Fully flexible ion-gated transistors

The flexibility of ion-gated transistors was studied in this work. The study could be extended to stretchable substrates obtained by employing polydimethylsiloxane (PDMS). However, the options for gate electrode remain open. These include metal nanoparticles, graphene, metal nanowires, etc. There still exist a number of challenges for fully flexible ion-gated transistors,

such as the balance between performance and stability. It will be appealing to carry out a thorough study on the electrical and mechanical properties of fully flexible devices.

(ii) Ion-gated light-emitting transistors: integration of light emitting and ion-gating

It is of great interest to equip ion-gated transistors with new functions. Light emitting is one of them as it will be combined with ion-gating in a transistor configuration. This will provide us with the opportunity to study how ion-gating modulates charge carrier density and emitted light simultaneously. How the doping process will work along with light emission is an intriguing question that remains for us to answer.

(iii) Towards green electronics

Ionic liquids possess the potential to work as green gating media. Thus, they open the possibility to be applied in green electronics which includes ion-gated transistors. With the development of materials engineering, more and more researchers are working on programming materials to be environmentally friendly. In addition, the biodegradability characteristic is particularly valued. Biosourced organic semiconductors could act as green channel materials for IGTs. This creates a new opportunity for ion-gated transistors to step closer to green electronics.

REFERENCES

1. J. A. F. Sir, The Thermionic Valve and Its Developments in Radio-telegraphy and Telephony, Andesite Press, 2017, 08.
2. L. J. Edgar, "Method and apparatus for controlling electric currents," United States Patent, 1930.
3. B. John, Brattain, Walter H., "Three-electrode circuit element utilizing semiconductive materials," United States Patent, 1950.
4. S. William, "Circuit element utilizing semiconductive material," United States Patent, 1951.
5. "The Nobel Prize in Physics 1956", Nobelprize.org. Nobel Media AB.
6. "1948: Conception of the Junction Transistor - The Silicon Engine - Computer History Museum". Retrieved August 10, 2016.
7. W. E. Bradley, PRO. I. R. E., 1953, 41, 1702.
8. "First Transistor IEEE Milestone Dedication" (PDF). IEEE Newsletter. North Jersey Section of the Institute of Electrical and Electronics Engineers, 2009, 56, 5.
9. ScienCentral. "The First Silicon Transistor". www.pbs.org. Archived from the original on November 2, 2017.
10. "1960 - Metal Oxide Semiconductor (MOS) Transistor Demonstrated". The Silicon Engine. Computer History Museum.
11. "1963: Complementary MOS Circuit Configuration is Invented". Computer History Museum. Retrieved July 6, 2019.
12. P. K. Weimer, Pro. IRE., 1962, 50, 1462.

13. P. V. Necliudov, M. S. Shur, D. J. Gundlach and T. N. Jackson, J. Appl. Phys., 2000, 88, 6594.

14. I. G. Hill, Appl. Phys. Lett., 2005, 87, 163505.

15. D. J. Gundlach, L. Zhou, J. A. Nichols, T. N. Jackson, P. V. Necliudov and M. S. Shur, J. Appl. Phys., 2006, 100, 024509.

16. D. Gupta, M. Katiyar and D. Gupta, Org. Electron., 2009, 10, 775.

17. C. H. Shim, F. Maruoka and R. Hattori, IEEE Trans. Electron Devices., 2010, 57, 195.

18. H. Klauk, Organic Electronics II More Materials and Applications, Wiley-VCH Verlag&Co. KGaA, 2012.

19. D. J. Gundlach, L. Jia and T. N. Jackson, IEEE Electron Device Lett., 2001, 22, 571.

20. Q. J. Cai, M. B. Chan-Park, Q. Zhou, Z. S. Lu, C. M. Li and B. S. Ong, Org. Electron., 2008, 9, 936.

21. H. Klauk, Chem. Soc. Rev., 2010, 39, 2643.

22. M. C. Buzzeo, R. G. Evans and R. G. Compton, Chem. Phys. Chem., 2004, 5, 1106.

23. R. Giles, J. Evett, and C. Liu, Schaum's Outline of Fluid Mechanics and Hydraulics, 3ed (McGraw Hill Professional, 2009).

24. P. Hapiot and C. Lagrost, Chem. Rew., 2008, 108, 2238.

25. S. Zhang, N. Sun, X. He, X. Lu, and X. J. Zhang, Phys. Chem. Ref. Data., 2006, 35, 1475.

26. E. I. Izgorodina, M. Forsyth, D. Aust. MacFarlane, J. Chem., 2007, 60, 15.

27. S. P. Ong, O. Andreussi, Y. Wu, N. Marzaria and G. Ceder, Chem. Mater., 2011, 23, 2979.

28. S. Z. Bisri, S. Shimizu, M. Nakano, and Y. Iwasa, Adv. Mater., 2017, 29, 1607054.

29. D. H. Wu, X. Lin, Z. M. Xu and D. W. Chu, J. Mater. Sci., 2010, 50, 5641.

30. T. Fujimoto and K. Awaga, Phys. Chem. Chem. Phys., 2013, 15, 8983.

31. T. Uemura, R. Hirahara, Y. Tominari, S. Ono, S. Seki and J. Takeya, Appl. Phys, 2008, 93, 263305.

32. Y. Xia, J. H. Cho, J. Lee, P. P. Ruden and C. D. Frisbie, Adv. Mater., 2009, 21, 2174.

33. T. Uemura, M. Yamagishi, S. Ono and J. Takeya, Jon. J. Appl. Phys., 2010, 49, 01AB13.

34. Q. S. Xie, E. P.-Cordero, and L. Echegoyen, J. Am. Chem. Soc., 1992, 114, 3978.

35. J. Chlistunoff, D. Cliffel and A. J. Bard, Thin Solid Films, 1995, 257, 166.

36. B. W. Larson, J. B. Whitaker, A. A. Popov, N. Kopidakis, G. Rumbles, O. V. Boltalina, and S. H. Strauss, Chem. Mater., 2014, 26, 2361.

37. B. W. Larson, J. B. Whitaker, X. B. Wang, A. A. Popov, G. Rumbles, N. Kopidakis, S. H. Strauss and O. V. Boltalina, J. Phys. Chem. C., 2013, 117, 14958.

38. D. Boucher and J. Howell, J. Phys. Chem. B., 2016, 120, 11556.

39. D. Ofer, R. M. Crooks and M. S. Wrighton, J. Am. Chem. Soc., 1990, 112, 7869.

40. E. W. Paul, A. J. Ricco and M. S. Wrighton, J. Phys. Chem., 1985, 89, 1441.

41. D. Ofer, T. M. Swager and M. S. Wrighton, Chem. Mater., 1995, 7, 418.

42. D. Ofer and M. S. Wrighton, J. Am. Chem. Soc., 1988, 110, 4468.

43. B. D. Paulsen and C. D. Frisbie, J. Phys. Chem. C., 2012, 116, 3132.

44. D. A. C. Brownson and C. E. Banks, The Handbook of Graphene Electrochemistry, Springer-Verlag London, 2014.

45. N. Elgrishi, K. J. Rountree, B. D. McCarthy, E. S. Rountree, T. T. Eisenhart and J. L. Dempsey, J. Chem. Educ., 2018, 95, 197.

46. R. G. Compton, E. Laborda and K. R. Ward, Understanding Voltammetry: Simulation of Electrode Processes, Imperial College Press, 2014.

47. I. Kymissis, Organic Field Effect Transistors: Theory, Fabrication and Characterization, Springer Science + Business Media, 2009.

48. S. Beaupré and M. Leclerc, J. Mater. Chem. A., 2013, 1, 11097.

49. D. M. de Leeuw, M. M. J. Simenon, A. R. Brown, R. E. F. Einerhand, Synth. Met., 1997, 87, 53.

50. S. Cho, J. H. Seo, S. H. Park, S. Beaupré, M. Leclerc and Alan J. Heeger, Adv. Mater., 2010, 22, 1253.

51. P. Jha, S. P. Koiry, V. Saxena, P. Veerender, A. Gusain, A. K. Chauhan, A. K. Debnath, D. K. Aswal and S. K. Gupta, Org. Electron., 2013, 14, 2635.

52. H. H. Xu, J. Li, B. H. K. Leung, C. C. Y. Poon, B. S. Ong, Y. T. Zhanga and N. Zhao, Nanoscale., 2013, 5, 11850.

53. H. J. Nam, J. Cha, S. H. Lee, W. J. Yoo and D. Y. Jung, Chem. Commun., 2014, 50, 1458.

54. F. Li, Y. Chen, C.Ma, U. Buttner, K. Leo and T. Wu, Adv. Electron. Mater., 2017, 3, 1600430.

55. Y. Liu, J. Zhao, Z. Li, C. Mu, W. Ma, H. Hu, K. Jiang, H. Lin, H. Ade, H. Yan, Nat. Commun., 2014, 5, 5293.

56. R. D. Jansen-van Vuuren, A. Armin, A. K. Pandey, P. L. Burn and P. Meredith, Adv. Mater., 2016, 28, 4766.

57. H. Sirringhaus, Adv. Mater., 2014, 26, 1319.

58. X. Guo, M. Baumgarten, K. Müllen, Prog. Polym. Sci., 2013, 38, 1832.

59. A. G. Dixon, R. Visvanathan, N. A. Clark, N. Stingelin, N. Kopidakis, S. E. Shaheen, J .Polym. Sci. B. Polym. Phys., 2018, 56, 31.

60. R. J. Kline, M. D. MaGehee, E. N. Kadnikova, J. S. Liu and J. M. Frechet, Adv. Mater., 2003, 15, 1519.

61. P. Pingel, A. Zen, R. D. Abellón, F. C. Grozema, L. D. A. Siebbeles and D. Neher, Adv. Funct. Mater., 2010, 20, 2286.

62. R. V. Giles, J. B. Evett and C. Liu, Schaum's Outline of Theory and Problems of Fluid Mechanics and Hydraulics, Third Edition, McGraw-Hill, 1994.

63. P. Ramm, J. J. Q. Lu and M. M. V. Taklo, Handbook of Wafer Bonding, WILEY-VCH Verlag GmbH & Co.KGaA, 2012.

64. J. Y. Na, B. Kang and Y. D. Park, J. Phys. Chem., 2019, 123, 17102.

65. J. Rivnay, S. Inal, A. Salleo, R. M. Owens, M. Berggren and G. G. Malliaras, Nat. Rev. Mater., 2008, 3, 17086.

66. S. R. Forrest, Nature, 2004, 428, 911.

67. S. Fabiano, S. Braun, M. Fahlman, X. Crispin and M. Berggren, Adv. Funct. Mater., 2014, 24, 695.

68. M. S. Thomas, S. P. White, K. D. Dorfman and C. D. Frisbie, J. Phys. Chem. Lett., 2018, 9, 1335.

69. T. Lan, F. Bélanger, F. Soavi and C. Santato, Org. Electron., 2019, 73, 265.

70. Z. Q. Xie, R. Avila, Y. G. Huang and J. A. Rogers, Adv. Mater., 2019, 32, 1902767.

71. M. S. White, M. Kaltenbrunner, E. D. Głowacki, K. Gutnichenko, G. Kettlgruber, I. Graz, S. Aazou, C. Ulbricht, D. A. M. Egbe, M. C. Miron, Z. Major, M. C. Scharber, T. Sekitani, T. Someya, S. Bauer and N. S. Sariciftci, Nat. Photonics., 2013, 07, 811.

72. G. D. Spyropoulos, J. N. Gelinas and D. Khodagholy, Sci. Adv., 2019, 5, 7378.

73. H. Tanaka, K. Kanahashi, N. Takekoshi, H. Mada, H. Ito, Y. Shimo, H. Ohta and T. Takenobu, Sci. Adv., 2020, 6, 8065.

74. S. P. Tiwari, E. B. Namdas, V. R. Rao, D. Fichou and S. G. Mhaisalkar, IEEE Electron Device Lett., 2007, 28, 880.

75. M. J. Earle, J. M. S. S. Esperança, M. A. Gilea, J. N. Canongia, L. P.N. Rebelo, J. W. Magee, K. R. Seddon, and J. A. Widegren, Nature, 2006, 439, 831.

76. D. D. Tullio, M. Magliulo, G, Colafemmina, K. Manoli, L. Torsi and G. Palazzo, Sci. Adv. Mater., 2013, 05, 1922.

77. S. E. Root, S. Savagatrup, A. D. Printz, D. Rodriquez and D. J. Liponmi, Chem. Rev., 2017, 117, 6467.

78. R. Noriega, J. Rivnay, K. Vandewal, F. P. V. Koch, N. Stingelin, P. Smith, M. F. Toney and A. Salleo, Nat. Mater., 2013, 12, 1038.

79. J. T. Friedlein, R. R. McLeod and J. Rivnay, Org. Electron., 2018, 63, 398.

80. R. G. Compton and J. D. Wadhawan, Electrochemistry Volume II Nanosystems Electrochemistry. The Royal Society of Chemistry, 2013.

81. https://www.ossila.com.

82. Y. Diao, L. Shaw, Z. N. Bao and S. C. B. Mannsfeld, Energy Environ. Sci., 2014, 7, 2145.

83. http://home.deib.polimi.it/sampietr/ESO/Grimoldi.pdf.

84. Data Measured and Provided by IoLiTec Ionic Liquids Technologies GmbH, Heilbronn/Germany, 2012.

85. A. J. Bard and L. R. Faulkner, Electrochemical Methods Fundamentals and Applications., John Wiley&Sons, INC, 2001.

86. G, Binnig, C. F. Quate, C. Gerber, Phys. Rev. Lett., 1986, 56, 930.

87. https://warwick.ac.uk/fac/sci/physics/current/postgraduate/regs/mpagswarwick/ex5/techniques/structural/afm/

88. Y. H. Seo and W. H. Jhe, Rep. Prog. Phys., 2008, 7, 016101.

89. E. Casero, L. Vázquez, A. M. P-Alfambra and E. Lorenzo, Analyst, 2010, 135, 1878.

90. https://www.freiberginstruments.com/x-ray-diffraction/technology/theta-scan.html

91. M. Ladd and R. Palmer, Structure Determination by X-ray Crystallography, Springer Science + Business Media New York, 2013.

92. G. Tarabella, F. M. Mohammadi, N. Coppedè, F. Barbero, S. Iannotta, C. Santato and F. Cicoira, Chem. Sci., 2013, 4, 1395.

93. T. Someya, Z. Bao and G. G. Malliaras, Nature, 2016, 540, 379.

94. S. H. Kim, K. Hong, W. Xie, K. H. Lee, S. Zhang, T. P. Lodge and C. D. Frisbie, Adv. Mater., 2013, 25, 1822.

95. F. Cicoira and C. Santato (Eds), Organic Electronics: Emerging Concepts and Technologies, J. Wiley & Sons, 2013.

96. O. G. Reid and G. Rumbles, J. Phys. Chem. C., 2016, 120, 87.

97. G. Yu, J. Gao, J. C. Hummelen, F. Wudl and A. J. Heeger, Science, 1995, 270, 1789.

98. P. H. Wöbkenberg, D. D. C. Bradley, D. Kronholm, J. C. Hummelen, D. M. de Leeuw, M. Cöll and T. D. Anthopoulos, Synth. Met., 2008, 158, 468.

99. F. Cicoira, C. M. Aguirre, and R. Martel, ACS Nano., 2011, 5, 283.

100. F. Paolucci, M. Marcaccio, S. Roffia, G. Orlandi, F. Zerbetto, M. Prato, M. Maggini and G. Scorrano, J. Am. Chem. Soc., 1995, 117, 6572.

101. M. Maggini, A. Karlsson, G. Scorrano, G. Sandonà, G. Farnia, M. Prato, J. Chem. Soc., Chem. Commun., 1994, 0, 589.

102. R. Mens, S. Chambon, S. Bertho, G. Reggers, B. Ruttens, J. D'Haen, J. Manca, R. Carleer, D. Vanderzande and P. Adriaensens, Magn. Reson. Chem., 2011, 49, 242.

103. J. Garshe, C. Dyer, P. Moseley, Z. Ogumi, D. Rand and B. Scrosati, Encyclopedia of Electrochemical Power Sources, Amsterdam, Elsevier, 2009, 1, 649.

104. J. Sayago, F. Soavi, Y. Sivalingam, F. Cicoira and C. Santato, J. Mater. Chem. C., 2014, 2, 5690.

105. N. Jackson, F. Stama, J. O'Brien, L. Kailas, A. Mathewson and C. O'Murchu, Thin Solid Films, 2016, 63, 371.

106. M. N. Kobrak, Green Chem., 2008, 10, 80.

107. J. Barthel, H. Krienke and W. Kunz, Physical Chemistry of Electrolyte Solutions: Modern Aspects, Springer, 1998.

108. G. Valenti, C. Bruno, S. Rapino, A. Fiorani, E. A. Jackson, L. T. Scott F. Paolucci, M. Marcaccio, J. Phys. Chem. C., 2010, 114, 19467.

109. T. D. Anthopoulos, C. Tanase, S. Setayesh, E. J. Meijer, J. C. Hummelen, P. W. M. Blom and D. M. de Leeuw, Adv. Mater., 2004, 16, 2175.

110. R. L. Fu, R. T. Fu and X. Sun, Phys. Rev. B,. 1993, 48, 17615.

111. K. Ueno, K. Yoshida, M. Tsuchiya, N. Tachikawa, K. Dokko and M. Watanabe, J. Phys. Chem. B., 2012, 116, 11323.

112. F. Messaggi, I. Ruggeri, D. Genovese, N. Zaccheroni, C. Arbizzani and F. Soavi, Electrochim. Acta., 2017, 245, 296.

113. F. Wu, Q. Z. Zhu, R. J. Chen, N. Chen, Y. Chen and L. Li, Electrochim. Acta., 2015, 184, 356.

114. M. J. Panzer and C. Daniel Frisbie, J. Am. Chem. Soc., 2007, 129, 6599.

115. M. Singh, K. Manoli, A. Tiwari, T. Ligonzo, C. Di Franco, N. Cioffi, G. Palazzo, G. Scamarcio and L. Torsi, J. Mater. Chem. C., 2017, 5, 3509.

116. T. Lan, F. Soavi, M. Marcaccio, P. L. Brunner, J. Sayago and C. Santato, Chem. Commun., 2018, 54, 5490.

117. T. Pajkossy and R. Jurczakowski, Curr. Opin. Electrochem., 2017, 1, 53.

118. N. Blouin, A. Michaud and M. Leclerc, Adv. Mater., 2007, 19, 2295.

119. K.J. Baeg, M. Binda, D. Natali, M. Caironi, Y. Y. Noh, Adv. Mater., 2013, 25, 4267.

120. N. Blouin, A. Michaud, D. Gendron, S. Wakim, E. Blair, R. Neagu-Plesu, M. Belletete, G. Durocher, Y. Tao, M. Leclerc, J. Am. Chem. Soc., 2008, 130, 732.

121. Y. Xia, J. H. Cho, B. Paulsen, C. D. Frisbie and M. J. Renn, Appl. Phys. Lett., 2009, 94, 013304.

122. L. Hrostea, M. Girtan, R. Mallet and L. Leontie, IOP Conf. Ser.: Mater. Sci. Eng., 2018, 374, 012015.

123. G. Dennler, M. C. Scharber and C. J. Brabec, Adv. Mater., 2009, 21, 1323.

124. N. E. Persson, P.-H. Chu, M. McBride, M. Grover and E. Reichmanis, Acc. Chem. Res., 2017, 50, 932.

125. O. G. Reid, J. A. N. Malik, G. Latini, S. Dayal, N. Kopidakis, C. Silva, N. Stingelin and G. Rumbles, J. Polym. Sci. B., 2012, 50, 27.

126. A. M. Ballantyne, L. Chen, J. Dane, T. Hammant, F. M. Braun, M. Heeney, W. Duff, I. McCulloch, D. D. C. Bradley and J. Nelson, Adv. Funct. Mater., 2008, 18, 2373.

127. H. Sirringhaus, P. J. Brown, R. H. Friend, M. M. Nielsen, K. Bechgaard, B. M. W. Langeveld-Voss, A. J. H. Spiering, R. A. J. Janssen, E. W. Meijer, P. Herwig and D. M. de Leeuw, Nature, 1999, 401, 686.

128. M. Roesing, J. Howell and D. Boucher, J. Polym. Sci. B., 2017, 55, 1075.

129. D. R. Morey and J. W. Tamblyn, J. Appl. Phys., 1945, 16, 419.

130. X. Li, R. Xing, Y. Zhang, Y. C. Han and L. J. An, Polymer., 2004, 45, 1637.

131. J. H. Cho, J. Lee, Y. Y. He, B. S. Kim, T. P. Lodge and C. D. Frisbie, Adv. Mater., 2008, 20, 686.

132. Y. Na and F. S. Kim, Chem. Mater., 2019, 31, 4759.

133. S. Zhang, E. Hubis, G. Tomasello, G. Soliveri, P. Kumar and F. Cicoira, Chem. Mater., 2017, 29, 3126.

APPENDIX A - SUPPORTING INFORMATION OF ARTICLE 1

Electrolyte-gated transistors based on phenyl-C61-butyric acid methyl ester (PCBM) films: bridging redox properties, charge carrier transport and device performance

Tian Lan, [a] Francesca Soavi, [b] Massimo Marcaccio, [b] Pierre-Louis Brunner, [c] Jonathan Sayago [d]* and Clara Santato [a] *

[a.] *Polytechnique Montréal, Département de Génie physique, Montréal, Québec H3C 3A7,*
[b.] *Department of Chemistry "Giacomo Ciamician", Università di Bologna, 40126, Italy*
[c.] *Solaris Chem Inc., 598 Chaline St., Saint-Lazare, Quebec, J7T 3E8, Canada*
[d.] *Instituto de Energías Renovables, Universidad Nacional Autónoma de México, Temixco, Morelos 62588, Mexico*

Experimental

SiO_2/Si substrates were photolithographically patterned with source and drain electrodes (Au 40 nm- thick on Ti adhesion film, 4 nm-thick) with interelectrode distance, *L*, of 10 μm and width, *W*, of 4 mm. A layer 1.6 μm-thick of Parylene C (Cookson Electronics, MW 500 kDa) was deposited on the patterned substrate and a rectangle of 1 mm × 5 mm, centered on the transistor channel, was etched away through photolithography and reactive ion etching. Prior to deposition of the PCBM semiconducting films, the substrates were cleaned with sequential steps of 5 min in isopropyl alcohol, 10 min in acetone and 5 min in isopropyl alcohol in ultrasonic baths. PCBM solutions consisting of 5 mg PCBM (Solaris Chem Inc) in 1 ml chlorobenzene stirred overnight in a N_2 glove box at room temperature were prepared. PCBM thin film were deposited by drop-cast on the substrates and set on a hot plate at 50 °C for 2 h in N_2 glove box (< 5 ppm O_2, H_2O). The typical thickness of the films measured with profilometer was 380 nm. [EMIM][TFSI] or [PYR_{14}][TFSI] (IoLiTec, >99%) ionic liquids were purified at 100 °C, 10^{-5} Torr overnight.

The ionic liquids were contained in a Durapore® membrane, 4 mm × 9 mm-sized, 125 μm-thick, laminated on top of the PCBM channel. The gate electrodes consisted of high surface area carbon paper (Spectracarb 2050), 6 mm × 3 mm, 170 μm thick, coated with an ink of activated carbon (PICACTIF SUPERCAP BP10, Pica, 28 mg ml^{-1}) and polyvinylidene fluoride (PVDF, KYNAR HSV900, 1.4 mg ml^{-1}) binder, in N-methyl pyrrolidone (NMP, Fluka). The microfabrication process flow is shown in S1. Transistor electric characteristics were acquired employing an Agilent B1500A semiconductor parameter analyzer connected to a house-made micromanipulated electrical probe station. Electrochemical characterizations were measured in situ with a VersaSTAT 4 potentiostat. X-ray diffraction (XRD) spectra of the PCBM thin films was taken using Bruker D8 diffractometer equipped with a copper source for X-rays with a wavelength (Cu K_a) of 1.54 Å. Scanning Electron Microscopy (SEM) images were taken in air, at room temperature on a Digital Instruments Dimension 3100 in tapping mode with Al-coated silicon cantilevers. 4M [Li][TFSI] (Sigma Aldrich, 99.95%) in tetraethylene glycol dimethyl ether (TEGDME) (Sigma Aldrich, ≥99%) was prepared stirring overnight in a N_2 glove box at room temperature.

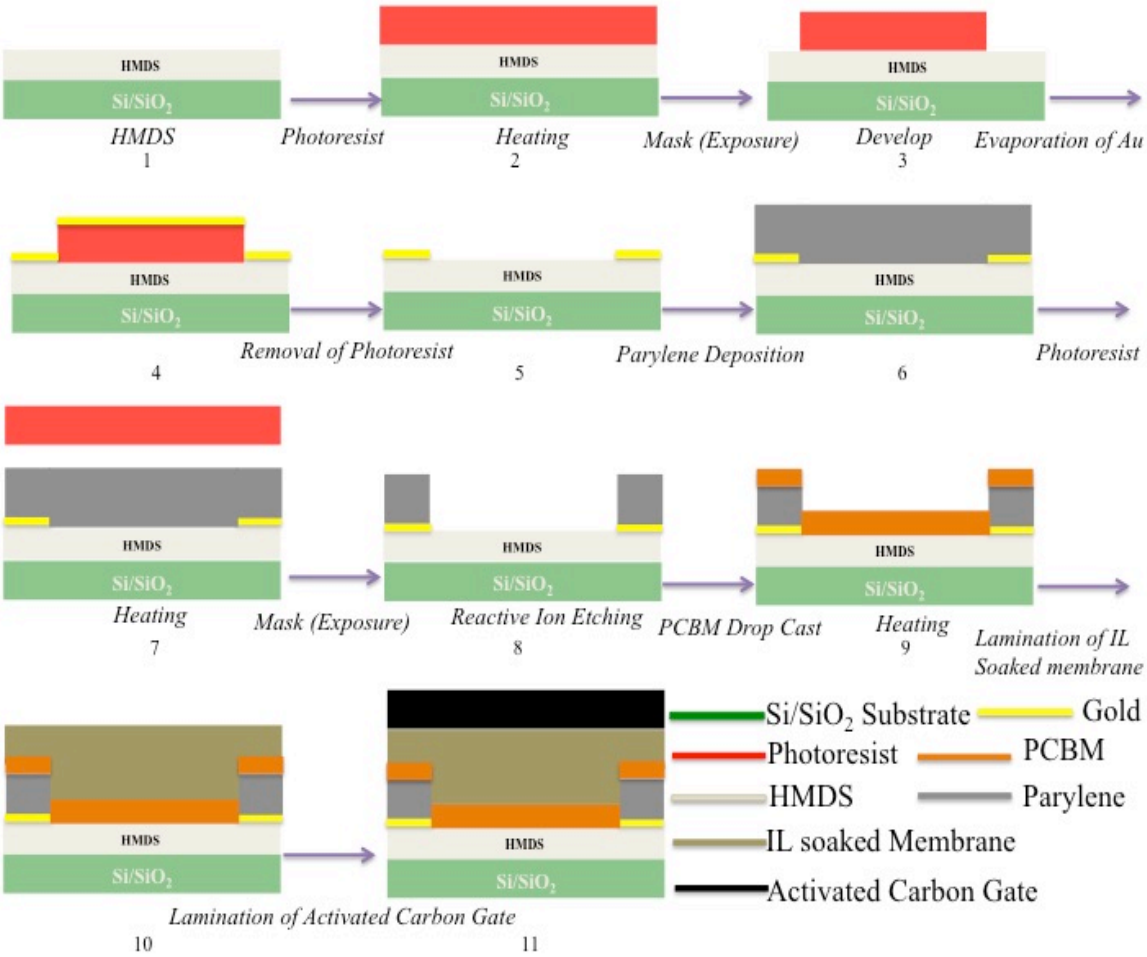

Fig. S1. Microfabrication process flow.

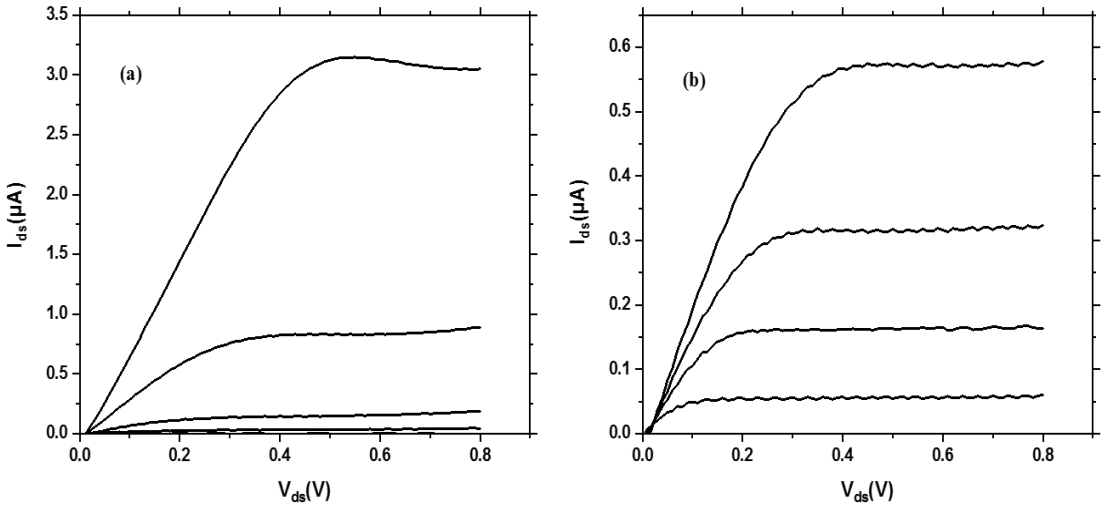

Fig. S2. Output characteristics for V_{gs} = 0, 0.8, 0.9, 1, 1.1 V, at 10 mVs^{-1}, for (a) [EMIM][TFSI]- and (b) [PYR_{14}][TFSI]- gated PCBM transistors.

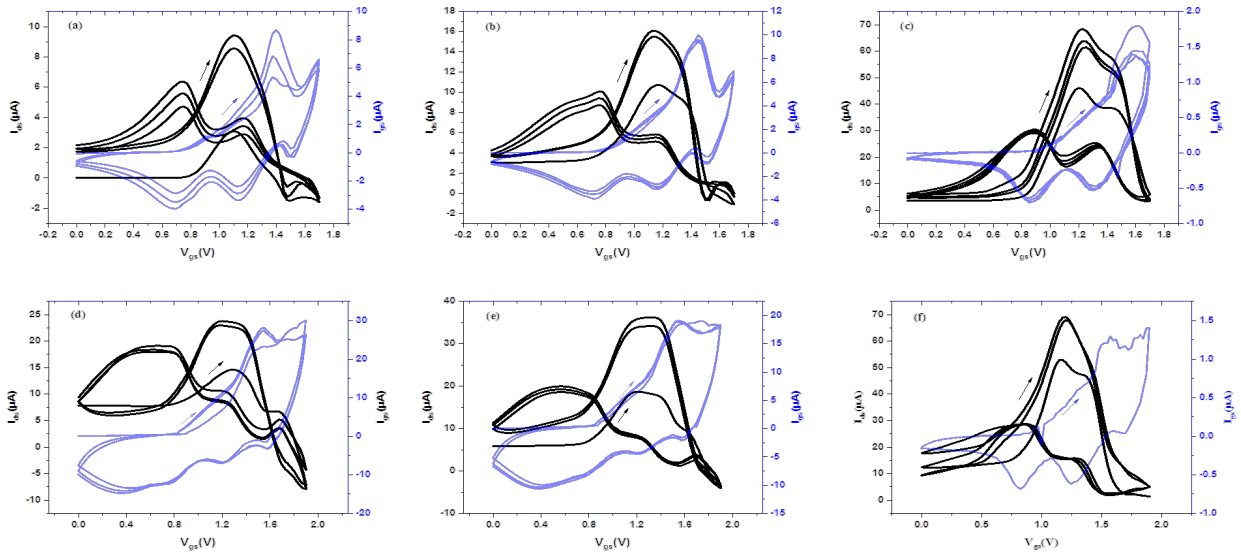

Fig. S3. Transfer characteristics obtained for increased values of V_{gs} for [EMIM][TFSI]-gated PCBM transistors. For (a) (b) (c) the interval is 0 V / 1.7 V. For (d) (e) (f) the interval is 0 V /1.9 V. V_{gs} sweeping rates: (a) and (d) 100 mVs^{-1}, (b) and (e) 50 mVs^{-1}, (c) and (f) 1 mVs^{-1}. In Fig. S4 f only the 3rd cycle of the I_{gs} vs V_{gs} is reported due to the weak (and as such relatively noisy) values of I_{gs} measured for the 1st and 2nd cycles.

In [EMIM][TFSI], for V_{gs} up to 1.7 V, at 100 mVs^{-1}, during the 1st forward scan of the I_{ds} vs V_{gs} plots (three cycles are shown in Fig. S3a) one peak is observable, located at ca 1.1 V. A peak shoulder is observable at 1.45 V (a second peak, of weak intensity, is located at ca.1.6 V). The peak at ca 1.1 V is more intense during the 2nd and 3rd cycle, with respect to the 1st one. In the backward scan, two peaks are observable; the peak position shift towards lower potentials from the 1st to the 3rd cycle. The decrease of the rate from 100 mVs^{-1} to 50 mVs^{-1} and 1 mVs^{-1} leads to a clear increase of the transistor current, as expected. The position of the peak current slightly shifts to higher potentials with the decrease of scan rate. I_{gs} vs V_{gs} plots recorded at 100 mVs^{-1}

and 50 mVs^{-1} (Fig. S3a and S3b) show, on the forward scan, one shoulder at ca 1 V and a peak at ca 1.375 (1.475) V for 100 (50) mVs^{-1}. There are three peaks in the I_{gs} vs V_{gs} backward scans at high sweeping rates whereas only two peaks are observable at 1 mVs^{-1}. I_{ds} vs V_{gs} and I_{gs} vs V_{gs} plots show comparable values of the current for 100 mVs^{-1} and 50 mVs^{-1} whereas I_{ds} has clearly higher values than I_{gs} at 1 mVs^{-1}.

In [EMIM][TFSI], for V_{gs} up to 1.9 V, during the first forward scan of the I_{ds} vs V_{gs} plots (three cycles are shown in Fig. S3d) one peak is observable, located at ca 1.275 V, 1.225 V and 1.175 V from the highest to the lowest scan rate. One shoulder is found at ca. 1.425 V. The peaks are more intense during the 2nd and 3rd cycle, with respect to the 1st one. In the backward scan, three peaks are observable at 100 mV s^{-1} and 50 mV s^{-1}, whereas only two peaks are observable at 1 mVs^{-1}. I_{gs} vs V_{gs} plots show, on the forward scan of the 1st cycle, one shoulder at ca 1.2 V, together with a peak at ca 1.55 V for 100 mVs^{-1} and 50 mVs^{-1}; on the other hand, three peaks are observable in the backward scans. I_{ds} vs V_{gs} and I_{gs} vs V_{gs} plots also show comparable values of the current for I_{ds} and I_{gs} for 100 mVs^{-1} and 50 mVs^{-1} whereas I_{ds} is clearly more intense than I_{gs} at 1 mVs^{-1}. With respect to [PYR14][TFSI] (see main file), I_{ds} vs V_{gs} plots observed with PCBM films in [EMIM][TFSI] seems mainly governed by the ionic component of the transport, in agreement with the results observed for excursions of V_{gs} carried out up to V_{gs}=1.25 V; in [EMIM][TFSI], it is more challenging to extract information on the electronic contribution of the transport.

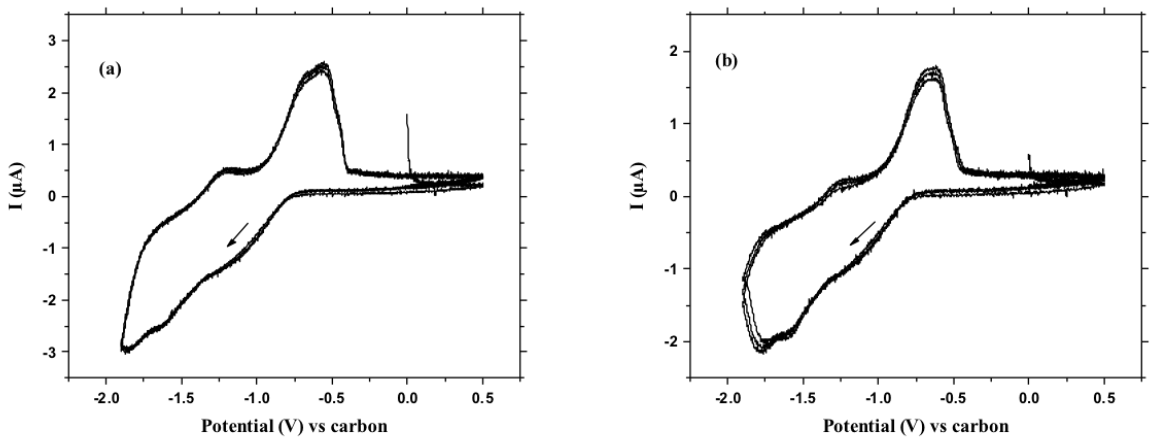

Fig. S4. Cyclic voltammograms in transistor configuration for PCBM films in 4 M [Li][TFSI] in tetraethylene glycol dimethyl-ether (TEGDME), with sweep rates of 100 $mV \cdot s^{-1}$ (a) and 50 $mV \cdot s^{-1}$ (b). The quasi reference electrode is made of high surface area activated carbon. Only the first three cycles are shown.

In 4 M [Li][TFSI] in TEGDME, PCBM electrodes feature, during the forward (cathodic) scan, two reduction processes located at around -1.0 V (shoulder) and -1.6 V (weak peak) at 100 $mV \cdot s^{-1}$ whereas three reduction processes are observable at 50 $mV \cdot s^{-1}$, located at around -1.0 V (shoulder), -1.6 V (weak peak) and -1.75 V (peak) vs carbon. During the backward (anodic) scan, two anodic processes are observed: one located at around -1.25 V (weak peak), both for 100 $mV \cdot s^{-1}$ and 50 $mV \cdot s^{-1}$, and another one located at around -0.5 V (peak with shoulder at -0.75 V) for 100 $mV \cdot s^{-1}$ and -0.7 V (*flat* peak), for 50 $mV \cdot s^{-1}$. It is possible to observe that the voltammograms are less resolved than in the [EMIM][TFSI] and [PYR14][TFSI] cases.

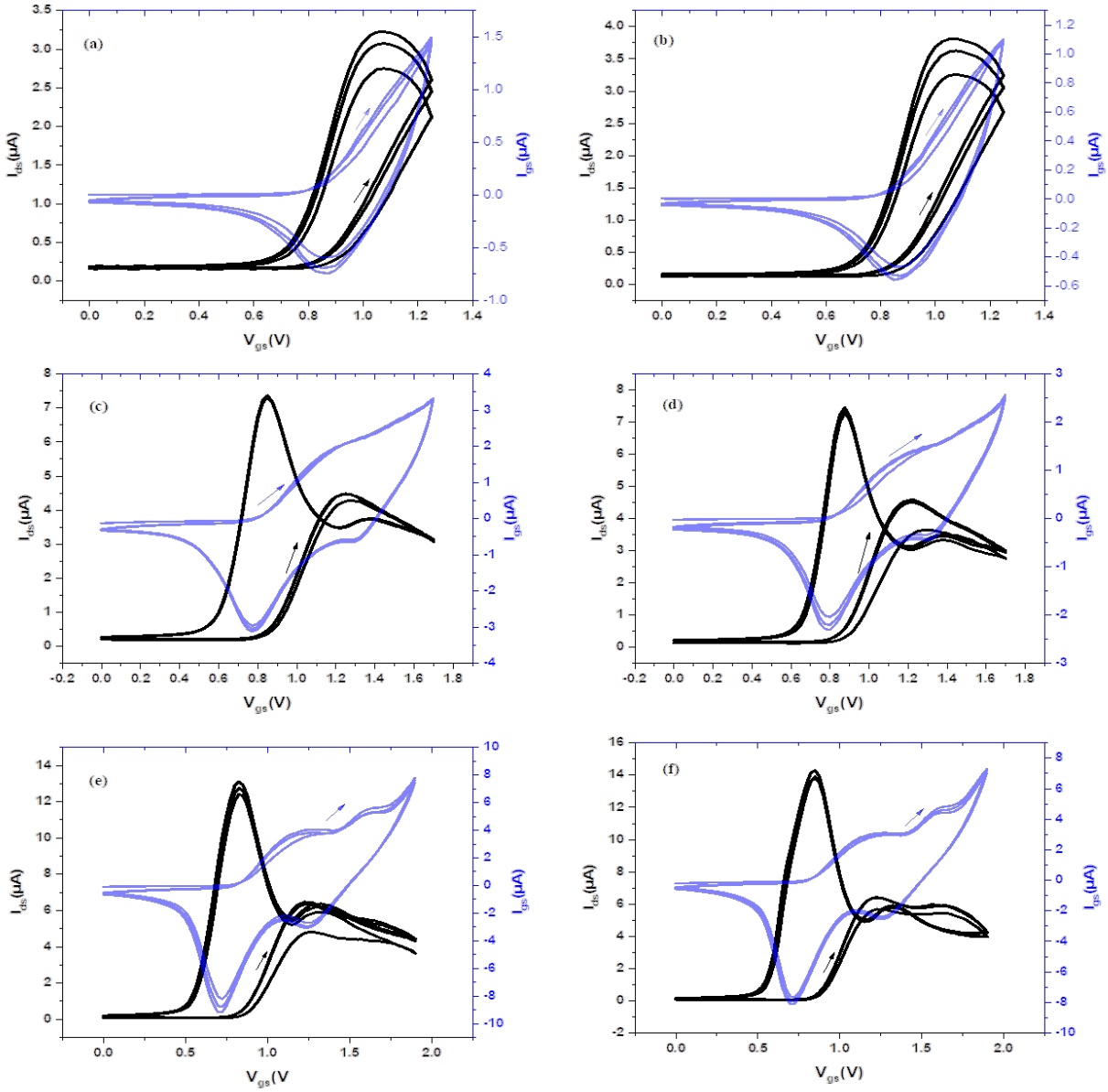

Fig. S5. Transfer characteristics obtained for PCBM transistors gated with 4 M [Li][TFSI] in TEGDME for increasing upper limits of V_{gs}. For (a) (b) the interval is 0 V/1.25 V. For (c) (d) the interval is 0 V/1.7 V. For (e) (f) the interval is 0 V/1.9 V. V_{gs} sweeping rates: (a), (c) and (e) 100 $mV \cdot s^{-1}$, (b), (d) and (f) 50 $mV \cdot s^{-1}$.

The linear transfer characteristics for 4 M [Li][TFSI] in TEGDME show that the transistor currents increase with the decrease of the sweep rate, as expected (see main text). For V_{gs} up to 1.25 V, I_{ds} vs V_{gs} plots at 100 mVs^{-1} and 50 mVs^{-1}, show one peak during the backward scan. For V_{gs} up to 1.7 and 1.9 V, during the forward scan, one broad peak is observable both at 100 $mV \cdot s^{-1}$ and 50 $mV \cdot s^{-1}$. At these two rates, in the backward scan, an intense peak is observable, located at lower potentials with respect to the peak observed during the forward scan. Overall, the behavior of the PCBM transistors gated in 4 M [Li][TFSI] in TEGDME resembles that one of analogous PCBM transistors gated with [EMIM][TFSI] ("bulk" doping as opposed to "surface-confined" doping observed with [PYR14][TFSI], see main text).

Ionic liquid **[EMIM][TFSI]**						
Scan rate of the electrochemical potential	Potential vs carbon	Current	Potential vs carbon	Current	Potential vs carbon	Current
Cathodic scan (third cycle)						
100mV/s	-0.99 V	-12.9 □A	-1.38 V	-39.8 µA	-1.67 V	-39.7 µA
50mV/s	-1.01 V	-9.2 µA	-1.35 V	-24.86 µA	-1.64 V	-24.75 µA
1mV/s	-0.83 V	-0.28 µA	-1.37 V	-1.52 µA	-1.71 V	-1.35 µA
Anodic scan (third cycle)						
100mV/s	-1.43 V	22.8 µA	-1.1 V	21.5 µA	-0.57 V	19.8 µA
50mV/s	-1.43 V	13.79 µA	-1.1 V	13.78 µA	-0.66 V	11.8 µA
1mV/s	-1.5 V	0.07 µA	-0.98 V	0.76 µA	-0.64 V	0.84 µA
Ionic liquid **[PYR14][TFSI]**						
Cathodic scan (third cycle)						
100mV/s	-0.99 V	-1.94 µA	-1.35 V	-3.80 µA	-1.62 V	-3.92 µA
50mV/s	-1.04 V	-1.78 µA	-1.37V	-3.55 µA	-1.64V	-3.87 µA
1mV/s	-0.95 V	-0.17 µA	-1.33 V	-0.79 µA	-1.72V	-0.94 µA
Anodic scan (third cycle)						
100mV/s	-1.49 V	1.82 µA	-1. 05 V	2.64 µA	-0.67 V	4.99 µA
50mV/s	-1.51 V	1.88 µA	-1.11 V	2.77 µA	-0.67 V	4.65 µA
1mV/s	-1.58 V	0.24 µA	-1.24 V	0.34 µA	-0.72 V	0.92 µA

Table S1. Cathodic and anodic current peak positions extracted at different scan rates, 100 mVs^{-1}, 50 mVs^{-1}, and 1 mVs^{-1}, for PCBM films in transistor configuration (see main text) in different ionic liquids, specified in the Table.

APPENDIX B - SUPPORTING INFORMATION OF ARTICLE 2

Supporting Information

Ambient-stable, ion-gated poly[N-9'-heptadecanyl-2,7-carbazole-alt-5,5-(4',7'-di-2-thienyl-2',1',3'-benzothiadiazole)] (PCDTBT) transistors and phototransistors

Tian Lan[1], Francis Bélanger [2], Francesca Soavi[3] and Clara Santato[1]*

1. Polytechnique Montreal, Engineering Physics Department, Montréal, Quebec, H3C 3A7, Canada

2. Seqens, 725 rue Trotter, St-Jean-sur-Richelieu, Quebec, Canada, J3B 8J8

3. Department of Chemistry, Università di Bologna, 40126, Italy

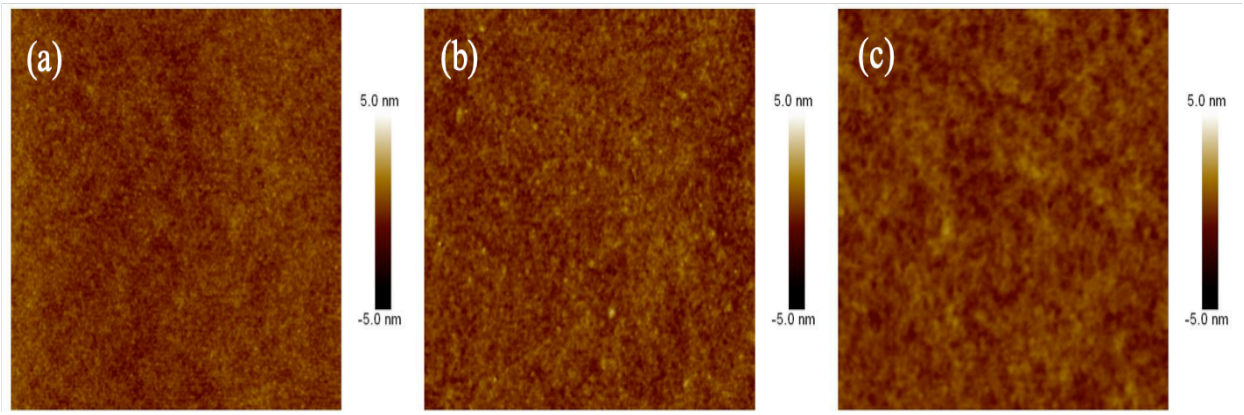

Fig. S1 AFM images of PCDTBT films deposited on SiO_2 by spin-coating : (a) 10 μm×10 μm, (b) 5 μm×5 μm and (c) 2 μm×2 μm.

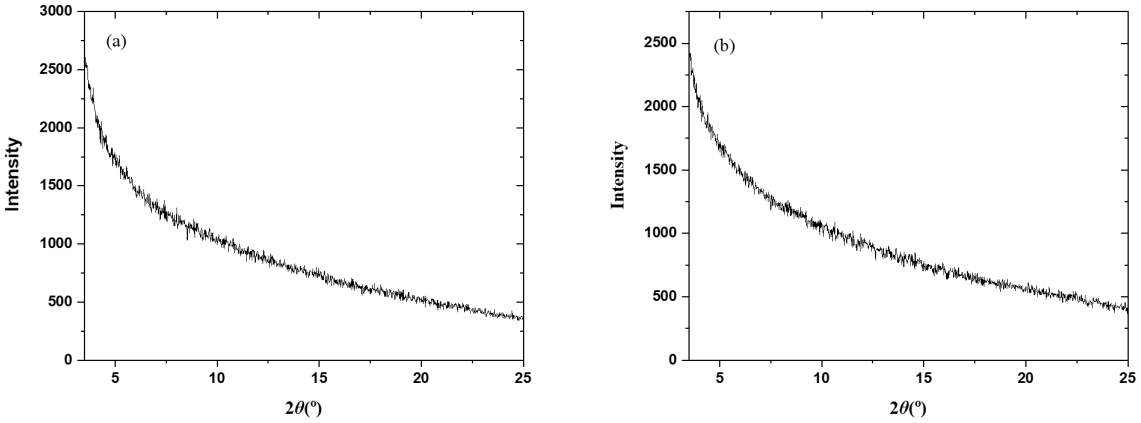

Fig. S2 XRD patterns of PCDTBT films deposited on SiO_2 via (a) spin-coating and (b) drop-casting.

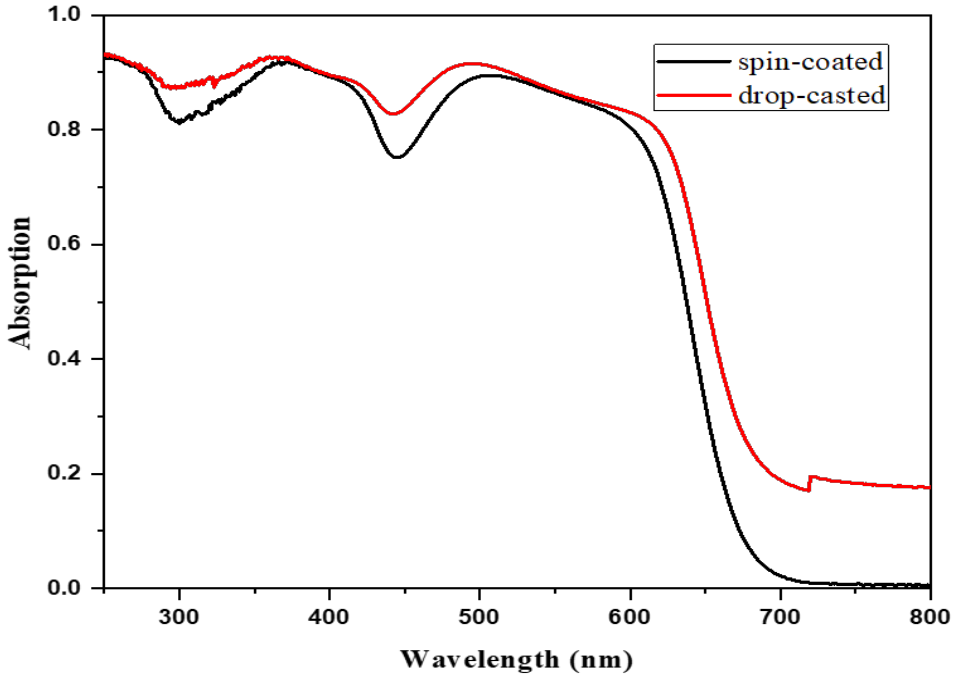

Fig. S3 UV-vis absorption spectra of spin-coated and drop-casted PCDTBT thin films on fused silica substrates.

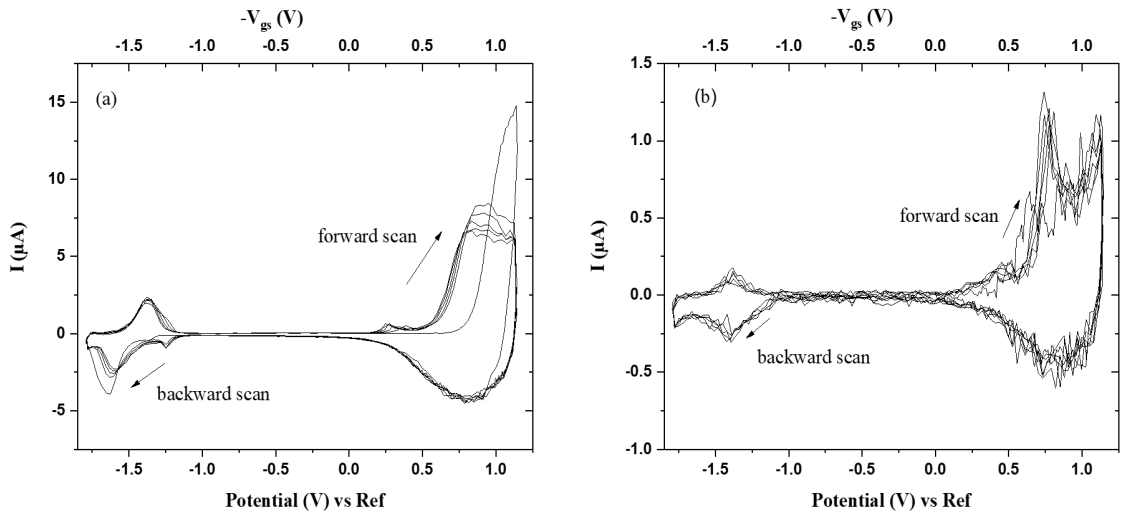

Fig. S4 Cyclic voltammograms obtained in transistor configuration for PCDTBT films fabricated via spin-coating in [EMIM][TFSI] with sweep rates of 10 $mV \cdot s^{-1}$ (a) 1 $mV \cdot s^{-1}$ (b). The quasi reference electrode is made of high surface area activated carbon. The first five cycles are shown.

Within the interval 0/+1.15 V, at 10 mV/s, we observe a peak at 1.15 V during the 1st cycle. With the increase of the cycle number, there are two peaks: one small peak at around 0.3 V and the other one at around 0.9 V; in the backward (cathodic) scan, there is a peak located at ca 0.8 V. At the same scan rate, in the interval of 0/ -1.8V, during the forward scan of the 1st cycle, there are two observable peaks: one pins at around -1.3 V and the other one locates at around -1.63 V, whose position shifts positively with the following scan. During the backward scan, there is an observable peak at -1.4 V.

At 1 mV/s, in the interval 0/+1.15 V, there is a peak at 0.75 V in the forward scan, in the 1st cycle; in the backward scan, a broad peak is observable at around 0.9 V. At the same scan rate, in

the interval 0/-1.8 V, during the forward scan of the 1st cycle, there is a peak at ca -1.4 V. In the backward scan, there is an oxidation peak located at ca -1.35 V.

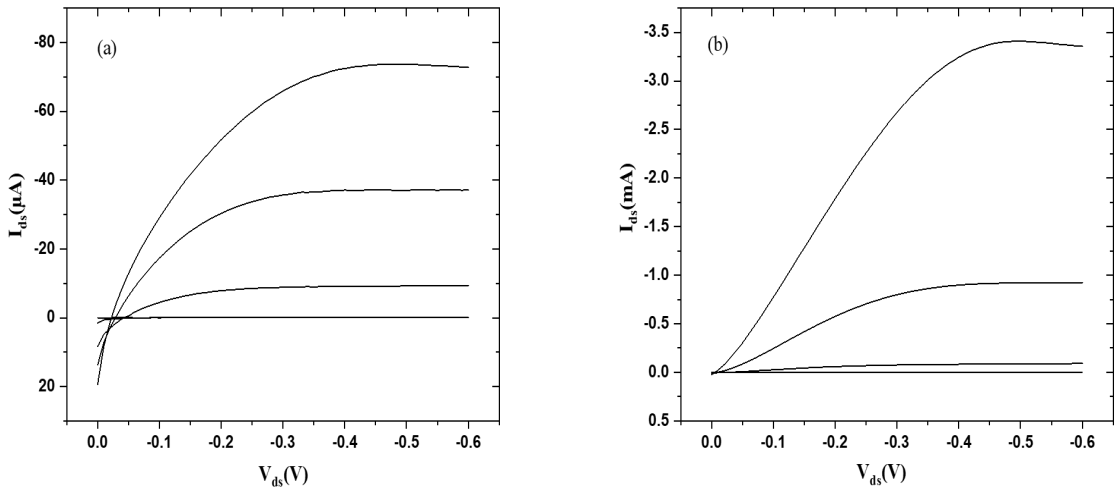

Fig. S5 [EMIM][TFSI]-gated PCDTBT transistors fabricated via (a) spin-coating and (b) drop-casting, characterized in the dark, under N_2 atmosphere. Output characteristics for V_{gs}=0, -0.55, -0.7, -0.85, -1V. Drain-source voltage scan rate is 10 mV s^{-1}. Output curves obtained for V_{gs}=0 V and -0.55 V superposed.

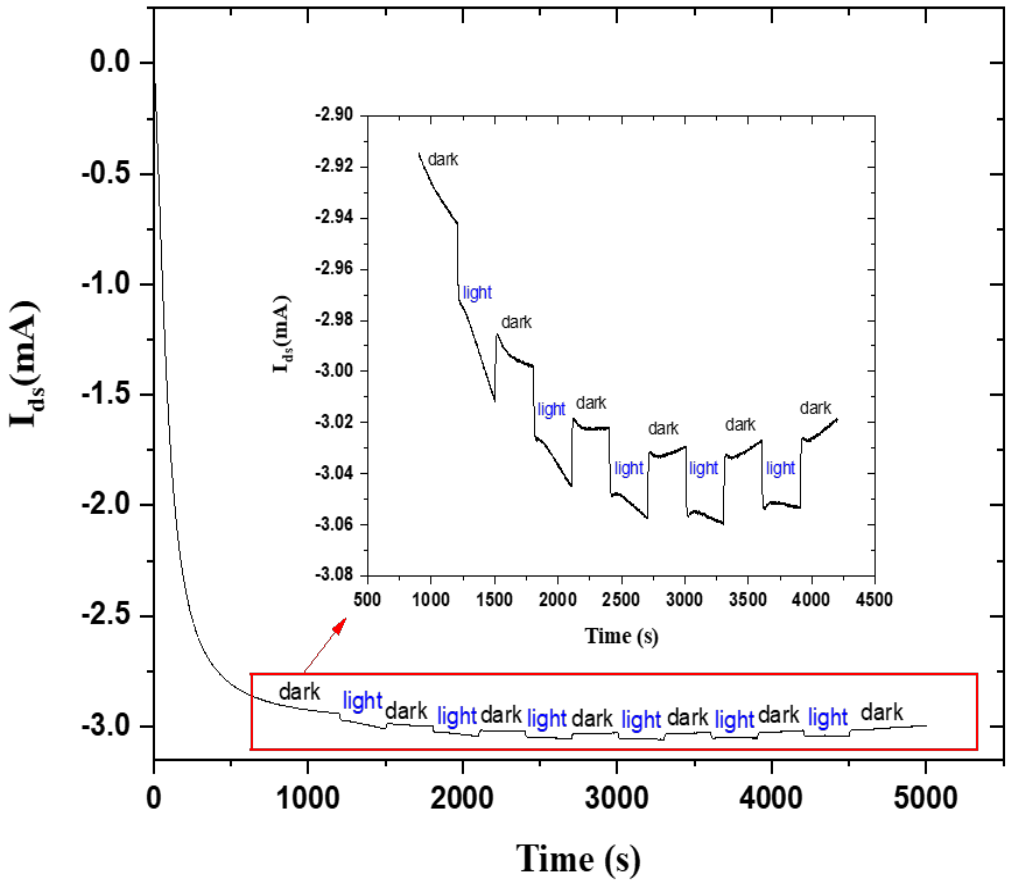

Fig. S6 Transient current measurement on [EMIM][TFSI]-gated PCDTBT transistors, under chopped, simulated solar light (time interval of 300 s), in vacuum. V_{ds}=-0.2 V, V_{gs}= -1.15 V.

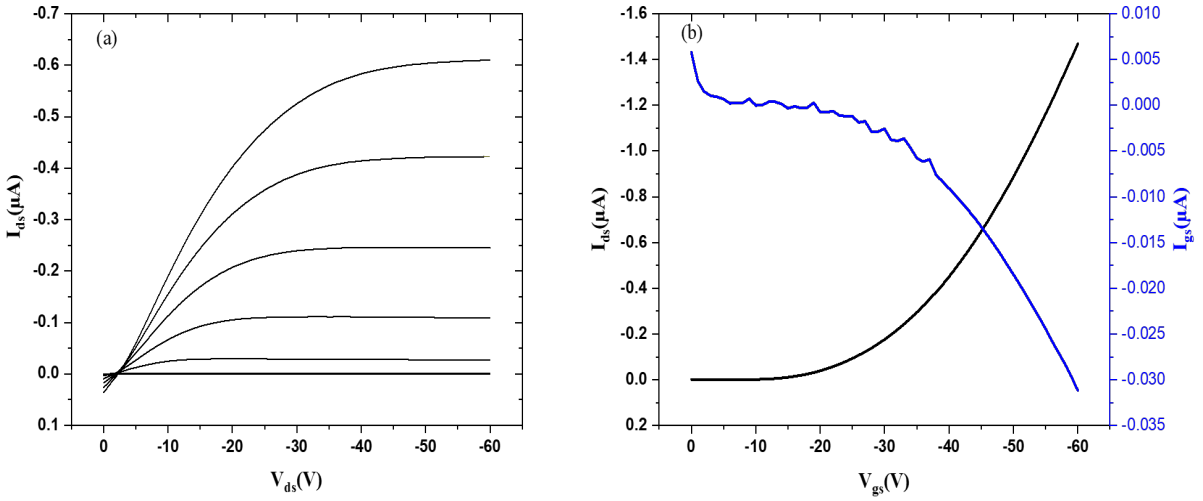

Fig. S7 PCDTBT-based field-effect transistor (FET) fabricated via drop-casting : (a) Output characteristics for V_{gs}= 0, -10, -20, -30, -40, -50, -60 V. (b) Transfer characteristics (V_{ds}= -60 V).

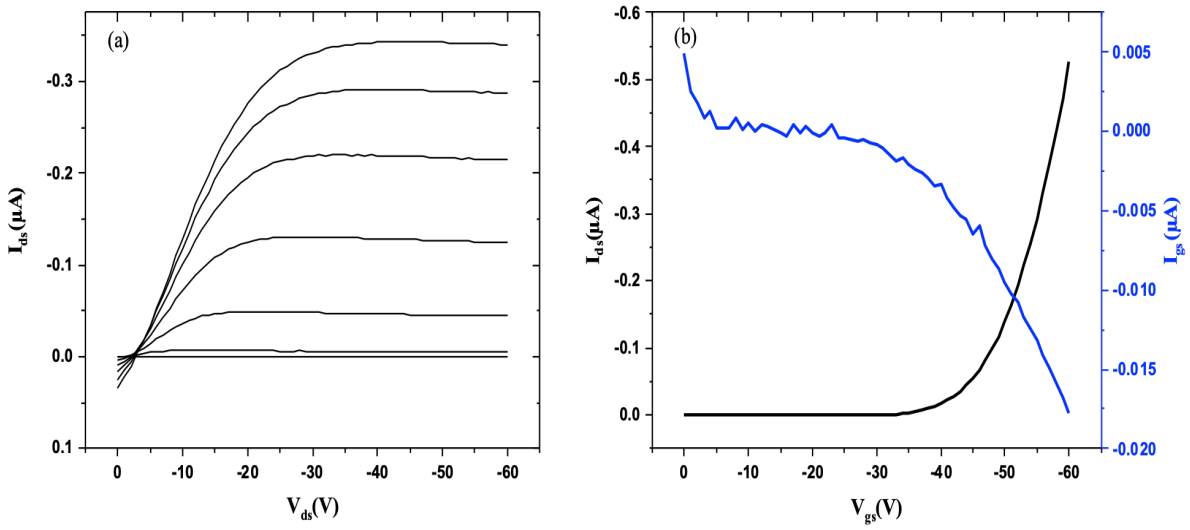

Fig. S8 PCDTBT-based field-effect transistor (FET) fabricated via spin-casting : (a) Output characteristics for V_{gs}= 0, -10, -20, -30, -40, -50, -60 V. (b) Transfer characteristics (V_{ds}= -60 V).

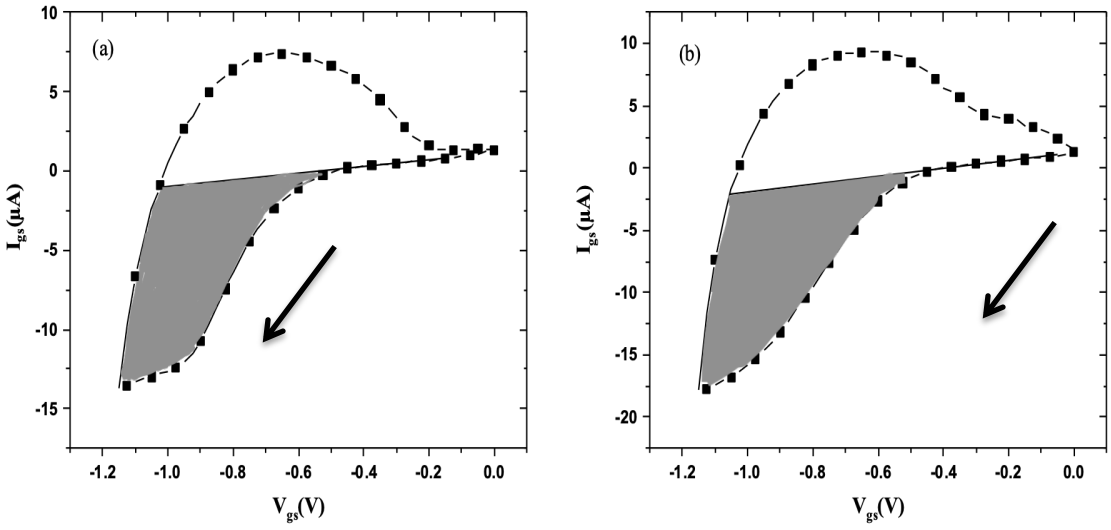

Fig. S9 I_{gs}-V_{gs} measured simultaneously for ion-gated PCTBT transistor under (a) dark and (b) light, with a gate voltage sweep rate of 10 mV/s. The gray shaded regions on the forward sweep of the I_{gs}-V_{gs} curves indicate the integrated areas used to calculate the total injected charge carrier (hole) densities by the application of V_{gs} up to -1.15 V.

The total hole density in the channel could be determined by integrating the displacement current I_{dis} versus time data, similar to the analysis of a cyclic voltammogram.[23-24] $I_{dis}=I_{gs}-I_{background}$, where $I_{background}$ is the displacement current before turn on.

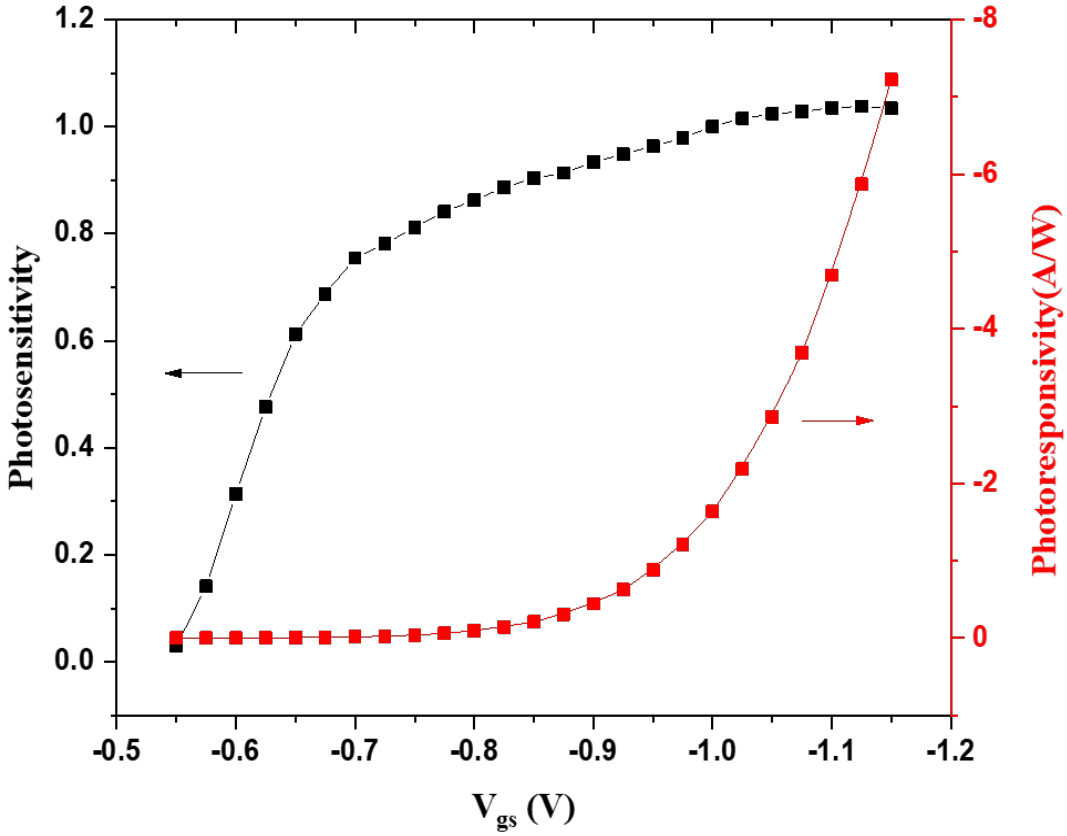

Fig. S10 Photosensitivity and photoresponsivity of [EMIM][TFSI]-gated PCDTBT transistors under simulated solar light conditions, measured at V_{ds}=-0.2 V, in vacuum conditions, at scan rate of 10 $mV \cdot s^{-1}$.

Table. S2 Key parameters for reported organic phototransistors, including materials used, light conditions (wavelength and power), gating medium, applied voltage, maximum photosensitivity and photoresponsivity.

	Channel Material	Gating Medium	Light Wavelength (nm)	Light Power ($mW\ cm^{-2}$)	Voltage	Figures of Merit		Ref
						Photosensitivity	Photoresponsivity (AW^{-1})	
P-type	PCDTBT	[EMIM][TFSI] liquid	White light	100	V_{gs}=-1.15V V_{ds}=-0.2V	1	7.3	This work
	CuPc	SiO_2	655	250	V_{gs}=-100V V_{ds}=-50V	2.5×10^3	0.02	[1]
	PBDFTDTBT	SiO_2	White light	100	V_{gs}=-40V V_{ds}=-50V	1.2×10^5	0.36	[2]
	CB-BTBT	SiO_2	365	30	V_{gs}=-60V V_{ds}=-30V	10^5	4×10^2	[3]
	PDA	SiO_2	808	19.3	V_{gs}=-12V V_{ds}=-30V	6.9×10^4	9	[4]
	DDTT-SBT-14	*h*TSO	Blue light	3	V_{gs}=-3V V_{ds}=-3V	3.8×10^3	2×10^2	[5]
	PQT12/PEO	PDMS	Poly-chromatic light	0.1	V_{gs}=-100V V_{ds}=-30V	2.76	9.3×10^2	[6]
	DNTT	AlO_x-SAM	450~490	0.005	V_{gs}=-5V V_{ds}=-5V	5	50	[7]
	TIPS-pentacene	HfO_2+PVP	365	1.8	V_{gs}=-10V V_{ds}=-5V	5×10^2	43	[8]
	P3HT	PMMA	550,800,1000	0.26	V_{gs}=-15V V_{ds}=-15V	N/A	747	[9]
	Pentacene	Al_2O_3	240~400	1.82	V_{gs}=-10V	1.5×10^3	4.5	[10]
N-type	BPE-PTCDI	SU-8	450	0.0015	V_{gs}=80V	N/A	7230	[11]
	PDIF-CN_2	SiO_2	White light	5.06	V_{gs}=60V V_{ds}=60V	1×10^3	2×10^3	[12]
	PTCDI-C_8	Cross-linked PVP	White light	10	V_{gs}=12V	1×10^3	3	[13]
Heterojunction	DPP-DTT: PCBM	SiO_2	808	67	V_{gs}=-30V	1.6×10^4	5×10^5	[14]
	P3HT: PDPPTTT	PMMA +PVA	450,555,795	1	V_{gs}=30V	8	1.65	[15]
	P3HT:THBT-ht	SiO_2	470,555,665	100	V_{gs}=10V	1.2×10^5	0.36	[16]
	C60:AlClPc	SiO_2	365	30	V_{gs}=60V	10^4	94.4	[17]
	P3HT:PEHTPPD-BT	PVP-MMF	550,1000	0.0022	V_{gs}=-80V V_{ds}=-80V	N/A	4.5×10^2	[18]
	MDMO-PPV:PCBM	Parylene	543	7.5	V_{gs}=-20V	N/A	1	[19]
	PDPP2T: $PC_{61}BM$	Ion-gel	808	50	V_{gs}=-1.5	7.5×10^5	1.5×10^3	[20]
ambipolar	PPhTQ	SiO_2	White light	15	V_{gs}=-80V V_{ds}=-80V	0.5	4×10^2	[21]
	PBIBDF-BT	SiO_2	White light	21.68	V_{gs}=-80V V_{ds}=-80V	4554	108	[22]

References

1. Xiao Luo et al, ACS Appl. Mater. Interfaces, **2018**, 10, 15352.

2. Wenlong Huang et al, Org. Electron., **2014**, 15, 1050.

3. Jia Huang et al, Adv. Funct. Mater., **2017**, 27, 1604163.

4. Hye Jin Nam et al, ChemComm., **2015**, 50, 1458.

5. Bo-Yi Jiang et al, J. Mater. Chem. C., **2017**, 5, 9838.

6. Moo Yeol Lee et al, Adv. Funct. Mater., **2016**, 26, 1445.

7. Fanfan Yu et al, RSC Adv., **2017**, 7, 11572.

8. Deepak Bharti et al, Superlattices Microstruct., **2017**, 109, 538.

9. Chulyeon Lee et al, IEEE J. Sel. Top. Quantum Electron., **2018**, 24, 6000307.

10. Shuo-Huang Yuan et al, IEEE Electr. Device L., **2015**, 36, 1186.

11. Xien Liu et al, ACS Appl. Mater. Interfaces., **2016**, 8, 7291.

12. Wassima Pekab et al, ACS Appl. Mater. Interfaces., **2016**, 8, 9829.

13. Biswanath Mukherjee, Optik., **2017**, 139, 48.

14. Haihua Xu et al, Nanoscale., **2013**, 5, 11850.

15. Sungho Nam et al, Adv. Electron. Mater., **2016**, 2, 1600264.

16. Wenlong Huang et al, Org Electron., **2014**, 15, 1050.

17. Lili Du et al, Carbon., **2016**, 96, 685.

18. Hyemi Han et al, Sci. Rep., **2015**, 5, 1.

19. Philip Chi Yung Chow et al, Nat. Commun., **2018**, 9, 1.

20. Haihua Xu et al, ACS Appl. Mater. Interfaces., **2017**, 9, 18134.

21. Mengmeng Li et al, Chem. Mater., **2015**, 27, 2218.

22. Qinghe Wang et al, J. Mater. Chem. C., **2015**, 3, 10734.

23. Panzer M. J. et al, AdV. Funct. Mater., **2006**, 16, 1051.

24. Yu Xia et al, Appl. Phys. Lett., **2009**, 94, 013304.

APPENDIX C - SUPPORTING INFORMATION OF ARTICLE 3

Support Information

Flexible ion-gated transistors making use of poly-3-hexylthiophene (P3HT): on the effect of the molecular weight on the effectiveness of gating and device performance

Tian Lan[1], Zhaojing Gao[1], Martin S Barbosa[1,2], and Clara Santato[1]*

1.Polytechnique Montreal, Engineering Physics Department, Montréal, Quebec, H3C 3A7, Canada

2. São Paulo State University, Departamento de Fisico-Química, São Paulo, 14800-060, Brazil.

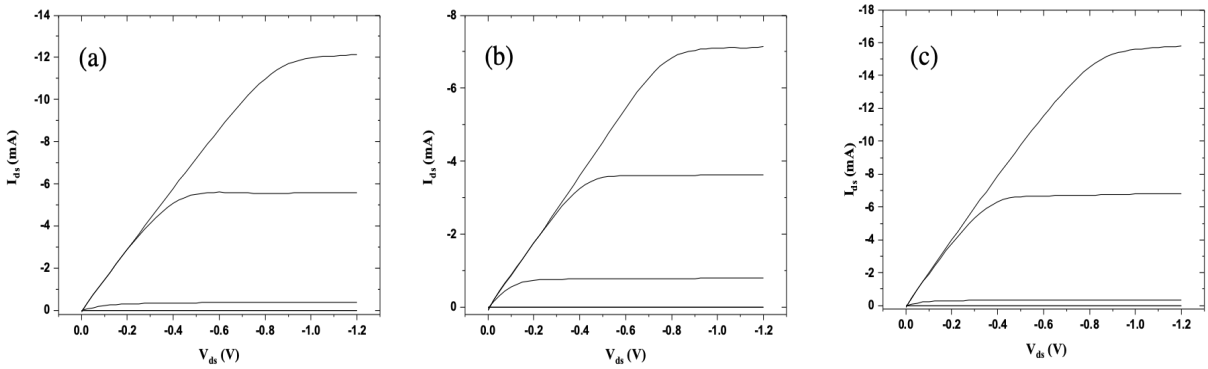

Fig. S1 [EMIM][TFSI]-gated P3HT films transistors (a: low MW; b: intermediate MW; c: high MW) fabricated on Si/SiO_2 via spin-coating. V_{gs}=0, -0.3, -0.6, -0.9, -1.2 V. Drain-source voltage scan rate is 50 mV s^{-1}. The output curves obtained for V_{gs}=0 V and -0.3 V are superposed.

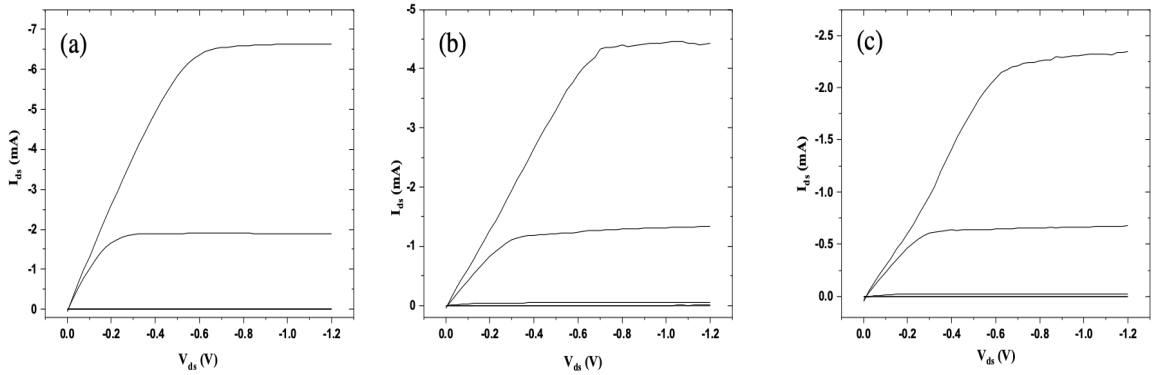

Fig. S2 [EMIM][TFSI]-gated low MW P3HT transistors on polyimide, at rest (a), under a bending radius of R=10 mm (b) and R= 5mm (c), under N_2 atmosphere. Output characteristics for V_{gs}=0, -0.3, -0.6, -0.9, -1.2 V. V_{ds} scan rate is 50 mV s^{-1}. Output curves obtained for V_{gs}=0 V and -0.3 V are superposed.

The output characteristics showed that $I_{ds,}$with a bending radius of R=10 mm, decreased, compared to the rest conditions. Further decrease in I_{ds} was observed with a bending radius of R=5

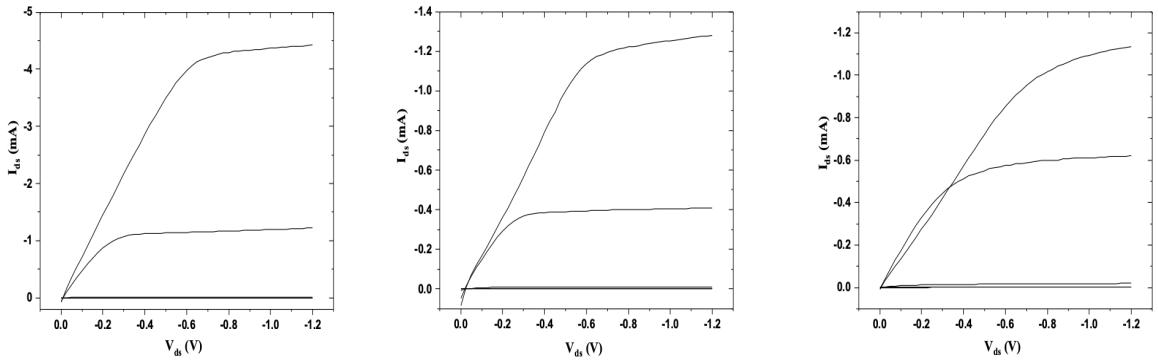

Fig. S3 [EMIM][TFSI]-gated intermediate MW P3HT transistors on polyimide, at rest (a), under a bending radius of R=10 mm (b) and R= 5mm (c), under N_2 atmosphere. Output characteristics for V_{gs}=0, -0.3, -0.6, -0.9, -1.2V. V_{ds} scan rate is 50 mV s^{-1}. Output curves for V_{gs}=0 V and -0.3 V are superposed.

Compared to the output characteristics of [EMIM][TFSI]-gated low MW P3HT transistors, the I_{ds} decrease from the rest conditions to the bending conditions with a bending radius of R=10 mm is more severe, here (i.e. for the intermediate MW case).

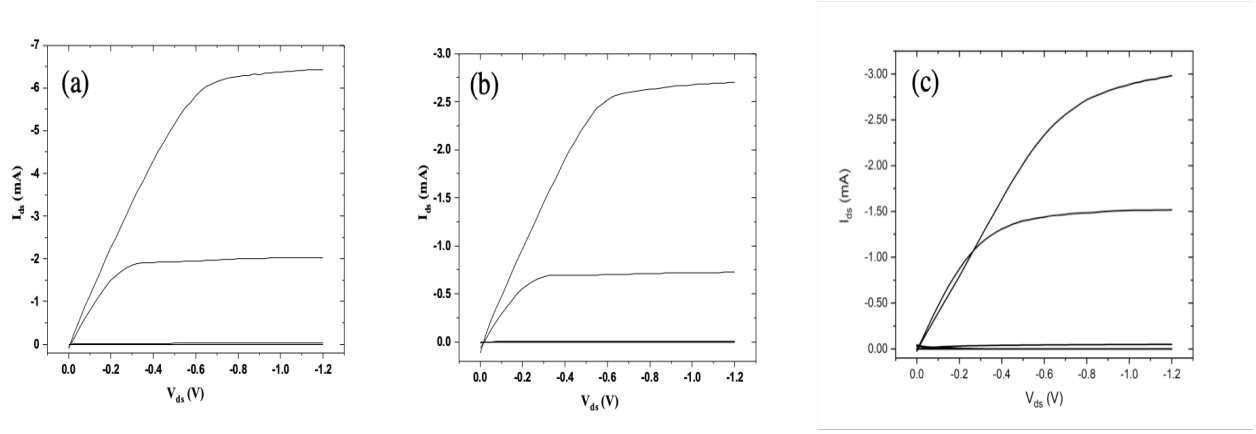

Fig. S4 [EMIM][TFSI]-gated high MW P3HT transistors on polyimide, at rest (a), under a bending radius of R=10 mm (b) and R= 5mm (c), under N_2 atmosphere. Output characteristics for V_{gs}=0, -0.3, -0.6, -0.9, -1.2V. V_{ds} scan rate is 50 mV s^{-1}. Output curves for V_{gs}=0 V and -0.3 V are superposed.

The output characteristics of [EMIM][TFSI]-gated high MW P3HT transistors, at rest or with the two bending radii R=10 mm and R= 5mm, share the same behavior of those observed with intermediate MW P3HT transistors.

APPENDIX D-PARTICIPATION IN CONFERENCES

1. **T. Lan**, J. Sayago, P.-L. Brunner, F. Cicoira and C. Santato “Electrolyte-Gated Transistors using n-type organic molecular semiconductors: the case of PCBM as Channel Material”, The 2nd edition of the Graphene & 2D Materials International Conference and Exhibition, Poster, Montreal, Canada, October 2016.
2. **T. Lan**, F. Soavi, J. Sayago and C. Santato, F. Soavi, J. Sayago and C. Santato, “PCBM (phenyl-C61-butyric acid methyl ester) working as channel nanomaterial in electrolyte-gated transistors”, Innovation 360, Nano Canada, Poster, Montreal, Canada, September 2017.
3. **T. Lan**, F. Soavi, J. Sayago and C. Santato “Electrolyte-Gated Transistors Based on N-Type Semiconductors Undergoing Several Redox Processes— Correlation of Electrochemical and Device Properties”, MRS Fall Meeting& Exhibit, Oral Presentation, Boston, USA, November 2017.
4. **T. Lan**, F. Soavi, P.-L. Brunner, J. Sayago and C. Santato “Correlation between redox, charge carrier transport and ion molecular structure properties in ion-gated PCBM films，MRS Fall Meeting& Exhibit, Oral Presentation, Boston, USA, November 2018